

IMPLEMENTATION AND COMPARISON OF DIFFERENT CONSTITUTIVE MODELS
IN DEEP DRAWING PROCESS

A THESIS SUBMITTED TO
THE GRADUATE SCHOOL OF NATURAL AND APPLIED SCIENCES
OF
MIDDLE EAST TECHNICAL UNIVERSITY

BY

FERAH OĐUN

IN PARTIAL FULFILLMENT OF THE REQUIREMENTS
FOR
THE DEGREE OF MASTER OF SCIENCE
IN
MECHANICAL ENGINEERING

SEPTEMBER 2013

Approval of the thesis:

**IMPLEMENTATION AND COMPARISON OF DIFFERENT CONSTITUTIVE
MODELS IN DEEP DRAWING PROCESS**

submitted by **FERAH OĐUN** in partial fulfillment of the requirements for the degree of
Master of Science in Mechanical Engineering, Middle East Technical University by,

Prof. Dr. Canan zgen
Dean, Graduate School of **Natural and Applied Sciences** _____

Prof. Dr. Suha Oral
Head of the Department, **Mechanical Engineering** _____

Prof. Dr. Haluk Darendeliler
Supervisor, **Mechanical Engineering Dept., METU** _____

Examining Committee Members:

Prof. Dr. Mustafa İ. Gkler
Mechanical Engineering Dept., METU _____

Prof. Dr. Haluk Darendeliler
Mechanical Engineering Dept., METU _____

Prof. Dr. Suha Oral
Mechanical Engineering Dept., METU _____

Prof. Dr. Levend Parnas
Mechanical Engineering Dept., METU _____

Prof. Dr. Mfit Glge
Mechatronics Engineering Dept., ankaya University _____

Date: September 3rd, 2013

I hereby declare that all information in this document has been obtained and presented in accordance with academic rules and ethical conduct. I also declare that, as required by these rules and conduct, I have fully cited and referenced all material and results that are not original to this work.

Name, Last name: Ferah ođun

Signature:

ABSTRACT

IMPLEMENTATION AND COMPARISON OF DIFFERENT CONSTITUTIVE MODELS IN DEEP DRAWING PROCESS

Çoğun, Ferah

M.Sc., Department of Mechanical Engineering

Supervisor: Prof. Dr. Haluk Darendeliler

September 2013, 88 pages

The aim of the study is to find out the effects of different models namely; BBC2008-8p, Yld2003-8p, Hu2003, isotropic hardening, kinematic hardening, combined hardening and Hill'48 on simulation of cylindrical, square and round bottom cup drawing processes. For this purpose two different sheet materials, SS304 stainless steel and DKP6112 steel with 1 mm thickness and three different punch travels were used in both computer simulation and experimental phase of this study. BBC2008-8p, Yld2003-8p and Hu2003 models were implemented to the software with the user material subroutine.

The thickness strain distributions obtained by simulations for the seven models were compared with the experimental findings to find out their consistency. It is found that the implemented recent models namely, BBC2008-8p, Yld2003-8p and Hu2003 models are better to predict the material behavior in deep drawing cases presented in the study.

Keywords: Sheet Metal, Deep Drawing, Constitutive Models, Yield Criteria, Finite Element Method.

ÖZ

DERİN ÇEKME İŞLEMİNDE FARKLI BÜNYE DENKLEMLERİNİN UYGULANMASI VE KARŞILAŞTIRILMASI

Çoğun, Ferah

Yüksek Lisans, Makina Mühendisliği Bölümü

Tez Yöneticisi: Prof. Dr. Haluk Darendeliler

Eylül 2013, 88 sayfa

Bu çalışmanın amacı silindirik, kare ve yarı küresel derin çekme işlemlerinin benzetiminde BBC2008-8p, Yld2003-8p, Hu2003, izotropik pekleşme, kinematik pekleşme, kombine pekleşme ve Hill'48 modellerinin kullanımının etkilerini tespit etmektir. Bu amaçla, çalışmanın bilgisayar benzetim ve deneysel aşamalarında 1 mm kalınlığında iki farklı sac malzeme, SS304 paslanmaz çelik ve DKP6112 çelik ve farklı zımba hareket boyları kullanılmıştır. BBC2008-8p, Yld2003-8p ve Hu2003 modelleri kullanıcı malzeme altyordamı aracılığıyla yazılıma uygulanmıştır.

Yedi model için benzetim sonuçlarından elde edilen kalınlık gerinim dağılımları deneysel bulgularla uyumluluk açısından karşılaştırılmıştır. Uygulanan güncel modellerden BBC2008-8p, Yld2003-8p ve Hu2003 modellerinin bu çalışmada sunulan derin çekme uygulamaları için malzeme davranışını daha iyi tahmin ettiği görülmüştür.

Keywords: Sac Malzeme, Derin Çekme, Bünye Denklemleri, Akma kriterleri, Sonlu Elemanlar Metodu.

To My Family

ACKNOWLEDGEMENTS

First and foremost, I would like to express my deepest gratitude to my supervisor Prof. Dr. Haluk DARENDELİLER for his valuable guidance, advices and time devoted to me.

Further, I wish to thank to Servet ŞEHİRLİ and Mehmet ERİLİ for their valuable support and assistance during the experimental phase of the thesis.

Finally, yet importantly, I am indebted to my beloved family; Can, Ferrin, Fuat and Tuğçe ÇOĞUN for their understanding, support, endless patience and encouragement through the study.

TABLE OF CONTENTS

ABSTRACT.....	v
ÖZ.....	vi
ACKNOWLEDGEMENTS.....	viii
TABLE OF CONTENTS.....	ix
LIST OF TABLES.....	xi
LIST OF FIGURES.....	xii
CHAPTERS	
1. INTRODUCTION.....	1
1.1 Background and Motivation.....	1
1.2 Deep (Cup) Drawing Process.....	1
1.3 Scope of Thesis.....	2
1.4 Outline of the Thesis.....	2
2. LITERATURE SURVEY.....	5
3. FINITE ELEMENT ANALYSIS.....	11
3.1 The Finite Element Method.....	11
3.1.1 Geometrical Nonlinearities.....	12
3.1.2 Material Nonlinearities.....	12
3.1.3 Boundary Nonlinearities.....	12
3.2 The Finite Element Formulation.....	12
3.3 The Finite Element Model.....	12
3.3.1 Cylindrical Cup Drawing.....	13
3.3.2 Square Cup Drawing.....	13
3.3.3 Round Bottom Cup Drawing.....	14
4. CONSTITUTIVE MODELS.....	17
4.1 Isotropic Hardening.....	17
4.2 Kinematic Hardening.....	19
4.3 Combined Hardening.....	21
4.4 Hill'48 Yield Criterion.....	22
4.5 Aretz 8 coefficients Yield Criterion (Yld2003-8p).....	25
4.6 Hu Yield Criterion (2003).....	29

4.7 BBC2008 Yield Criterion.....	32
5. EXPERIMENTAL STUDIES.....	39
5.1 Tension Test.....	39
5.2 Erichsen Test.....	43
5.3 Deep Drawing Tests.....	45
5.3.1 Cylindrical Cup Drawing.....	45
5.3.2 Square Cup Drawing.....	46
5.3.3 Round Bottom Cup Drawing.....	47
5.4 Material Constants.....	48
6. RESULTS AND DISCUSSION.....	51
6.1 Stainless steel 304 material	51
6.1.1 Cylindrical Cup Drawing.....	51
6.1.2 Square Cup Drawing.....	55
6.1.3 Round Bottom Cup Drawing.....	59
6.2 DKP6112 material.....	61
6.2.1 Cylindrical Cup Drawing.....	61
6.2.2 Square Cup Drawing.....	65
6.2.3 Round Bottom Cup Drawing.....	68
7. CONCLUSION AND FUTURE WORK.....	73
REFERENCES.....	75
APPENDIX A	
SAMPLE FEA RESULTS.....	81

LIST OF TABLES

TABLES

Table 5.1 Elastic Modulus, Poisson's ratio of SS304 and DKP 6112 steels.....	42
Table 5.2 Mechanical properties of SS304 and DKP 6112 steels.....	42
Table 5.3 The equibiaxial yield stresses (σ_b) and r-values (r_b) of SS304 and DKP6112 steels.....	44
Table 5.4 Material constants of BBC2008-8p yield criterion for SS304 and DKP6112 steels.....	49
Table 5.5 Material constants of Yld2003-8p yield criterion for SS304 and DKP6112 steels.....	50

LIST OF FIGURES

FIGURES

Figure 3.1 The FEM model of cylindrical cup drawing.....	13
Figure 3.2 Meshing of a quarter circle blank.....	13
Figure 3.3 The FEM model of square cup drawing.....	14
Figure 3.4 Meshing of a quarter square blank.....	14
Figure 3.5 The FEM model of round bottom cup drawing.....	15
Figure 3.6 Meshing of a quarter circle blank.....	15
Figure 4.1 π - plane and uniaxial test for isotropic hardening.....	17
Figure 4.2 π - plane and uniaxial test for kinematic hardening and Bauschinger effect...	19
Figure 4.3 Schematic view of combined hardening.....	21
Figure 4.4 Flow chart of the BBC2008 model.....	37
Figure 5.1 Strains on a tensile specimen.....	39
Figure 5.2 Zwick/Roel Z020 tension machine.....	40
Figure 5.3 The SS304 specimens.....	40
Figure 5.4 Tensile test specimens dimensions.....	41
Figure 5.5 The SS304 specimens after tensile testing.....	41
Figure 5.6 True stress-strain behaviors of SS304 material.....	42
Figure 5.7 True stress-strain behaviors of DKP6112 material.....	43
Figure 5.8 Erichsen test setup.....	44
Figure 5.9 10, 14, 18, 22 and 24 mm drawn SS304 steel cups.....	44
Figure 5.10 Tinius-Olsen deep drawing machine.....	45
Figure 5.11 20, 35, 45 mm drawn SS304 steel cylindrical cups.....	46
Figure 5.12 15, 20, 25 mm drawn SS304 steel square cups.....	47
Figure 5.13 25 and 45 mm drawn SS304 steel round cups.....	47
Figure 5.14 Laser markings of blanks: (a) Circular blanks for cylindrical and round bottom cup drawing, (b) square blanks for square cup drawing, (c) circular blanks for Erichsen tests.....	48
Figure 5.15 The deformed patterns on the drawn cup.....	49
Figure 6.1 Thickness strain distributions obtained from different models and experiment at 20 mm punch travel (SS304, cylindrical, rolling direction).....	52

Figure 6.2 Thickness strain distributions obtained from different models and experiment at 20 mm punch travel (SS304, cylindrical, transverse direction).....	52
Figure 6.3 Thickness strain distributions obtained from different models and experiment at 35 mm punch travel (SS304, cylindrical, rolling direction).....	53
Figure 6.4 Thickness strain distributions obtained from different models and experiment at 35 mm punch travel (SS304, cylindrical, transverse direction).....	53
Figure 6.5 Thickness strain distributions obtained from different models and experiment at 45 mm punch travel (SS304, cylindrical, rolling direction).....	54
Figure 6.6 Thickness strain distributions obtained from different models and experiment at 45 mm punch travel (SS304, cylindrical, transverse direction).....	54
Figure 6.7 Thickness strain distributions obtained from different models and experiment at 15 mm punch travel (SS304, square, rolling direction).....	55
Figure 6.8 Thickness strain distributions obtained from different models and experiment at 15 mm punch travel (SS304, square, diagonal direction).....	56
Figure 6.9 Thickness strain distributions obtained from different models and experiment at 20 mm punch travel (SS304, square, rolling direction).....	56
Figure 6.10 Thickness strain distributions obtained from different models and experiment at 20 mm punch travel (SS304, square, diagonal direction).....	57
Figure 6.11 Thickness strain distributions obtained from different models and experiment at 25 mm punch travel (SS304, square, rolling direction).....	58
Figure 6.12 Thickness strain distributions obtained from different models and experiment at 25 mm punch travel (SS304, square, diagonal direction).....	58
Figure 6.13 Thickness strain distributions obtained from different models and experiment at 25 mm punch travel (SS304, round, rolling direction).....	59
Figure 6.14 Thickness strain distributions obtained from different models and experiment at 25 mm punch travel (SS304, round, transverse direction).....	60
Figure 6.15 Thickness strain distributions obtained from different models and experiment at 45 mm punch travel (SS304, round, rolling direction).....	60
Figure 6.16 Thickness strain distributions obtained from different models and experiment at 45 mm punch travel (SS304, round, transverse direction).....	61
Figure 6.17 Thickness strain distributions obtained from different models and experiment at 15 mm punch travel (DKP6112, cylindrical, rolling direction).....	62
Figure 6.18 Thickness strain distributions obtained from different models and experiment at 15 mm punch travel (DKP6112, cylindrical, transverse direction).....	62
Figure 6.19 Thickness strain distributions obtained from different models and experiment at 25 mm punch travel (DKP6112, cylindrical, rolling direction).....	63
Figure 6.20 Thickness strain distributions obtained from different models and experiment at 25 mm punch travel (DKP6112, cylindrical, transverse direction).....	63

Figure 6.21 Thickness strain distributions obtained from different models and experiment at 35 mm punch travel (DKP6112, cylindrical, rolling direction).....	64
Figure 6.22 Thickness strain distributions obtained from different models and experiment at 35 mm punch travel (DKP6112, cylindrical, transverse direction).....	64
Figure 6.23 Thickness strain distributions obtained from different models and experiment at 15 mm punch travel (DKP6112, square, rolling direction).....	65
Figure 6.24 Thickness strain distributions obtained from different models and experiment at 15 mm punch travel (DKP6112, square, diagonal direction).....	66
Figure 6.25 Thickness strain distributions obtained from different models and experiment at 20 mm punch travel (DKP6112, square, rolling direction).....	66
Figure 6.26 Thickness strain distributions obtained from different models and experiment at 20 mm punch travel (DKP6112, square, diagonal direction).....	67
Figure 6.27 Thickness strain distributions obtained from different models and experiment at 25 mm punch travel (DKP6112, square, rolling direction).....	68
Figure 6.28 Thickness strain distributions obtained from different models and experiment at 25 mm punch travel (DKP6112, square, diagonal direction).....	68
Figure 6.29 Thickness strain distributions obtained from different models and experiment at 20 mm punch travel (DKP6112, round, rolling direction).....	69
Figure 6.30 Thickness strain distributions obtained from different models and experiment at 20 mm punch travel (DKP6112, round, diagonal direction).....	69
Figure 6.31 Thickness strain distributions obtained from different models and experiment at 35 mm punch travel (DKP6112, round, rolling direction).....	70
Figure 6.32 Thickness strain distributions obtained from different models and experiment at 35 mm punch travel (DKP6112, round, transverse direction).....	70
Figure 6.33 Thickness strain distributions obtained from different models and experiment at 45 mm punch travel (DKP6112, round, rolling direction).....	71
Figure 6.34 Thickness strain distributions obtained from different models and experiment at 45 mm punch travel (DKP6112, round, transverse direction).....	71
Figure A.1 The cylindrical cup drawn (SS304 steel) according to Hu2003 model (45 mm punch travel)	81
Figure A.2 The cylindrical cup drawn (DKP6112 steel) according to Yld2003 model (35 mm punch travel).....	81
Figure A.3 The cylindrical cup drawn (DKP6112 steel) according to Hu2003 model (35 mm punch travel).....	82
Figure A.4 The cylindrical cup drawn (SS304 steel) according to Hu2003 model (20 mm punch travel)	82
Figure A.5 The square cup drawn (SS304 steel) according to Hu2003 model (15 mm punch travel).....	83

Figure A.6 The square cup drawn (SS304 steel) according to Yld2003 model (25 mm punch travel).....	83
Figure A.7 The square cup drawn (SS304 steel) according to Yld2003 model (15 mm punch travel).....	84
Figure A.8 The square cup drawn (DKP6112) according to Yld2003 model (25 mm punch travel).....	84
Figure A.9 The square cup drawn (DKP6112) according to Hu2003 model (25 mm punch travel).....	85
Figure A.10 The square cup drawn (SS304 steel) according to Hu2003 model (25 mm punch travel).....	85
Figure A.11 The round bottom cup drawn (SS304 steel) according to Yld2003 model (45 mm punch travel).....	86
Figure A.12 The round bottom cup drawn (SS304 steel) according to BBC2008 model (25 mm punch travel).....	86
Figure A.13 The round bottom cup drawn (DKP6112) according to BBC2008 model (20 mm punch travel).....	87
Figure A.14 The round bottom cup drawn (DKP6112) according to Yld2003 model (20 mm punch travel).....	87
Figure A.15 The round bottom cup drawn (DKP6112) according to Hu2003 model (20 mm punch travel).....	88
Figure A.16 The round bottom cup drawn (SS304 steel) according to Hu2003 model (25 mm punch travel).....	88

CHAPTER 1

INTRODUCTION

1.1 Background and Motivation

The yield surface defines elastic and plastic stress states and shows the potential for the strain increments. The yield surface is defined analytically by a yield criterion [1]. A yield criterion is used to define the constitutive model of a material to simulate the process in finite element analysis (FEA). Since, variety of engineering applications related with the use of a yield criterion are existing, a suitable yield criterion need to be selected not only to predict the yield attitude of the material, but also to constitute plastic stress-strain relations [2].

For the precision of sheet metal forming process simulations, correct selection of the material constitutive model in FEA is crucially important as the selection of forming conditions (i.e. friction, die, punch, blankholder geometry). The constitutive models (relations) are extremely important in defining the deformation characteristics of the sheet material to obtain correct stress-strain distributions in the formed part [3]. In FEA of a sheet metal forming process, a proper constitutive model should describe different behaviors, like the strain hardening, anisotropic yielding behavior and Bauschinger effect [4].

In literature, various yield criteria were presented to explain the experimental behavior of the material. Among those criteria, the Tresca and von Mises are the oldest yield criteria for isotropic materials [5-8]. In 1948, Hill [9, 10] presented quadratic anisotropic yield criterion. This is the first and the most comprehensive yield criteria in generalizing the von Mises yield criterion although it shows some discrepancies for some materials (like aluminum and its alloys). The published experimental studies in the last four decades indicated that the earlier material models are not describing the material behaviors precisely [11]. In recent decades, numbers of non-quadratic anisotropic yield criteria were introduced [12-21]. However, in most of the anisotropic models the main problem is the requirement of excessive amount of experimentation to find the model coefficients to describe the anisotropic attitude of the material with accuracy. So, if possible, the model to be selected should have minimum number of coefficients to reduce the experimental efforts, the cost of experimentation and computational efforts with a best possible consistency with material deformation behavior [4].

It is evident that there is a strong need of testing number of proposed models to find the ones having the highest possible fit to the experimentally found (actual) material behaviors with the less number of model coefficients.

1.2 Deep (Cup) Drawing Process [22]

In deep drawing a punch pushes the sheet metal downward to force it into the die cavity. Tensile forces are applied to blank to result the plastic deformation of the part. Some

examples of deep drawn parts are cans, cups, automotive bodies, kitchen sinks, fuel tanks, pots, etc. In deep drawing process the blank is a raw sheet metal piece trimmed into the desired shape. The blank is clamped and pressed towards the die by means of a blankholder. Die has a cavity in the external form of the cup to be drawn.

The formability of a sheet depends on the various factors, like the die-punch clearance, lubrication conditions, friction coefficients, blankholder force, punch radius, die radius, mechanical properties of blank material, sheet thickness, final form of the part, etc. Wrinkling and fracturing are the two main failure modes in sheet metal forming. The blankholder force is the main factor to control the wrinkling and to avoid tearing of the blank sheet, if the other sheet metal forming parameters are set correctly. If the blankholder pressure is higher than the required, the sheet could not have drawn easily into the die which causes tearing. On the other hand, if the blankholder pressure is less than the required then wrinkling of the sheet metal is observed. For a good deep drawing process, the recommended blankholder pressure is about 2-3% of the yield strength of the sheet material. Previous research on the tearing and wrinkling failure modes showed the effects of blankholder pressure on forming. The recommendations of blankholder force application schemes to eliminate wrinkling and tearing occurrences were introduced in the previous research studies [23–28].

1.3 Scope of Thesis

The main aim of this study is to compare the numerical results of the recently proposed models of the researchers for various deep drawing processes. The efforts will be spent to choose the models which define the material behavior accurately considering the real (experimental) cases. One of the other aims of the study is to contribute the literature by providing extensive experimental data related to deep drawing process for different cup shapes and material types.

In this thesis, the effect of seven different models on simulation of deep (cup) drawing process for three different cup drawing models (cylindrical cup drawing, square cup drawing and round bottom cup) at three different punch travels will be investigated. Two different types of steels (SS304 stainless steel and DKP6112 steel) with 1 mm thickness were chosen for both the numerical analyses and the experimentation phases of the study. The numerical analyses were performed by using ABAQUS software. The eight parameters BBC2008 model, eight parameters Yld2003 model and Hu2003 model were implemented to ABAQUS software via the user material subroutine (VUMAT). The other models, namely; Hill'48, isotropic hardening, kinematic hardening and combined hardening, were directly used in the ABAQUS software to simulate the cup drawing cases.

1.4 Outline of the Thesis

This thesis is structured as follows. Chapter 2 will give information about the literature survey related to the implementation of models to finite element software for cup drawing processes and the comparison of the simulation results with the experimental findings. In Chapter 3, the finite element method and brief information about the formulation used in this study will be introduced. In the following chapter, Chapter 4, the models formulations used

in this study will be given. Chapter 5 will contain the experimental phase of this study including tension, Erichsen and deep drawing tests as well as the findings about the material constants. In Chapter 6, the results and the discussion of the FEA (thickness strain distribution) of different cup drawing models at different punch travels will be given. The chapter also contains the comparison of the models with the experimental findings of this study for different cup drawing geometries, materials and different punch travels. The closing chapter, Chapter 7, contains the conclusion of the study and suggestions for future work. The Appendix A contains some additional thickness strain distributions of the sheet metals used in this study for various models.

CHAPTER 2

LITERATURE SURVEY

Although, there is a vast amount of information available in the literature about the constitutive models and their implementations to various forming processes, this part of the thesis is dedicated on the research works related to the implementation of constitutive models to cup drawing processes by means of ABAQUS software and the comparison of the simulation results of relevant constitutive models with the experimental findings.

In Vrh et al. work [29], plane-stress orthotropic yield criterion BBC2008 [30] was implemented to ABAQUS/Explicit with VUMAT subroutine to model the deep drawing process. The AA5042-H2 and AA2090-T3 sheet materials were used to test the validity of the model. In the study, NICE scheme was used for the integration of the constitutive model. The 16 parameters and the 8 parameters of the BBC2008 yield criterion were calculated using the normalized yield stress and r values found experimentally from uniaxial and biaxial tension tests. The ear profiles were compared with the experimental findings and the CPB06ex2 [31] model for the AA5042-H2 alloy. The results were found in good agreement with the CPB06ex2 model for the prediction of the ears. The earing profiles were also compared with the experimental findings and the Yld2004-18p [13] model for the AA2090-T3 alloy. The results were also found in good agreement. It was stated that the 16 parameters BBC2008 model was able to predict the formation of more than four ears and their locations.

In Moreira et al. study [32], a plane-stress orthotropic yield criterion of Ferron [33] was implemented to ABAQUS with VUMAT subroutine. Deep drawings of cylindrical cup experiments were performed. Two different materials which are IF steel and thin plate steel were used in the study. Uniaxial tension test was performed to define the material behavior. The predicted earing profiles and strain distribution by means of simulation were compared with the experimental datas, the Hill's quadratic model [36] and the Ferron's model. The results were found close to each other.

The Yld2000-2d model [34] was implemented as a VUMAT subroutine for ABAQUS/Explicit in Guner et al. work [35]. The AA6016-T4 alloy material was used in the analysis of deep drawn car hood geometry. Tensile and equibiaxial tests were performed to find the material parameters. Yield loci and thickness variations were obtained. The comparison of the Yld2000-2d model and the Hill'48 [36] model showed that the Hill'48 model was predicted 12% lower thickness than the actual measurements at the corner regions of the geometry. The Yld2000-2d model prediction was found closer to the measured thicknesses.

In Eggertsen et al. study [37], the Hill'48 [36], the Barlat–Lian Yld89 [19] and the eight parameter criterion BBC2005 [12] were implemented with the Yoshida–Uemori kinematic hardening law [38] in LS-DYNA. In the experimental phase of the study, two DP600 steels,

the DX56 mild steel and the 220IF steel materials were used. The material parameters were obtained from uniaxial and equibiaxial tension tests. The U-bend springback behavior was found in the transverse, rolling and diagonal directions. In the rolling direction, fairly good predictions were obtained for the three yield criteria. An accurate springback prediction was obtained only for the BBC2005 yield criterion for the other directions. In their other work [39], the researchers emphasized the importance of the correct selection of kinematic hardening law and the unloading modulus to get accurate springback predictions.

Homogeneous polynomials with different orders were investigated by Soare et al. [40] as orthotropic plane stress yield criteria. In their work, a set of analytic formulas for the fourth order polynomial and an optimization procedure for the sixth and eight order polynomials were proposed to describe the material coefficients. They suggested a technique for extending the plane stress criteria to full 3D stress states. The yield criteria were implemented into ABAQUS with user subroutines. AA2008-T4, AA2090-T3 and mild steel materials were used in the study. In their work, the square (mild steel) and cylindrical (AA2090-T3) drawings were simulated. For the two cases, very good fit with experimental results was found.

In Laurent et al. study [41], various yield criteria for isotropic and mixed (isotropic + kinematic) hardening were investigated to define the behavior of the AA5754-0 aluminum alloy during a forming process and springback evolution using the split-ring test. The amount of change in the ring's diameter was used as the measure of residual stresses released and springback. Isotropic and kinematic hardening models were combined with the von Mises, Hill'48 [36] and Barlat'91 [42] models. The von Mises yield criteria is directly used in ABAQUS/Standard code with an elasto-plastic approach. The von Mises yield criterion with isotropic and kinematic hardening, Hill'48 yield criterion with isotropic hardening, and Barlat91 (with or without kinematic hardening) models were implemented with ABAQUS subroutine (UMAT). Numerical results show good agreement with the experimental findings. The predicted behavior of the material (thickness distribution) during forming process using von Mises and Hill'48 criteria with kinematic hardening was less accurate than Barlat'91 model. The predicted thickness distribution was little higher than the experimental thickness distribution in the Hill'48 criteria with isotropic hardening and slightly higher than with the two others yield criteria. It is found that if the kinematic hardening is taken into account, the quality of the thickness evolution slightly improves only for Barlat'91 criterion. Simulations using the von Mises model showed fairly good results for the thickness distribution along the rolling direction.

In Aretz study [43], a new plane stress yield criterion with eight anisotropic parameters Yld2003-8p was introduced for orthotropic materials. The yield stresses and r-values were obtained from uniaxial and equibiaxial tensile tests. The test data were used for calculating the anisotropy parameters. The AA2090-T3, AA6111-T4 and low-carbon steel materials were used in the study. The experimentally obtained yield stresses, yield surfaces and r values at rolling direction were compared with the Yld2000-2d [14] and the Yld2003-8p models. The results showed that Yld2003-8p yield criterion is as flexible as the Yld2000-2d yield criterion. The Yld2003-8p has a simpler mathematical form and more efficient than the Yld2000-2d in computational analysis. Yoon and Hong [44] were implemented the Yld2000-

2d and the Yld2004-18p [13] yield criteria to LS-DYNA with user subroutine to test the validity of earing prediction in the cup drawing and automotive stamping analysis. The imaginary material (FM8) was simulated depend on Yld2004-18p model. AA5182-0 aluminum alloy with 1.6 mm thickness was selected for the comparison purpose with the Yld2004-18p and Yld2000-2d models. The yield stresses and r-values obtained from Yld2004-18p and Yld2000-2d were compared with the experimental findings. It was found that two yield criteria coincide exactly and the Yld2000-2d exhibited very good computational efficiency. Later Aretz et al. [11] were proposed a new yield criterion known as Yld2011-18p which is the improved version of the well-known yield criterion Yld2004-18p [13, 45]. In this study, the Yld2011 criterion with 18 parameters and 27 parameters were proposed for orthotropic sheet metals and AA2090-T3 and AA3104-H19 aluminum alloys and AISI409L steel were used as sheet materials. Both yield criteria were implemented to ABAQUS/Explicit and ABAQUS/Standard by means of the user material subroutines VUMAT and UMAT. The purpose of the implementations was to understand the capability of the yield criteria to predict the earing formation in cylindrical cup-drawing. It was emphasized that the Yld2004-18p and the Yld2011-18p models are similar but both yield criteria were predicted different yield surfaces in the isotropic case. It was also stated that, the Yld2011-18p produces a flattened yield surface in the region around equibiaxial tension. On the other hand, the Yld2011-27p predicts a nicely rounded yield surface.

Hu [46] proposed a new anisotropic yield criterion (called as “Hu”). In applications of this criteria, “anomalous behavior” does not exist which based on the improper construction of the yield criteria. Hot dipped galvanized HSLA material was selected for this study. The r - values and yield stresses for angles from rolling to transverse directions were compared for Hosford 1979 [47], Hill’48 [36], Hu yield criteria and experimental data. Very consistent results were found between Hu yield criterion and experimental data. It is clear that this criterion define anisotropic behaviors of stress-strain states accurately under the equibiaxial and uniaxial tensions in the transverse, rolling and diagonal directions.

Xu et al. [48] performed uniaxial tensile tests, hydraulic bulge tests and disk compression tests using AISI409L and AISI430 ferritic stainless steel materials. The yield stresses and r values obtained from uniaxial and biaxial tension tests (hydraulic bulge tests and disk compression tests) were used to calculate the anisotropic model parameters of Hill’48 [36], Karafillis and Boyce 1993 [15], Yld2000-2d [13] and Yld2004-18p [13, 14] yield criteria. The results show that the Yld2004-18p and Yld2000-2d were consistent with the experimental results for the r values and flow stresses. Yet, the Hill’48, Karafillis and Boyce 1993 criteria were not consistent with the experimental findings especially for r values.

A simple constitutive model of plastic deformation was adopted by Soare et al. [49] to study the effect of the initial anisotropy on earing predictions. The performance of the new polynomial implementation of Yld2004 [13] yield criteria was tested in the FEA of the cylindrical cup drawing. The materials used in the study were the AA2090-T3, AA3104-H19 and a theoretical material (RMAT). Some deviations from previous reports are noticed in AA2090-T3 for Yld2004 criterion. The authors stated that if earing prediction is of primary importance, than the extensions of classical uniaxial directional properties to biaxial stress

states should also be done in cup drawing applications. To achieve this goal, the authors extended the Yld2004 criterion to Yld2004B.

Banabic et al [50] derived a new yield criterion for orthotropic sheet metals under plane-stress conditions. The A6XXX-T4 aluminum alloy sheet with 1.0 mm and a cold-rolled steel sheet (Ti-added IF-steel) with 0.8 mm thick were used in the study. The seven material constants of the yield criteria were found by using the error function minimization method. The predicted yield surfaces, uniaxial yield stress and r-coefficient with respect to rolling direction angle were obtained. It is found that the predicted yield surfaces for two materials were consistent with the experimental findings of Kuwabara et al. [1, 51] and the associated flow rule gives the distribution of the Lankford coefficients and uniaxial yield stress very accurately [52, 53].

Mattiaasson et al. [54] introduced a six parameter yield criterion MS6p. Yld2000 [14] and BBC2000 [55] were examined for anisotropic metal sheets. The DC0 mild steel and AA2090-T3 aluminum alloy were used in the study. The Newton–Raphson and the minimization of error function (downhill simplex) method were used to find the material coefficients. The Yld2000, BBC2000, MS6p, and Yld89 [19] material models were implemented with user materials in the LS-DYNA. The BBC2000 and MS6p were coincident, however the Yld89 showed a deviation in the equibiaxial area for the yield loci for the DC06 material. The yield locus predicted by the Yld89 was completely unrealistic and the MS6p was deviated substantially from the BBC2000 due to the strong anisotropy of the AA2090-T3. The main conclusions drawn from the study were; i) the MS6p gives a good fit with materials exhibiting a moderate in-plane anisotropy, ii) the Yld89 gives mostly a poor fit in the equibiaxial area of the yield locus. The authors recommended the use of 8p models of BBC2000 or Yld2000 for materials exhibiting strong anisotropy.

Butuc et al. [56] coupled five hardening models, MicMod [57], the Swift law (isotropic hardening model) [58] with and without kinematic hardening, and the Voce law (isotropic hardening model) [59] with and without kinematic hardening with the Yld2000-2d [14] yield criterion to predict the forming limits for DC06 steel. The localized necking was simulated by using Marciniak-Kuczinsky [60] analysis which assumes an infinite sheet metal containing a region of local imperfection where heterogeneous plastic flow develops and localizes, has become one of the most important tools in predicting the sheet metal formability. It is found that MicMod fit perfectly with the experimental findings for all selected tests and the Swift + kinematic hardening and Voce + kinematic hardening were also able to adequately fit the general level of stress, except for the work-hardening stagnation or softening predictions.

In Wu study [61], a combined isotropic-kinematic hardening rule was proposed. In the study, the Hill'48 quadratic yield criterion [36] was also used for comparison. The proposed model showed good fit with experimental data of the AA6061-O and AA7108-T1 aluminum materials in yield stress and r-ratio aspects of anisotropy. A good agreement between the theoretical findings of this study and other published experimental data [62] was also shown. Wu stated that the present model could be a good tool for analyses of sheet metal forming.

Some of the findings of this work [61] were also introduced and used in the previous works of the author [63, 64].

Dasappa et al. [65] compared five different yield criteria (Hill (1948, 1990, 1993) [66, 17, 18], Barlat and Lian (1989) [19], and CPB06 [67]) to predict the forming limit diagram (FLD) with experimental data. As a sheet material AA5754 aluminum sheet were used. The FLDs were calculated with Marciniak-Kuczinsky [60] approach. Except CPB06, the other yield criteria predicted the behavior in variation of either the yield stress or the r-values. Hill'48 yield criterion, accurately predict the behavior of the limit strains while the Barlat and Lian (1989) under-estimate the strains in the biaxial stretching region. The CPB06 yield criterion provided the most accurate forming and showed resembling behavior with Hill'93.

Hu [2] proposed a hypothesis on an anisotropic yield criterion containing three-yield-system. High strength steels (galvanized and cold rolled) and aluminum alloys (AA2090-T3 [46] AA5182-0 [68] and AA3104-H19 [68]) were used in the study. The Yld96 [21, 69] and Yld2000-2d [14] yield criteria were also compared with the experimental data of the aluminum alloy sheet. The proposed yield criterion showed similar result for the strain ratio and the yield stress with Yld96 and Yld2000-2d in aluminum material property predictions. However, the Hill'48 criterion was only matched with the strain ratio. The proposed criterion exhibited acceptable results in describing the yielding behavior from uniaxial tension to equibiaxial tension.

In Choi work [70], a new hardening model (Rotational-Isotropic-Kinematic (RIK)) which describe the growth of the yield surface (isotropic hardening), its transition (kinematic hardening), and its rotation (anisotropy axes rotation via plastic spin) was proposed. Two types of steel sheets were used in the experimental phase of this study. The isotropic, nonlinear kinematic and RIK hardening models were compared with experimental data of Numisheet'93 benchmark results. The proposed model was good in prediction of earing and stress-strain behavior.

CHAPTER 3

FINITE ELEMENT ANALYSIS

3.1 The Finite Element Method

Finite element method (FEM) is a numerical technique that could be applied to various physical problems. The technique basically consists of assuming the piecewise continuous function for the solution and obtaining the parameters of the functions to reduce the error in the solution [71].

The FEM is used to get close solutions of boundary value problems in engineering. A boundary value problem (sometimes called “field problems”) is a mathematical problem in which one or more dependent variables must satisfy a differential equation everywhere. The field generally represents a physical structure and field variables are the dependent variables of the differential equation. The boundary conditions are the described values of the field variables on the boundaries. The field variables may be displacement, fluid velocity, temperature, heat flux, etc. The finite element software first combines the related algebraic equations in matrix form. Then, it computes the unknown values of the primary field variable(s). The computed values are used by back substitution to compute derived variables, like stresses, forces, temperature, heat flow, etc. [72].

The assumptions of engineering problems that depend on linear approximations can be given as follows:

- The displacements are small enough to be neglected in equilibrium equations.
- The strain is proportional to the stress.
- The loads are independent on displacements.
- The structure supports do not change during loading.

Then, the main features of solution of linear problems are:

- The displacements are proportional to the loads.
- The structure stiffness is independent of the load level.

Actually, the behavior of structures is nonlinear, but divergences from linear response are usually small and can be neglected in engineering problems designed for elastic limits. However, the solution of engineering problems mostly requires the abandonment of linear approximations. Many engineering materials attitude is nonlinear or linear material model cannot be used if stress values are high. In real problems, the loads possibly change their directions, and depend on displacements, and supports may change during loading. So, the structure behaves nonlinearly. If these phenomena are included in a finite element analysis (FEA), the equilibrium equations turn to nonlinear form. The structural nonlinearity types

are; material, geometry and boundary nonlinearities such as contact [73, 74]. The strain-displacement relations are not linear in most of the engineering problems. An example to the geometrical nonlinearity is the large deflection of thin structures. The stress-strain relation of the material may not be linear and may be time-dependent. In addition, the stress-strain relation is nonlinear beyond the yielding which also results in material nonlinearity [74]. Nonlinear elastic, elastoplastic, viscoelastic, viscoplastic material models are some examples for material nonlinearity [73].

3.2 The Finite Element Formulation

In this thesis, finite element analyses of the cylindrical, square and round bottom cup drawings processes were simulated by using a commercial finite element code, ABAQUS/Explicit (version 6.10).

In this study, a nonlinear analysis was used since the deep drawing process shows geometrically and materially nonlinear characteristics. The updated Lagrangian formulation was used implicitly in ABAQUS software [75]. In this study, the elasto-plastic material models, in which the constitutive relations were found using the sum of the elastic and plastic strain increments, were used.

The isotropic hardening, kinematic hardening, combined hardening and Hill'48 models were available in the ABAQUS software. The von Mises yield criterion was used in the isotropic hardening, kinematic hardening and combined hardening models. The other models which are not available in the ABAQUS library were implemented by preparing separate FORTRAN subroutines (VUMAT). In this study, three VUMAT subroutines were prepared to implement BBC2008-8p, Yld2003-8p and Hu2003 models to the ABAQUS. The reasons for selecting these recent models in this study were due to their consistency with the experimental data and requirement of less number of model parameters. Microsoft Visual Studio 2008 and Fortran 11.1 compiler were linked to the ABAQUS software in order to execute the prepared VUMAT subroutines (i.e the models).

3.3 The Finite Element Model

The cylindrical, square and round bottom cup drawing processes were modeled and analyzed with a FEA package (ABAQUS) at three different punch travels and two types of steels (DKP6112 and SS304) considering different constitutive relations.

In all considered models, only the quarter of the cups were modeled and analyzed due to the symmetry of the cups drawn. By this way the computational time of the simulations were reduced significantly. In order to model the blanks, S4R 4 node shell elements with reduced integration control were used. The punch, die and blankholder were defined as rigid parts (bodies) in all cases only, the blank was defined as deformable part in the simulations.

3.3.1 Cylindrical cup drawing

In cylindrical cup drawing analyses, the blank, die, punch and blankholder geometries were modeled as shown in Figure 3.1. There are 720 elements in the quarter cup model shown in Figure 3.2. The sample drawn cups were given in Appendix A.1-A.4.

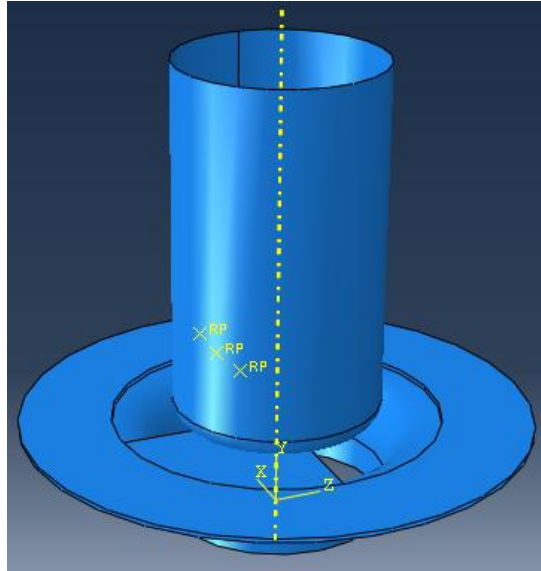


Figure 3.1 The FEM model of cylindrical cup drawing.

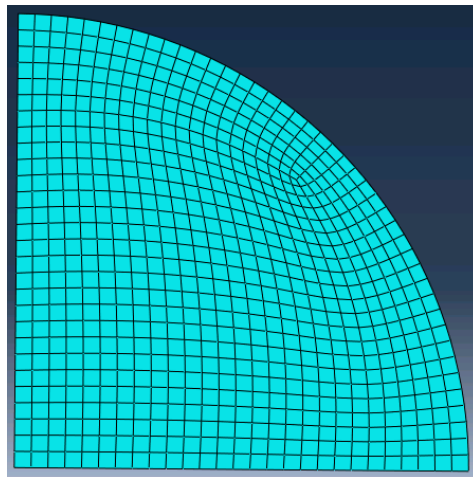


Figure 3.2 Meshing of a quarter circle blank.

3.3.2 Square cup drawing

In square cup drawing analyses, the blankholder, blank, die and punch geometries were modeled as shown in Figure 3.3. There are 400 elements in the quarter cup model shown in Figure 3.4. The sample drawn cups were given in Appendix A.5-A.10.

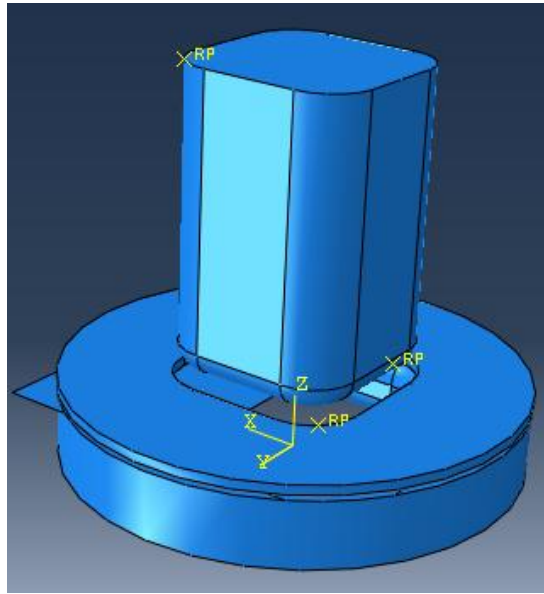


Figure 3.3 The FEM model of square cup drawing.

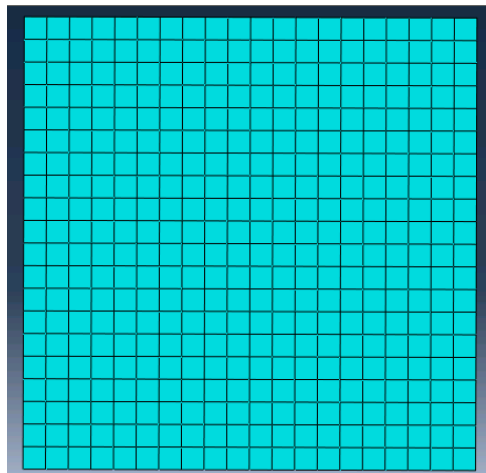


Figure 3.4 Meshing of a quarter square blank.

3.3.3 Round Bottom Cup Drawing

In round bottom cup drawing analyses, the blankholder, blank, die and punch geometries were modeled as shown in Figure 3.5. There are 720 elements in the quarter cup model shown in Figure 3.6. The sample drawn cups were given in Appendix A.11-A.16.

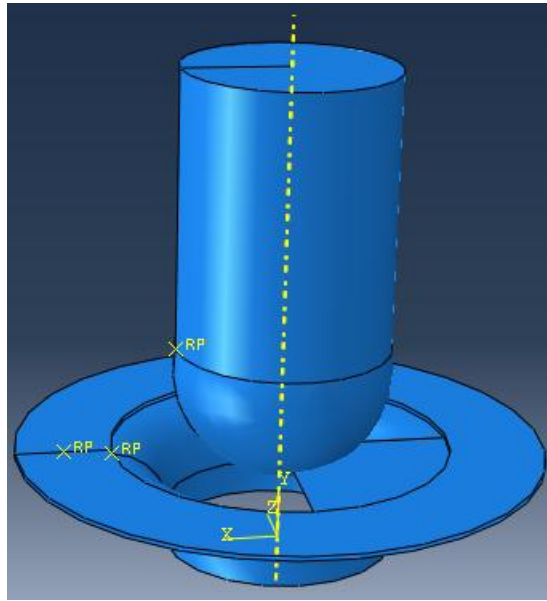


Figure 3.5 The FEM model of round bottom cup drawing.

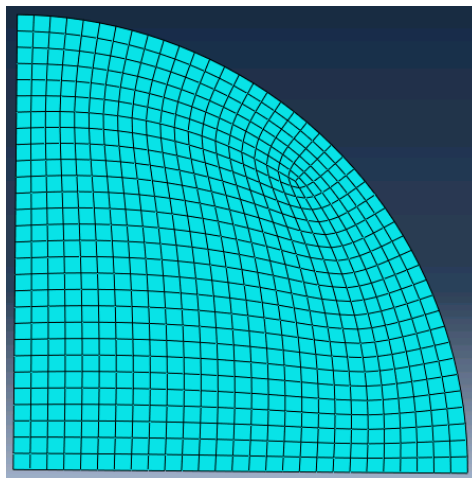


Figure 3.6 Meshing of a quarter circle blank.

CHAPTER 4

CONSTITUTIVE MODELS

In this part of the thesis, the well-known hardening models and yield criteria will be given.

4.1 Isotropic Hardening

The yield function for isotropic hardening is

$$f = F(J_2', J_3') - K(\alpha) = 0 \quad (4.1)$$

where J_2' and J_3' are the second and third invariants of the deviatoric stress tensor. K is a monotonically increasing function of α and α characterizes the isotropic hardening simply the function. $F(J_2', J_3')$ is assumed to be von Mises type. Then

$$f = J_2' - \frac{1}{3}\sigma_y^2(\alpha) = 0 \quad (4.2)$$

where σ_y is the current uniaxial yield strength that increase with α .

The von Mises yield surface in Cartesian coordinates is expressed as[76]

$$\begin{aligned} (\sigma_{22} - \sigma_{33})^2 + (\sigma_{33} - \sigma_{11})^2 + (\sigma_{11} - \sigma_{22})^2 + 6(\sigma_{23}^2 + \sigma_{13}^2 + \sigma_{12}^2) \\ = 2\bar{\sigma}^2 \end{aligned} \quad (4.3)$$

A constitutive model is called as isotropic hardening case if it corresponds to a uniform (isotropic) expansion of the initial yield surface without any translation [77] (Figure 4.1).

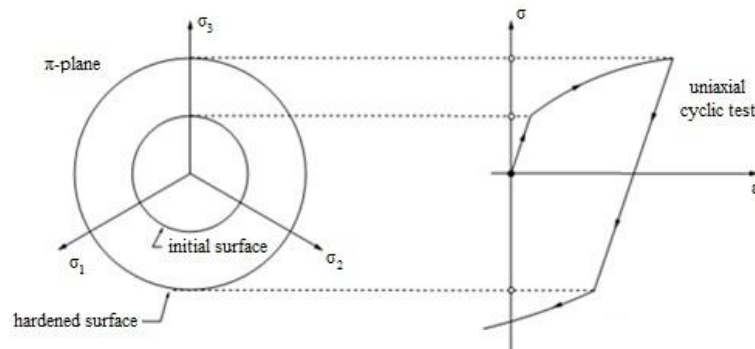


Figure 4.1 π - plane and uniaxial test for isotropic hardening [77].

During plastic flow,

$$df = 0 \quad (4.4)$$

Then,

$$df = \frac{\partial f}{\partial \sigma_{ij}} d\sigma_{ij} - \frac{\partial f}{\partial \bar{\varepsilon}^p} d\bar{\varepsilon}^p = 0 \quad (4.5)$$

Since,

$$\frac{\partial f}{\partial \sigma_{ij}} = \frac{3}{2} \frac{\sigma_{ij}}{\bar{\sigma}} \quad (4.6)$$

This gives,

$$\frac{3}{2} \frac{\sigma_{ij}}{\bar{\sigma}} d\sigma_{ij} - \frac{\partial f}{\partial \bar{\varepsilon}^p} d\bar{\varepsilon}^p = 0 \Rightarrow \bar{\varepsilon}^p = \frac{\frac{3}{2} \frac{\sigma_{ij}}{\bar{\sigma}} d\sigma_{ij}}{\frac{\partial f}{\partial \bar{\varepsilon}^p}} \quad (4.7)$$

The definition of [for instance, Eqn. (4.4)] and the general flow rule

$$d\varepsilon_{ij}^p = d\lambda \frac{\partial f}{\partial \sigma_{ij}} \quad (4.8)$$

also

$$\bar{\varepsilon}^p = \int_0^{\varepsilon_{ij}^p} \frac{d\varepsilon_{ij}^p}{\bar{\varepsilon}^p} = \int_0^{\varepsilon_{ij}^p} \sqrt{\frac{2}{3}} d\varepsilon_{ij}^p \quad (4.9)$$

gives a simple relation between $d\lambda$ and $\bar{\varepsilon}^p$

$$\bar{\varepsilon}^p = \sqrt{\frac{2}{3}} d\lambda \frac{\partial f}{\partial \sigma_{ij}} \frac{\partial f}{\partial \sigma_{ij}} = d\lambda \sqrt{\frac{2}{3} \frac{3}{2} \frac{\sigma_{ij}}{\bar{\sigma}} \frac{3}{2} \frac{\sigma_{ij}}{\bar{\sigma}}} = \sqrt{\frac{3}{2} \frac{\sigma_{ij} \sigma_{ij}}{(\bar{\sigma})^2}} \quad (4.10)$$

which gives the final expression for $d\lambda$

$$d\lambda = \frac{\frac{3}{2} \frac{\sigma_{ij}}{\bar{\sigma}} d\sigma_{ij}}{\frac{\partial f}{\partial \bar{\varepsilon}^p}} \quad (4.11)$$

Combining Eqns. (4.6), (4.8) and (4.11) gives the flow rule

$$d\varepsilon_{ij}^p = \frac{\frac{3}{2} \frac{\sigma_{kl}}{\bar{\sigma}} d\sigma_{kl}}{\frac{\partial f}{\partial \bar{\varepsilon}^p}} \frac{3}{2} \frac{\sigma_{ij}}{\bar{\sigma}} = \frac{9}{4} \frac{\sigma_{kl} d\sigma_{kl}}{\frac{\partial f}{\partial \bar{\varepsilon}^p} (\bar{\sigma})^2} \sigma_{ij} \quad (4.12)$$

The constitutive relations can be determined from above equations.

4.2 Kinematic Hardening

Most of the materials show decreasing resistance to plastic yielding in the opposite direction when they are loaded in one direction which is called as Bauschinger effect [77]. This effect must be included in the model with the introduction of kinematic hardening. Kinematic hardening takes place when the yield surfaces conserve their shape and size while there is a translation in the stress space as a rigid body [3]. Kinematic hardening is described by the translation of its center, expressed with back stress tensor (Figure 4.2).

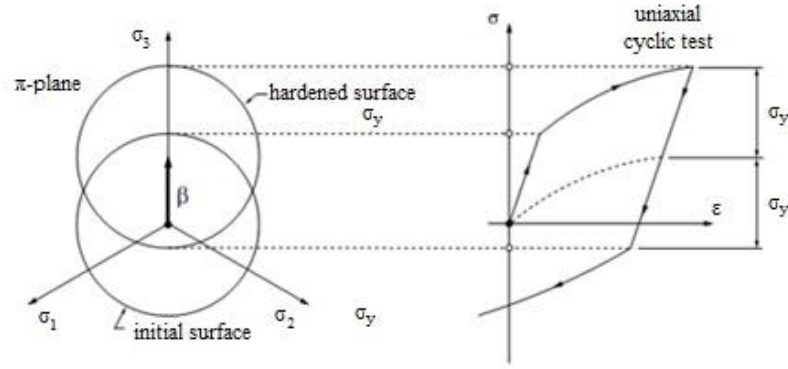


Figure 4.2 π - plane and uniaxial test for kinematic hardening and Bauschinger effect [77].

Bauschinger effect can be expressed as,

$$f = f(\sigma_{ij}, \alpha_{ij}) = \bar{\sigma}(\sigma_{ij} - \alpha_{ij}) - \sigma_s \quad (4.13)$$

where α_{ij} is a 2nd order tensor:

$$\alpha_{ij} = \alpha_{ij}(\epsilon_{kl}^p) \quad (4.14)$$

often called the backstress, and σ_s is the initial yield strength of the original material. Eqn. (4.13) states that after plastic flow, $\bar{\sigma}$ can be found from $\sigma_{ij} - \alpha_{ij}$ instead of σ_{ij} .

To establish the function $\alpha_{ij} = \alpha_{ij}(\epsilon_{kl}^p)$. The two most frequent relations introduced by Prager and Ziegler, respectively are

$$d\alpha_{ij} = c^{(k)} d\epsilon_{ij}^p \quad (\text{Prager}) \quad (4.15)$$

$$d\alpha_{ij} = d\mu(\sigma_{ij} - \alpha_{ij}) \quad (\text{Ziegler}) \quad (4.16)$$

where $c^{(k)}$ is a constant that is characteristic for the material (in analogy with $c^{(i)}$ in the isotropic hardening) and $d\mu = d\mu(d\epsilon_{ij}^p)$ is a function of the increment of plastic strain which is also characteristic for a material. In the von Mises case, the two models are identical.

Since $c^{(k)}$ is a constant, Eqn. (4.15) can be directly integrated to give

$$\alpha_{ij} = c^{(k)} \varepsilon_{ij}^p \quad (4.17)$$

and, further,

$$\alpha_{kk} = c^{(k)} \varepsilon_{kk}^p = 0 \quad (4.18)$$

With the consistency condition $df = 0$,

$$df = \frac{\partial f}{\partial \sigma_{ij}} d\sigma_{ij} + \frac{\partial f}{\partial \alpha_{ij}} \frac{\partial \alpha_{ij}}{\partial \varepsilon_{kl}^p} d\varepsilon_{kl}^p = 0 \quad (4.19)$$

From the using the definition of F given in Eqn. (4.13), we can differentiate to find $\partial f/(\partial \sigma_{ij})$ and $\partial f/(\partial \alpha_{ij})$:

$$\frac{\partial f}{\partial \sigma_{ij}} = \frac{\partial \bar{\sigma}}{\partial (\sigma_{ij} - \alpha_{ij})} \frac{\partial (\sigma_{ij} - \alpha_{ij})}{\partial \sigma_{ij}} = \frac{\partial \bar{\sigma}}{\partial (\sigma_{ij} - \alpha_{ij})} \quad (4.20)$$

$$\frac{\partial f}{\partial \alpha_{ij}} = \frac{\partial \bar{\sigma}}{\partial (\sigma_{ij} - \alpha_{ij})} \frac{\partial (\sigma_{ij} - \alpha_{ij})}{\partial \alpha_{ij}} = -\frac{\partial \bar{\sigma}}{\partial (\sigma_{ij} - \alpha_{ij})} = -\frac{\partial f}{\partial \sigma_{ij}} \quad (4.21)$$

Eqns. (4.19) and (4.21) together with the fundamental normality rule give

$$df = \frac{\partial f}{\partial \sigma_{ij}} d\sigma_{ij} - \frac{\partial f}{\partial \alpha_{ij}} \frac{\partial \alpha_{ij}}{\partial \varepsilon_{kl}^p} d\varepsilon_{kl}^p = \frac{\partial f}{\partial \sigma_{ij}} d\sigma_{ij} - \frac{\partial f}{\partial \sigma_{ij}} \frac{\partial \alpha_{ij}}{\partial \varepsilon_{kl}^p} d\varepsilon_{kl}^p = 0 \quad (4.22)$$

and

$$d\varepsilon_{ij}^p = \frac{\frac{\partial f}{\partial \sigma_{mn}} d\sigma_{mn}}{\frac{\partial f}{\partial \sigma_{ij}} \frac{\partial \alpha_{ij}}{\partial \varepsilon_{kl}^p} \frac{\partial f}{\partial \sigma_{kl}}} \quad (4.23)$$

and, consequently,

$$d\varepsilon_{ij}^p = d\lambda \frac{\partial f}{\partial \sigma_{ij}} = \frac{\frac{\partial f}{\partial \sigma_{mn}} d\sigma_{mn}}{\frac{\partial f}{\partial \sigma_{pq}} \frac{\partial \alpha_{pq}}{\partial \varepsilon_{kl}^p} \frac{\partial f}{\partial \sigma_{kl}}} \frac{\partial f}{\partial \sigma_{ij}} \quad (4.24)$$

Then, the constitutive relations can be determined from above equations.

Although, the above hardening models are useful for predicting the material characteristics, but they are mostly unsuccessful in predicting highly nonlinear materials. However, it is clear from the previous works that some hardening models characterize highly nonlinear materials in a better way. These are the multi-surface hardening models introduced by Mronz [76] and the family of nonlinear kinematic hardening models proposed by Armstrong and Frederick [76]. These models were revised and extended by the other researchers (Chaboche, Geng and Teodoisu [76]).

4.3 Combined Hardening

The materials commonly show the combination of isotropic hardening and kinematic hardening characteristics (Figure 4.3). In combined hardening, the material yield surface both expands and translates at the same time. The combination type hardening (shortly combined hardening) law predicts the springback and failure behaviors better in forming operations. The yield function for combined hardening is,

$$f(\sigma_{ij}, \alpha_{ij}, R) = \bar{\sigma}(\sigma_{ij} - \alpha_{ij}) - |\sigma_{y0} + R(\bar{\epsilon}^p)| = 0 \quad (4.25)$$

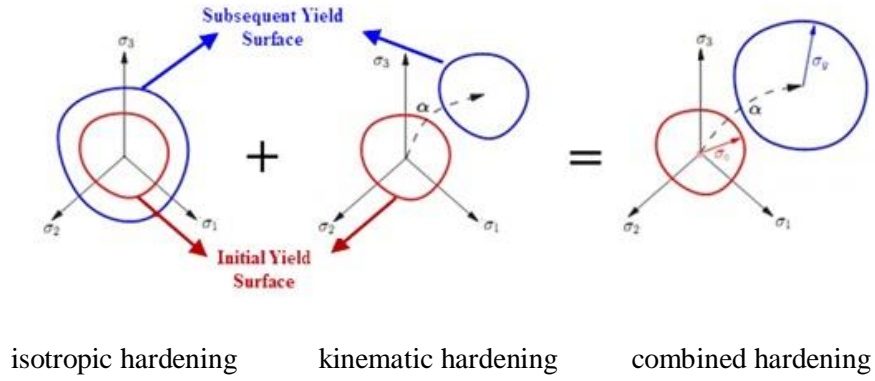


Figure 4.3 Schematic view of combined hardening [3].

For the von Mises yield criterion the combined hardening rule can be expressed as

$$(\sigma_{ij} - \alpha_{ij})(\sigma_{ij} - \alpha_{ij}) = \frac{2}{3} \bar{\sigma}^2 \quad (4.26)$$

The right-hand side of Eqn. (4.26) is the square of the current radius of the displaced yield cylinder.

The associated plastic strain increment $d\epsilon_{ij}^p$ in the kinematic hardening can be expressed as

$$d\epsilon_{ij}^p = d\lambda \frac{\partial f}{\partial \sigma_{ij}} = (\sigma_{ij} - \alpha_{ij}) d\lambda \quad (4.27)$$

By substituting Eqn. (4.27) into Eqn. (4.9) and using Eqn. (4.26)

$$d\lambda = \frac{3d\bar{\epsilon}^p}{2\bar{\sigma}} \quad (4.28)$$

The plastic strain increment therefore becomes

$$d\epsilon_{ij}^p = (\sigma_{ij} - \alpha_{ij}) \frac{3d\bar{\epsilon}^p}{2\bar{\sigma}} = (\sigma_{ij} - \alpha_{ij}) \frac{d\bar{\sigma}}{h\bar{\sigma}} \quad (4.29)$$

Here, the h is a measure of the isotropic part of the rate of hardening. Differentiation of the yield criterion Eqn. (4.26) gives

$$\frac{2}{3}\bar{\sigma}d\bar{\sigma} = (\sigma_{kl} - \alpha_{kl})(d\sigma_{kl} - cd\varepsilon_{kl}^p) \quad (4.30)$$

in view of Eqn. (4.15) and the fact that $d\sigma_{kk} = 0$. Here, c is the anisotropic part. Substituting from Eqn. (4.29) and using Eqn. (4.26), we obtain the relation

$$\left(1 + \frac{c}{h}\right)d\bar{\sigma} = \frac{3}{2\bar{\sigma}}(\sigma_{kl} - \alpha_{kl})d\sigma_{kl} \quad (4.31)$$

The flow rule is defined by Eqn. (4.29) and Eqn. (4.31). The elastic strain increment, which is given by the generalized Hooke's law, may be written as

$$d\varepsilon_{ij}^e = \frac{1}{2G}\left\{d\sigma_{ij} + \frac{1}{3}\left(\frac{1-2\nu}{1+\nu}\right)d\sigma_{kk}\delta_{ij}\right\} \quad (4.32)$$

Here, ν is Poisson's ratio and G is the shear modulus. The scalar product of Eqn. (4.32) and the tensor $\sigma_{ij} - \alpha_{ij}$ and using Eqn. (4.31),

$$(\sigma_{ij} - \alpha_{ij})d\varepsilon_{ij}^e = \left(\frac{c+h}{2G}\right)\bar{\sigma}d\varepsilon^p \quad (4.33)$$

The scalar product of Eqn. (4.29) with the same tensor $\sigma_{ij} - \alpha_{ij}$ gives

$$(\sigma_{ij} - \alpha_{ij})d\varepsilon_{ij}^p = (\sigma_{ij} - \alpha_{ij})(\sigma_{ij} - \alpha_{ij})\frac{3\bar{\sigma}d\varepsilon^p}{2\bar{\sigma}} \quad (4.34)$$

Using Eqn. (4.26),

$$(\sigma_{ij} - \alpha_{ij})d\varepsilon_{ij}^p = \bar{\sigma}d\varepsilon^p \quad (4.35)$$

in view of Eqn. (4.26). Eqns (4.33) and (4.35) are added together to get

$$(\sigma_{ij} - \alpha_{ij})d\varepsilon_{ij} = \left(\frac{1+H}{3G}\right)\bar{\sigma}d\varepsilon^p \quad (4.36)$$

H is the plastic modulus of the current stress state which is expressed as

$$H = \frac{3}{2}(c+h) \quad (4.37)$$

H is the slope of the uniaxial stress–plastic strain curve.

The constitutive relations can be determined from above equations.

4.4 Hill'48 Yield Criterion [36]

Hill [36] proposed an anisotropic yield criterion (f) which is expressed in the quadratic form:

$$2f(\sigma_{ij}) \equiv F(\sigma_{22} - \sigma_{33})^2 + G(\sigma_{33} - \sigma_{11})^2 + H(\sigma_{11} - \sigma_{22})^2 + 2L(\sigma_{23})^2 + 2M(\sigma_{31})^2 + 2N(\sigma_{12})^2 = 1 \quad (4.38)$$

Where F, G, H, L, M and N are the material anisotropy constants. Axis 1 is parallel to the rolling direction, 2 is parallel to the transverse direction and 3 is collinear with the normal direction for sheet metals. If the tensile yield stresses in the principal anisotropy directions are expressed by X, Y and Z,

$$\frac{1}{X^2} = G + H \quad (4.39)$$

$$\frac{1}{Y^2} = H + F \quad (4.40)$$

$$\frac{1}{Z^2} = F + G \quad (4.41)$$

F, G and H terms can also be represented by uniaxial yield stresses:

$$2F = \frac{1}{Y^2} + \frac{1}{Z^2} - \frac{1}{X^2} \quad (4.42)$$

$$2G = \frac{1}{Z^2} + \frac{1}{X^2} - \frac{1}{Y^2} \quad (4.43)$$

$$2H = \frac{1}{X^2} + \frac{1}{Y^2} - \frac{1}{Z^2} \quad (4.44)$$

R, S and T are the shear yield stresses associated to the same directions, then

$$2L = \frac{1}{R^2} \quad (4.45)$$

$$2M = \frac{1}{S^2} \quad (4.46)$$

$$2N = \frac{1}{T^2} \quad (4.47)$$

For plane stress ($\sigma_{33} = \sigma_{31} = \sigma_{23} = 0; \sigma_{11} \neq 0; \sigma_{22} \neq 0; \sigma_{12} \neq 0$), the yield criterion becomes

$$2f(\sigma_{ij}) \equiv \sigma_{11}^2 (G + H) - 2H\sigma_{11}\sigma_{22} + \sigma_{22}^2 (H + F) + 2N(\sigma_{12})^2 = 1 \quad (4.48)$$

r_0, r_{45}, r_{90} are the anisotropy coefficients and $X = \sigma_0, Y = \sigma_{90}$ are the yield stresses in the principal directions. The relations between the r_0, r_{45}, r_{90} and the F, G, H... can be found from the flow rule:

$$r_0 = \frac{H}{G} \quad (4.49)$$

$$r_{45} = \frac{N}{F + G} - \frac{1}{2} \quad (4.50)$$

$$r_{90} = \frac{H}{F} \quad (4.51)$$

The associated flow rule can be expressed as

$$\frac{d\varepsilon_{ij}^p}{d\lambda} = \frac{\partial f}{\partial \sigma_{ij}} \quad (4.52)$$

This implies that

$$\frac{d\varepsilon_{11}^p}{d\lambda} = H(\sigma_{11} - \sigma_{22}) + G(\sigma_{11} - \sigma_{33}) \quad (4.53)$$

$$\frac{d\varepsilon_{22}^p}{d\lambda} = F(\sigma_{22} - \sigma_{33}) + H(\sigma_{22} - \sigma_{11}) \quad (4.54)$$

$$\frac{d\varepsilon_3^p}{d\lambda} = G(\sigma_{33} - \sigma_{11}) + F(\sigma_{33} - \sigma_{22}) \quad (4.55)$$

Hill proposed that equivalent stress should be defined as

$$\bar{\sigma} = \sqrt{\frac{3}{2} \left(\frac{F(\sigma_{22} - \sigma_{33})^2 + G(\sigma_{33} - \sigma_{11})^2 + H(\sigma_{11} - \sigma_{22})^2 + 2L(\sigma_{23})^2 + 2M(\sigma_{31})^2 + 2N(\sigma_{12})^2}{F + G + H} \right)} \quad (4.56)$$

Using Eqn. (4.38) and Euler's theorem on homogeneous functions, plastic potential function

$$dw = \sigma_{ij} \frac{\partial f}{\partial \sigma_{ij}} d\lambda = fd\lambda = d\lambda \quad (4.57)$$

From Eqns. (4.53-4.55),

$$Gd\varepsilon_{22} - Hd\varepsilon_{33} = (FG + GH + HF)(\sigma_{22} - \sigma_{33})d\lambda \quad (4.58)$$

$$Hd\varepsilon_{33} - Fd\varepsilon_{11} = (FG + GH + HF)(\sigma_{33} - \sigma_{11})d\lambda \quad (4.59)$$

$$Fd\varepsilon_{11} - Gd\varepsilon_{22} = (FG + GH + HF)(\sigma_{11} - \sigma_{33})d\lambda \quad (4.60)$$

The generalized strain increment $d\bar{\varepsilon}$ can therefore be defined from $dw = \bar{\sigma}d\bar{\varepsilon}$ as

$$d\bar{\varepsilon} = \frac{d\lambda}{\bar{\sigma}} = \sqrt{\frac{2}{3} [F + G + H]} \sqrt{\left[F \left(\frac{Gd\varepsilon_{22} - Hd\varepsilon_{33}}{(FG + GH + HF)} \right)^2 + \dots \frac{2d\varepsilon_{23}^2}{L} \right]} \quad (4.61)$$

For a sheet material subjected to plane stress, with rotational symmetry about z axis,

$$r = \frac{H}{G} = \frac{H}{F} \quad (4.62)$$

Eqn. (4.56) and (4.61) reduce to,

$$\bar{\sigma} = \sqrt{\frac{3}{2} \left[\frac{\sigma_{11}^2 + \sigma_{22}^2 + r(\sigma_{11} - \sigma_{22})^2}{2 + r} \right]} \quad (4.63)$$

$$d\bar{\varepsilon} = \sqrt{\frac{2}{3} \left[\frac{2 + r}{(1 + 2r)^2} \{ (d\varepsilon_{22} - rd\varepsilon_{33})^2 + (d\varepsilon_{11} - rd\varepsilon_{33})^2 + r(d\varepsilon_{11} - d\varepsilon_{22})^2 \} \right]} \quad (4.64)$$

The constitutive relations can be determined from above equations.

4.5 Aretz 8 coefficients Yield Criterion (Yld2003-8p) [43]

Aretz [43] proposed a plane stress yield function, which contains eight anisotropy parameters, as shown below.

$$|\sigma'_1|^m + |\sigma'_2|^m + |\sigma''_1 - \sigma''_2|^m = 2Y_{\text{ref}}^m \quad (4.65)$$

with the generalized principal stress transformations

$$\sigma'_1 = \frac{a_8\sigma_{11} + a_1\sigma_{22}}{2} + \sqrt{\left(\frac{a_2\sigma_{11} - a_3\sigma_{22}}{2}\right)^2 + (a_4)\sigma_{12}\sigma_{21}} \quad (4.66.a)$$

$$\sigma'_2 = \frac{a_8\sigma_{11} + a_1\sigma_{22}}{2} - \sqrt{\left(\frac{a_2\sigma_{11} - a_3\sigma_{22}}{2}\right)^2 + (a_4)\sigma_{12}\sigma_{21}} \quad (4.66.b)$$

$$\sigma''_1 = \frac{\sigma_{11} + \sigma_{22}}{2} + \sqrt{\left(\frac{a_5\sigma_{11} - a_6\sigma_{22}}{2}\right)^2 + (a_7)\sigma_{12}\sigma_{21}} \quad (4.67.a)$$

$$\sigma''_2 = \frac{\sigma_{11} + \sigma_{22}}{2} - \sqrt{\left(\frac{a_5\sigma_{11} - a_6\sigma_{22}}{2}\right)^2 + (a_7)\sigma_{12}\sigma_{21}} \quad (4.67.b)$$

The anisotropy parameters a_1, \dots, a_8 that are given in Eqns. (4.66) and (4.67) can be used to fit the yield criterion to selected experimental data obtained from mechanical tests or calculated from polycrystalline models. Y_{ref} is a reference yield stress of the considered material. m is a material constant depends on the material crystal structure. The yield function f corresponding to Eqn. (4.66) is given by

$$f(a_i, \sigma) = \bar{\sigma}(a_i, \sigma) - Y_{\text{ref}} \leq 0 \quad (4.68)$$

with the equivalent stress

$$\bar{\sigma}(a_i, \sigma) = \left\{ \frac{1}{2} (|\sigma'_1|^m + |\sigma'_2|^m + |\sigma''_1 - \sigma''_2|^m) \right\}^{1/m} \quad (4.69)$$

and σ'_1 , σ'_2 , σ''_1 , σ''_2 are defined by Eqns. (4.66) and (4.67).

For BCC crystal structure m is 6 and for FCC crystal structure m is 8. In the case of the von Mises yield criterion, for plane stress case $a_1 = \dots = a_8 = 1$ and $m = 2$.

Three directional yield stresses obtained from uniaxial tensile tests at specimens having an orientation of 0° , 45° and 90° (Y_0 , Y_{45} , Y_{90}) and three r -values corresponding to (r_0 , r_{45} , r_{90}), one equibiaxial yield stress (Y_b) and one equibiaxial r -value (r_b) obtained from a cross tensile test or a bulge test are required to obtain the material parameters. This makes 8 experimental data points which are proposed to calibrate the Yld2003 parameters a_i , $i = 1, \dots, 8$.

For the adjustment of the anisotropy parameters the Y_0 , Y_{45} , Y_{90} , Y_b , r_0 , r_{45} , r_{90} , r_b experimental data must be found. Commonly, $Y_{\text{ref}} = Y_0$ is used in sheet forming. But, Y_{ref} can also identified with any other yield stress of the considered material. The stress components in a tensile test specimen with orientation angle ϕ with respect to the original rolling direction and subjected to uniaxial loading are given as

$$\sigma_{11} = Y_\phi \cos^2 \phi \quad (4.70)$$

$$\sigma_{22} = Y_\phi \sin^2 \phi \quad (4.71)$$

$$\sigma_{12} = \sigma_{21} = Y_\phi \cos \phi \sin \phi \quad (4.72)$$

Y_ϕ is the yield stress of the tensile test specimen under uniaxial load. This gives three stress tensors σ_0 , σ_{45} and σ_{90} related to the orientation angle $\phi \in \{0, 45, 90\}$, respectively. For an equibiaxial tensile test (cross tensile test or bulge test) the stress tensor components are given by $\sigma_{11} = \sigma_{22} = Y_b$, $\sigma_{12} = \sigma_{21} = 0$.

A directional r -value, r_ϕ , can be expressed as

$$r_\phi = - \left. \frac{\sin^2 \phi \left(\frac{\partial f}{\partial \sigma_{11}} \right) - \sin 2\phi \left(\frac{\partial f}{\partial \sigma_{12}} \right) + \cos^2 \phi \left(\frac{\partial f}{\partial \sigma_{22}} \right)}{\left(\frac{\partial f}{\partial \sigma_{11}} \right) + \left(\frac{\partial f}{\partial \sigma_{22}} \right)} \right|_{\sigma_\phi} \quad (4.73)$$

with $\phi \in \{0, 45, 90\}$. The equibiaxial r -value, r_b follows from

$$r_b = \frac{\left(\frac{\partial f}{\partial \sigma_{22}} \right)}{\left(\frac{\partial f}{\partial \sigma_{11}} \right)} \quad (4.74)$$

Finally, the following equations can be obtained:

$$\bar{\sigma}(\sigma_0, a_1, \dots, a_8) - Y_{\text{ref}} = 0 \quad (4.75)$$

$$\bar{\sigma}(\sigma_{45}, a_1, \dots, a_8) - Y_{\text{ref}} = 0 \quad (4.76)$$

$$\bar{\sigma}(\sigma_{90}, a_1, \dots, a_8) - Y_{\text{ref}} = 0 \quad (4.77)$$

$$\bar{\sigma}(\sigma_b, a_1, \dots, a_8) - Y_{\text{ref}} = 0 \quad (4.78)$$

$$r_0(\sigma_0, a_1, \dots, a_8) - r_0^{\text{exp}} = 0 \quad (4.79)$$

$$r_{45}(\sigma_{45}, a_1, \dots, a_8) - r_{45}^{\text{exp}} = 0 \quad (4.80)$$

$$r_{90}(\sigma_{90}, a_1, \dots, a_8) - r_{90}^{\text{exp}} = 0 \quad (4.81)$$

$$r_b(\sigma_b, a_1, \dots, a_8) - r_b^{\text{exp}} = 0 \quad (4.82)$$

r^{exp} expresses the experimentally found r-values where r are calculated from above formulas.

The increment associated flow rule can be expressed as,

$$\Delta \varepsilon_{ij}^p = \Delta \lambda \frac{\partial f}{\partial \sigma_{ij}} \quad (4.83)$$

From Eqn (4.68) yield function can be rewritten in the following form

$$f = \frac{\bar{\sigma}^m}{Y_{\text{ref}}^m} - 1 = \frac{\hat{\sigma}}{Y_{\text{ref}}^m} - 1 \quad (4.84)$$

where

$$\hat{\sigma} = \left\{ \frac{1}{2} (|\sigma'_1|^m + |\sigma'_2|^m + |\sigma'_1 - \sigma'_2|^m) \right\} \quad (4.85)$$

here

$$\frac{\partial f}{\partial \sigma_{ij}} = \frac{\partial f}{\partial \hat{\sigma}} \left[\frac{\partial \hat{\sigma}}{\partial \sigma'_1} \frac{\partial \sigma'_1}{\partial \sigma_{ij}} + \frac{\partial \hat{\sigma}}{\partial \sigma'_2} \frac{\partial \sigma'_2}{\partial \sigma_{ij}} + \frac{\partial \hat{\sigma}}{\partial \sigma''_1} \frac{\partial \sigma''_1}{\partial \sigma_{ij}} + \frac{\partial \hat{\sigma}}{\partial \sigma''_2} \frac{\partial \sigma''_2}{\partial \sigma_{ij}} \right] \quad (4.86)$$

here

$$\frac{\partial f}{\partial \hat{\sigma}} = \frac{1}{Y_{\text{ref}}^m} \quad (4.87)$$

$$\frac{\partial f}{\partial Y} = -m \frac{\hat{\sigma}}{Y_{\text{ref}}^{m+1}} \quad (4.88)$$

$$\frac{\partial \acute{\sigma}}{\partial \sigma'_1} = \frac{1}{2} m |\sigma'_1|^{m-1} a \begin{cases} \sigma'_1 > 0 \Rightarrow a = 1 \\ \sigma'_1 < 0 \Rightarrow a = -1 \end{cases} \quad (4.89)$$

$$\frac{\partial \acute{\sigma}}{\partial \sigma'_2} = \frac{1}{2} m |\sigma'_2|^{m-1} b \begin{cases} \sigma'_2 > 0 \Rightarrow b = 1 \\ \sigma'_2 < 0 \Rightarrow b = -1 \end{cases} \quad (4.90)$$

$$\frac{\partial \acute{\sigma}}{\partial \sigma''_1} = \frac{1}{2} m |\sigma''_1 - \sigma''_2|^{m-1} \quad (4.91)$$

$$\frac{\partial \acute{\sigma}}{\partial \sigma''_2} = -\frac{1}{2} m |\sigma''_1 - \sigma''_2|^{m-1} \quad (4.92)$$

$$\begin{aligned} \frac{\partial \sigma'_1}{\partial \sigma_{11}} &= \frac{1}{2} a_8 + \frac{1}{2} \left[\left(\frac{a_2 \sigma_{11} - a_3 \sigma_{22}}{2} \right)^2 \right. \\ &\quad \left. + (a_4^2) \sigma_{12}^2 \right]^{-1/2} \left(\frac{a_2^2 \sigma_{11} - a_2 a_3 \sigma_{22}}{2} \right) \end{aligned} \quad (4.93)$$

$$\begin{aligned} \frac{\partial \sigma'_1}{\partial \sigma_{22}} &= \frac{1}{2} a_1 + \frac{1}{2} \left[\left(\frac{a_2 \sigma_{11} - a_3 \sigma_{22}}{2} \right)^2 \right. \\ &\quad \left. + (a_4^2) \sigma_{12}^2 \right]^{-1/2} \left(\frac{a_3^2 \sigma_{11} - a_2 a_3 \sigma_{11}}{2} \right) \end{aligned} \quad (4.94)$$

$$\frac{\partial \sigma'_1}{\partial \sigma_{12}} = \frac{1}{2} \left[\left(\frac{a_2 \sigma_{11} - a_3 \sigma_{22}}{2} \right)^2 + (a_4^2) \sigma_{12}^2 \right]^{-1/2} (2 \sigma_{12} a_4^2) \quad (4.95)$$

$$\begin{aligned} \frac{\partial \sigma'_2}{\partial \sigma_{11}} &= \frac{1}{2} a_8 - \frac{1}{2} \left[\left(\frac{a_2 \sigma_{11} - a_3 \sigma_{22}}{2} \right)^2 \right. \\ &\quad \left. + (a_4^2) \sigma_{12}^2 \right]^{-1/2} \left(\frac{a_2^2 \sigma_{11} - a_2 a_3 \sigma_{22}}{2} \right) \end{aligned} \quad (4.96)$$

$$\begin{aligned} \frac{\partial \sigma'_2}{\partial \sigma_{22}} &= \frac{1}{2} a_1 - \frac{1}{2} \left[\left(\frac{a_2 \sigma_{11} - a_3 \sigma_{22}}{2} \right)^2 \right. \\ &\quad \left. + (a_4^2) \sigma_{12}^2 \right]^{-1/2} \left(\frac{a_3^2 \sigma_{11} - a_2 a_3 \sigma_{11}}{2} \right) \end{aligned} \quad (4.97)$$

$$\frac{\partial \sigma'_2}{\partial \sigma_{12}} = -\frac{1}{2} \left[\left(\frac{a_2 \sigma_{11} - a_3 \sigma_{22}}{2} \right)^2 + (a_4^2) \sigma_{12}^2 \right]^{-1/2} (2 \sigma_{12} a_4^2) \quad (4.98)$$

$$\frac{\partial \sigma''_1}{\partial \sigma_{11}} = \frac{1}{2} + \frac{1}{2} \left[\left(\frac{a_5 \sigma_{11} - a_6 \sigma_{22}}{2} \right)^2 + (a_7^2) \sigma_{12}^2 \right]^{-1/2} \left(\frac{a_5^2 \sigma_{11} - a_5 a_6 \sigma_{22}}{2} \right) \quad (4.99)$$

$$\frac{\partial \sigma''_1}{\partial \sigma_{22}} = \frac{1}{2} + \frac{1}{2} \left[\left(\frac{a_5 \sigma_{11} - a_6 \sigma_{22}}{2} \right)^2 + (a_7^2) \sigma_{12}^2 \right]^{-1/2} \left(\frac{a_5^2 \sigma_{22} - a_5 a_6 \sigma_{11}}{2} \right) \quad (4.100)$$

$$\frac{\partial \sigma_1''}{\partial \sigma_{12}} = \frac{1}{2} \left[\left(\frac{a_5 \sigma_{11} - a_6 \sigma_{22}}{2} \right)^2 + (a_7^2) \sigma_{12}^2 \right]^{-1/2} (2\sigma_{12} a_7^2) \quad (4.101)$$

$$\frac{\partial \sigma_2''}{\partial \sigma_{11}} = \frac{1}{2} - \frac{1}{2} \left[\left(\frac{a_5 \sigma_{11} - a_6 \sigma_{22}}{2} \right)^2 + (a_7^2) \sigma_{12}^2 \right]^{-1/2} \left(\frac{a_5^2 \sigma_{11} - a_5 a_6 \sigma_{22}}{2} \right) \quad (4.102)$$

$$\frac{\partial \sigma_2''}{\partial \sigma_{22}} = \frac{1}{2} - \frac{1}{2} \left[\left(\frac{a_5 \sigma_{11} - a_6 \sigma_{22}}{2} \right)^2 + (a_7^2) \sigma_{12}^2 \right]^{-1/2} \left(\frac{a_5^2 \sigma_{22} - a_5 a_6 \sigma_{11}}{2} \right) \quad (4.103)$$

$$\frac{\partial \sigma_2''}{\partial \sigma_{12}} = -\frac{1}{2} \left[\left(\frac{a_5 \sigma_{11} - a_6 \sigma_{22}}{2} \right)^2 + (a_7^2) \sigma_{12}^2 \right]^{-1/2} (2\sigma_{12} a_7^2) \quad (4.104)$$

The increment plastic multiplier can be found from consistency condition,

$$\Delta \lambda = \frac{f + \frac{df}{d\sigma_{ij}} C_{ijkl} \Delta \varepsilon_{kl}}{\frac{df}{d\sigma_{ij}} C_{ijkl} \frac{df}{d\sigma_{kl}} - \frac{df}{dY} \frac{dY}{d\varepsilon_{eq}^p} \frac{\sigma_{kl}}{Y} \frac{df}{d\sigma_{kl}}} \quad (4.105)$$

The constitutive relations can be determined from above equations. The following error function is minimized to calculate the anisotropy parameters:

$$\begin{aligned} \varepsilon(a_1, \dots, a_8) = & \left(\frac{\bar{\sigma}_b - Y_{ref}}{Y_{ref}} \right)^2 + \sum_{i=1}^3 \left(\frac{\bar{\sigma}_{\phi_i} - Y_{ref}}{Y_{ref}} \right)^2 + \left(\frac{r_b - r_b^{exp}}{r_b^{exp}} \right)^2 \\ & + \sum_{i=1}^3 \left(\frac{r_{\phi_i} - r_{\phi_i}^{exp}}{r_{\phi_i}^{exp}} \right)^2 = \min \end{aligned} \quad (4.106)$$

where $\{\phi_1, \phi_2, \phi_3\} = \{0, 45, 90\}$.

4.6 Hu Yield Criterion (2003) [46]

The loading functions proposed by Hu [46] can be expressed as

$$f_1(\sigma_{ij}) = A_1 \sigma_{11}^2 + B_1 \sigma_{22}^2 + C_1 \sigma_{11} \sigma_{22} + D_1 \sigma_{12}^2 = 1 \quad (4.107.a)$$

$$f_2(\sigma_{ij}) = A_2 \sigma_{11}^2 + B_2 \sigma_{22}^2 + C_2 \sigma_{11} \sigma_{22} + D_2 \sigma_{12}^2 = 1 \quad (4.107.b)$$

where $f_1(\sigma_{ij})$ and $f_2(\sigma_{ij})$ are the loading functions with respect to the slip plane. A_1, B_1, C_1, D_1 and A_2, B_2, C_2, D_2 are the constants related to the slip planes orientation.

The loading function should satisfy both yielding properties in 1 and 2 directions, which is expressed as

$$\begin{aligned}
f(\sigma_{ij}) &= f_1(\sigma_{ij})f_2(\sigma_{ij}) \\
&= (A_1\sigma_{11}^2 + B_1\sigma_{22}^2 + C_1\sigma_{11}\sigma_{22} + D_1\sigma_{12}^2)(A_2\sigma_{11}^2 + B_2\sigma_{22}^2 \\
&\quad + C_2\sigma_{11}\sigma_{22} + D_2\sigma_{12}^2) = 1
\end{aligned} \tag{4.108}$$

Evolution of Eqn. (4.108),

$$\begin{aligned}
A_1A_2\sigma_{11}^4 + (A_1C_2 + A_2C_1)\sigma_{11}^3\sigma_{22} + (A_1B_2 + A_2B_1 + C_1C_2)\sigma_{11}^2\sigma_{22}^2 \\
+ (B_1C_2 + B_2C_1)\sigma_{11}\sigma_{22}^3 + B_1B_2\sigma_{22}^4 \\
+ [(A_1D_2 + A_2D_1)\sigma_{11}^2 + (B_1D_2 + B_2D_1)\sigma_{22}^2 \\
+ (C_1D_2 + C_2D_1)\sigma_{11}\sigma_{22}]\sigma_{12}^2 + D_1D_2\sigma_{12}^4 = 1
\end{aligned} \tag{4.109}$$

where 1 and 2 axes are the transverse and rolling directions. If experimental data with respect to the transverse, rolling and diagonal directions used to define the anisotropic properties of sheet metals, the parameters in the first five items of Eqn. (4.109) are related to the associated experimental data in the rolling and transverse directions. Then,

$$A_1A_2 = \frac{1}{\sigma_0^4} \tag{4.110.a}$$

$$A_1C_2 + A_2C_1 = -\frac{4R_0}{(1 + R_0)\sigma_0^4} \tag{4.110.b}$$

$$A_1B_2 + A_2B_1 + C_1C_2 = \frac{1}{\sigma_b^4} - \frac{1}{\sigma_0^4} - \frac{1}{\sigma_{90}^4} + \frac{4R_0}{(1 + R_0)\sigma_0^4} + \frac{4R_{90}}{(1 + R_{90})\sigma_{90}^4} \tag{4.110.c}$$

$$B_1C_2 + B_2C_1 = -\frac{4R_{90}}{(1 + R_{90})\sigma_{90}^4} \tag{4.110.d}$$

$$B_1B_2 = \frac{1}{\sigma_{90}^4} \tag{4.110.e}$$

The constants of the last two terms in Eqn. (4.108) include the experimental findings in the diagonal. Then, a relation can be obtain with respect to the sixth item in Eqn. (4.108) as

$$\begin{aligned}
(A_1D_2 + A_2D_1)\sigma_{11}^2 + (B_1D_2 + B_2D_1)\sigma_{22}^2 + (C_1D_2 + C_2D_1)\sigma_{11}\sigma_{22} \\
= \Omega(\sigma_{11}^2 + \sigma_{22}^2 - \sigma_{11}\sigma_{22})
\end{aligned} \tag{4.111}$$

Depend on the related experiments in the diagonal directions,

$$A_1D_2 + A_2D_1 + B_1D_2 + B_2D_1 + C_1D_2 + C_2D_1 = \Omega = \frac{16}{(1 + R_{45})\sigma_{45}^4} - \frac{2}{\sigma_b^4} \tag{4.112.a}$$

$$D_1D_2 = \frac{1}{\sigma_b^4} + \frac{16R_{45}}{(1 + R_{45})\sigma_{45}^4} \tag{4.112.b}$$

Thus, Eqn. (4.108) can be rewritten as

$$\begin{aligned}
f(\sigma_{ij}) = & \frac{1}{\sigma_0^4} \sigma_{11}^4 - \frac{4R_0}{(1+R_0)\sigma_0^4} \sigma_{11}^3 \sigma_{22} \\
& + \left[\frac{1}{\sigma_b^4} - \frac{1}{\sigma_0^4} - \frac{1}{\sigma_{90}^4} + \frac{4R_{90}}{(1+R_{90})\sigma_{90}^4} + \frac{4R_0}{(1+R_0)\sigma_0^4} \right] \sigma_{11}^2 \sigma_{22}^2 \\
& - \frac{4R_{90}}{(1+R_{90})\sigma_{90}^4} \sigma_{11} \sigma_{22}^3 + \frac{1}{\sigma_{90}^4} \sigma_{22}^4 \\
& + \left[\frac{16}{(1+R_{45})\sigma_{45}^4} - \frac{2}{\sigma_b^4} \right] (\sigma_{11}^2 + \sigma_{22}^2 - \sigma_{11} \sigma_{22}) \sigma_{12}^2 \\
& + \left[\frac{1}{\sigma_b^4} + \frac{16R_{45}}{(1+R_{45})\sigma_{45}^4} \right] \sigma_{12}^4 = 1
\end{aligned} \tag{4.113}$$

Eqn. (4.113) is a general form of anisotropic yield criterion for sheet metal forming. After some mathematical manipulations the yield criterion is written as,

$$\begin{aligned}
f(\sigma_i) = & \frac{1}{\sigma_0^4} \sigma_1^4 - \frac{4R_0}{(1+R_0)\sigma_0^4} \sigma_1^3 \sigma_2 \\
& + \left[\frac{1}{\sigma_b^4} - \frac{1}{\sigma_0^4} - \frac{1}{\sigma_{90}^4} + \frac{4R_{90}}{(1+R_{90})\sigma_{90}^4} + \frac{4R_0}{(1+R_0)\sigma_0^4} \right] \sigma_1^2 \sigma_2^2 \\
& - \frac{4R_{90}}{(1+R_{90})\sigma_{90}^4} \sigma_1 \sigma_2^3 + \frac{1}{\sigma_{90}^4} \sigma_2^4 = 1
\end{aligned} \tag{4.114}$$

The increment associated flow rule can be expressed as,

$$\Delta \varepsilon_{ij}^p = \Delta \lambda \frac{\partial f}{\partial \sigma_{ij}} \tag{4.115}$$

From Eqn. (4.113)

$$\begin{aligned}
\frac{\partial f}{\partial \sigma_{11}} = & \frac{1}{Y} \left(\frac{4}{\sigma_0^4} \sigma_1^3 - \frac{12R_0}{(1+R_0)\sigma_0^4} \sigma_1^2 \sigma_2 \right. \\
& + 2 \left[\frac{1}{\sigma_b^4} - \frac{1}{\sigma_0^4} - \frac{1}{\sigma_{90}^4} + \frac{4R_{90}}{(1+R_{90})\sigma_{90}^4} + \frac{4R_0}{(1+R_0)\sigma_0^4} \right] \sigma_1 \sigma_2^2 \\
& - \frac{4R_{90}}{(1+R_{90})\sigma_{90}^4} \sigma_2^3 \\
& \left. + \left[\frac{16}{(1+R_{45})\sigma_{45}^4} - \frac{2}{\sigma_b^4} \right] (2\sigma_1 - \sigma_2) \sigma_{12}^2 \right)
\end{aligned} \tag{4.116}$$

$$\begin{aligned}
\frac{\partial f}{\partial \sigma_{22}} = \frac{1}{Y} & \left(-\frac{4R_0}{(1+R_0)\sigma_0^4} \sigma_1^3 \right. \\
& + 2 \left[\frac{1}{\sigma_b^4} - \frac{1}{\sigma_0^4} - \frac{1}{\sigma_{90}^4} + \frac{4R_{90}}{(1+R_{90})\sigma_{90}^4} + \frac{4R_0}{(1+R_0)\sigma_0^4} \right] \sigma_2 \sigma_1^2 \\
& - \frac{12R_{90}}{(1+R_{90})\sigma_{90}^4} \sigma_1 \sigma_2^2 + \frac{4}{\sigma_{90}^4} \sigma_2^3 \\
& \left. + \left[\frac{16}{(1+R_{45})\sigma_{45}^4} - \frac{2}{\sigma_b^4} \right] (2\sigma_2 - \sigma_1) \sigma_{12}^2 \right)
\end{aligned} \tag{4.117}$$

$$\begin{aligned}
\frac{\partial f}{\partial \sigma_{12}} = \frac{1}{Y} & \left(2 \left[\frac{16}{(1+R_{45})\sigma_{45}^4} - \frac{2}{\sigma_b^4} \right] (\sigma_1^2 + \sigma_2^2 - \sigma_1 \sigma_2) \sigma_{12} \right. \\
& \left. + 4 \left[\frac{1}{\sigma_b^4} + \frac{16R_{45}}{(1+R_{45})\sigma_{45}^4} \right] \sigma_{12}^3 \right)
\end{aligned} \tag{4.118}$$

where Y is the yield stress of the material.

The increment plastic multiplier can be found from consistency condition,

$$\Delta \lambda = \frac{f + \frac{df}{d\sigma_{ij}} C_{ijkl} \Delta \varepsilon_{kl}}{\frac{df}{d\sigma_{ij}} C_{ijkl} \frac{df}{d\sigma_{kl}} - \frac{df}{dY} \frac{dY}{d\varepsilon_{eq}^p} \frac{\sigma_{kl}}{Y} \frac{df}{d\sigma_{kl}}} \tag{4.119}$$

The constitutive relations can be determined from above equations.

4.7 BBC2008 Yield Criterion [30]

The BBC2008 yield criterion [30] is a plane-stress criterion developed to describe the plastic behavior of highly orthotropic sheet metals. The yield surface defined by this model results from the implicit equation

$$f(\sigma_{11}, \sigma_{22}, \sigma_{12}, Y) = \bar{\sigma}(\sigma_{11}, \sigma_{22}, \sigma_{12}) - Y = 0 \tag{4.120}$$

where $\bar{\sigma}(\sigma_{11}, \sigma_{22}, \sigma_{12} = \sigma_{21})$ is the equivalent stress (see below) $Y > 0$ is the yield stress, while σ_{11} , σ_{22} and $\sigma_{12} = \sigma_{21}$ are planar components of the stress tensor expressed in an orthonormal basis superimposed to the local axes of plastic orthotropy. One assumes that the third unit vector of the local basis is always perpendicular to the mid-surface of the sheet metal.

In the particular case of the BBC2008 yield criterion, the equivalent stress is defined as follows:

$$\frac{\bar{\sigma}^{2k}}{w-1} = \sum_{r=1}^s \left\{ w^{r-1} \left\{ [L^{(r)} + M^{(r)}]^{2k} + [L^{(r)} - M^{(r)}]^{2k} \right\} \right. \\ \left. + w^{s-r} \left\{ [M^{(r)} + N^{(r)}]^{2k} + [M^{(r)} - N^{(r)}]^{2k} \right\} \right\} \quad (4.121)$$

$$L^{(r)} = \ell_1^{(r)} \sigma_{11} + \ell_2^{(r)} \sigma_{22} \quad (4.122)$$

$$M^{(r)} = \sqrt{\left[m_1^{(r)} \sigma_{11} - m_2^{(r)} \sigma_{22} \right]^2 + \left[m_3^{(r)} (\sigma_{12} + \sigma_{21}) \right]^2} \quad (4.123)$$

$$N^{(r)} = \sqrt{\left[n_1^{(r)} \sigma_{11} - n_2^{(r)} \sigma_{22} \right]^2 + \left[n_3^{(r)} (\sigma_{12} + \sigma_{21}) \right]^2} \quad (4.124)$$

$$w = \left(\frac{3}{2}\right)^{1/s} > 1 \quad (4.125)$$

k , $\ell_1^{(r)}$, $\ell_2^{(r)}$, $m_1^{(r)}$, $m_2^{(r)}$, $m_3^{(r)}$, $n_1^{(r)}$, $n_2^{(r)}$ and $n_3^{(r)}$ ($r = 1, \dots, s$) are the material parameters. It is clear that the equivalent stress given in Eqns. (4.120-4.125) reduces to the isotropic formulation proposed by Barlat and Richmond [78] if $\ell_1^{(r)} = \ell_2^{(r)} = m_1^{(r)} = m_2^{(r)} = m_3^{(r)} = n_1^{(r)} = n_2^{(r)} = \frac{1}{2}$, $r = 1, \dots, s$.

Under these circumstances, the value of the integer exponent k may be adopted according to the crystallographic structure of the sheet metal, as in Barlat and Richmond's model [78]; $k = 3$ for BCC alloys, and $k = 4$ for FCC alloys.

The other material parameters involved in Eqn. (4.120-4.125) are evaluated upon a corresponding identification procedure. Their number is $n_p = 8s$, where s is the summation limit. Let n_e be the number of experimental values describing the plastic anisotropy of the sheet metal. If $n_e \geq 8$, the summation limit s must be chosen according to the constraint $s \leq n_e/8$. When $n_e < 8$, the minimum value $s = 1$ must be adopted. In this case, the identification constraints obtained from experiments should be accompanied by at least $8 - n_e$ artificial conditions involving the material parameters. For example, if $n_e = 6$, one may enforce $m_1^{(r)} = n_1^{(r)}$ and $m_2^{(r)} = n_2^{(r)}$.

Comsa and Banabic [30] developed a numerical method depend on the minimization of an error-function operating only with normalized yield stresses and r -coefficients found from uniaxial and biaxial tension tests.

If Y_θ is the yield stress predicted by the yield criterion by the angle θ from rolling direction, then the planar components of the stress tensor are

$$\sigma_{11}|_\theta = Y_\theta \cos^2 \theta \quad (4.126)$$

$$\sigma_{22}|_\theta = Y_\theta \sin^2 \theta \quad (4.127)$$

$$\sigma_{12}|_{\theta} = \sigma_{21}|_{\theta} = Y_{\theta} \sin \theta \cos \theta \quad (4.128)$$

After replacing them in Eqns. (4.120-4.125), associated equivalent stress was obtained

$$\bar{\sigma}|_{\theta} = Y_{\theta} F_{\theta} \quad (4.129)$$

where F_{θ} is defined by the relationships

$$\begin{aligned} \frac{F_{\theta}^{2k}}{w-1} = \sum_{i=1}^s \left\{ w^{i-1} \left\{ [L_{\theta}^{(i)} + M_{\theta}^{(i)}]^{2k} + [L_{\theta}^{(i)} - M_{\theta}^{(i)}]^{2k} \right\} \right. \\ \left. + w^{s-i} \left\{ [M_{\theta}^{(i)} + N_{\theta}^{(i)}]^{2k} + [M_{\theta}^{(i)} - N_{\theta}^{(i)}]^{2k} \right\} \right\} \end{aligned} \quad (4.130)$$

$$L_{\theta}^{(i)} = \ell_1^{(i)} \cos^2 \theta + \ell_2^{(i)} \sin^2 \theta \quad (4.131)$$

$$M_{\theta}^{(i)} = \sqrt{[m_1^{(i)} \cos^2 \theta - m_2^{(i)} \sin^2 \theta]^2 + [m_3^{(i)} \sin 2\theta]^2} \quad (4.132)$$

$$N_{\theta}^{(i)} = \sqrt{[n_1^{(i)} \cos^2 \theta - n_2^{(i)} \sin^2 \theta]^2 + [n_3^{(i)} \sin 2\theta]^2} \quad (4.133)$$

Eqns. 4.120 and 4.127 lead to the following

$$y_{\theta} = \frac{Y_{\theta}}{Y} = \frac{1}{F_{\theta}} \quad (4.134)$$

After some simple mathematical manipulations r-coefficients become,

$$r_{\theta} = \frac{F_{\theta}}{G_{\theta}} - 1 \quad (4.135)$$

where G_{θ} is defined by the relationships

$$\begin{aligned} \frac{F_{\theta}^{2k-1} G_{\theta}}{w-1} = \sum_{i=1}^s \left\{ w^{i-1} [\hat{L}_{\theta}^{(i)} + \hat{M}_{\theta}^{(i)}] [L_{\theta}^{(i)} + M_{\theta}^{(i)}]^{2k-1} \right. \\ + w^{i-1} [\hat{L}_{\theta}^{(i)} - \hat{M}_{\theta}^{(i)}] [L_{\theta}^{(i)} - M_{\theta}^{(i)}]^{2k-1} \\ + w^{s-i} [\hat{M}_{\theta}^{(i)} + \hat{N}_{\theta}^{(i)}] [M_{\theta}^{(i)} + N_{\theta}^{(i)}]^{2k-1} \\ \left. + w^{s-i} [\hat{M}_{\theta}^{(i)} - \hat{N}_{\theta}^{(i)}] [M_{\theta}^{(i)} - N_{\theta}^{(i)}]^{2k-1} \right\} \end{aligned} \quad (4.136)$$

$$\hat{L}_{\theta}^{(i)} = \ell_1^{(i)} + \ell_2^{(i)} \quad (4.137)$$

$$\hat{M}_{\theta}^{(i)} = [m_1^{(i)} - m_2^{(i)}] [m_1^{(i)} \cos^2 \theta - m_2^{(i)} \sin^2 \theta] / M_{\theta}^{(i)} \quad (4.138)$$

$$\hat{N}_{\theta}^{(i)} = [n_1^{(i)} - n_2^{(i)}] [n_1^{(i)} \cos^2 \theta - n_2^{(i)} \sin^2 \theta] / N_{\theta}^{(i)} \quad (4.139)$$

together with Eqn (4.130-4.133). Denoting the yield stress predicted by Y_b along rolling and transverse direction, the corresponding planar components of the stress tensor are

$$\sigma_{11}|_b = Y_b, \sigma_{22}|_b = Y_b, \sigma_{12}|_b = \sigma_{21}|_b = 0 \quad (4.140)$$

Substituting them in Eqn. (4.120), the associated equivalent stress

$$\bar{\sigma}|_b = Y_b F_b \quad (4.141)$$

where F_b is defined by the relationships

$$\begin{aligned} \frac{F_b^{2k}}{w-1} = \sum_{i=1}^s \left\{ w^{i-1} \left\{ [L_b^{(i)} + M_b^{(i)}]^{2k} + [L_b^{(i)} - M_b^{(i)}]^{2k} \right\} \right. \\ \left. + w^{s-i} \left\{ [M_b^{(i)} + N_b^{(i)}]^{2k} + [M_b^{(i)} - N_b^{(i)}]^{2k} \right\} \right\} \end{aligned} \quad (4.142)$$

$$L_b^{(i)} = \ell_1^{(i)} + \ell_2^{(i)} \quad (4.143)$$

$$M_b^{(i)} = m_1^{(i)} + m_2^{(i)} \quad (4.144)$$

$$N_b^{(i)} = n_1^{(i)} + n_2^{(i)} \quad (4.145)$$

Eqn (4.120) and (4.141) give the normalized biaxial yield stress

$$y_b = \frac{Y_b}{Y} = \frac{1}{F_b} \quad (4.146)$$

After some simple mathematical manipulations r_b become,

$$r_b = \frac{F_b}{G_b} - 1 \quad (4.147)$$

where G_b is defined by the relationships

$$\begin{aligned} \frac{F_b^{2k-1} G_b}{w-1} = \sum_{i=1}^s \left\{ w^{i-1} [\hat{L}_b^{(i)} + \hat{M}_b^{(i)}] [L_b^{(i)} + M_b^{(i)}]^{2k-1} \right. \\ + w^{i-1} [\hat{L}_b^{(i)} - \hat{M}_b^{(i)}] [L_b^{(i)} - M_b^{(i)}]^{2k-1} \\ + w^{s-i} [\hat{M}_b^{(i)} + \hat{N}_b^{(i)}] [M_b^{(i)} + N_b^{(i)}]^{2k-1} \\ \left. + w^{s-i} [\hat{M}_b^{(i)} - \hat{N}_b^{(i)}] [M_b^{(i)} - N_b^{(i)}]^{2k-1} \right\} \end{aligned} \quad (4.148)$$

$$\hat{L}_b^{(i)} = \ell_1^{(i)} \quad (4.149)$$

$$\widehat{M}_b^{(i)} = m_1^{(i)} \quad (4.150)$$

$$\widehat{N}_b^{(i)} = n_1^{(i)} \quad (4.151)$$

together with Eqn. (4.142-4.145). The increment associated flow rule is

$$\Delta \varepsilon_{ij}^p = \Delta \lambda \frac{\partial f}{\partial \sigma_{ij}} \quad (4.152)$$

Yield function can be rewritten in the following form (Eqn. 4.120) (for eight parameter of BBC2008 yield criterion $r = 1$)

$$f = \frac{\bar{\sigma}^{2k}(\sigma_{ij})}{Y^{2k}} - 1 = \frac{\dot{\sigma}(\sigma_{ij})}{Y^{2k}} - 1 = 0 \quad (4.153)$$

$$\frac{\partial f}{\partial \sigma_{ij}} = \frac{\partial f}{\partial \dot{\sigma}} \sum_{r=1}^s \left[\frac{\partial \dot{\sigma}}{\partial L^{(r)}} \frac{\partial L^{(r)}}{\partial \sigma_{ij}} + \frac{\partial \dot{\sigma}}{\partial M^{(r)}} \frac{\partial M^{(r)}}{\partial \sigma_{ij}} + \frac{\partial \dot{\sigma}}{\partial N^{(r)}} \frac{\partial N^{(r)}}{\partial \sigma_{ij}} \right] \quad (4.154)$$

$$\frac{\partial f}{\partial \dot{\sigma}} = \frac{1}{Y^{2k}} \quad (4.155)$$

$$\frac{\partial \dot{\sigma}}{\partial L^{(r)}} = 2k(w-1)w^{r-1} \left[(L^{(r)} + M^{(r)})^{2k-1} + (L^{(r)} - M^{(r)})^{2k-1} \right] \quad (4.156)$$

$$\frac{\partial \dot{\sigma}}{\partial N^{(r)}} = 2k(w-1)w^{s-r} \left[(M^{(r)} + N^{(r)})^{2k-1} - (M^{(r)} - N^{(r)})^{2k-1} \right] \quad (4.157)$$

$$\begin{aligned} \frac{\partial \dot{\sigma}}{\partial M^{(r)}} = 2k(w-1) & \left[w^{r-1} \left[(L^{(r)} + M^{(r)})^{2k-1} - (L^{(r)} - M^{(r)})^{2k-1} \right] \right. \\ & \left. + w^{s-r} \left[(M^{(r)} + N^{(r)})^{2k-1} - (M^{(r)} - N^{(r)})^{2k-1} \right] \right] \end{aligned} \quad (4.158)$$

$$\frac{\partial L^{(r)}}{\partial \sigma} = \{ \ell_1^{(r)}, \ell_2^{(r)}, -(\ell_1^{(r)} + \ell_2^{(r)}), 0 \} \quad (4.159)$$

$$\frac{\partial M^{(r)}}{\partial \sigma} = \frac{1}{M^{(r)}} \{ \widehat{M}^{(r)} m_1^{(r)}, -\widehat{M}^{(r)} m_2^{(r)}, \widehat{M}^{(r)} (m_2^{(r)} - m_1^{(r)}), m_3^{(r)} 2\sigma_{12} \} \quad (4.160)$$

$$\frac{\partial N^{(r)}}{\partial \sigma} = \frac{1}{N^{(r)}} \{ \widehat{N}^{(r)} n_1^{(r)}, -\widehat{N}^{(r)} n_2^{(r)}, \widehat{N}^{(r)} (n_2^{(r)} - n_1^{(r)}), n_3^{(r)} 2\sigma_{12} \} \quad (4.161)$$

$$\widehat{M}^{(r)} = m_1^{(r)} \sigma_{11} - m_2^{(r)} \sigma_{22} \quad (4.162)$$

$$\widehat{N}^{(r)} = n_1^{(r)} \sigma_{11} - n_2^{(r)} \sigma_{22} \quad (4.163)$$

The increment plastic multiplier can be found from consistency condition,

$$\Delta\lambda = \frac{f + \frac{df}{d\sigma_{ij}} C_{ijkl} \Delta\varepsilon_{kl}}{\frac{df}{d\sigma_{ij}} C_{ijkl} \frac{df}{d\sigma_{kl}} - \frac{df}{dY} \frac{dY}{d\varepsilon_{eq}^p} \frac{\sigma_{kl}}{Y} \frac{df}{d\sigma_{kl}}} \quad (4.164)$$

The constitutive relations can be determined from above equations. The following error function is minimized to calculate the anisotropy parameters:

$$\begin{aligned} \varepsilon \left(\ell_1^{(i)}, \ell_2^{(i)}, m_1^{(i)}, m_2^{(i)}, m_3^{(i)}, n_1^{(i)}, n_2^{(i)}, n_3^{(i)} \mid i = 1, \dots, s \right) \\ = \sum_{\theta_j} \left[\frac{y_{\theta_j}^{\text{exp}}}{y_{\theta_j}} - 1 \right]^2 + \sum_{\theta_j} \left[r_{\theta_j}^{\text{exp}} - r_{\theta_j} \right]^2 + \left[\frac{y_b^{\text{exp}}}{y_b} - 1 \right]^2 \\ + \left[r_b^{\text{exp}} - r_b \right]^2 = \min \end{aligned} \quad (4.165)$$

where θ_j defines the orientation of the specimens used in the uniaxial tensile tests.

The flow chart given in Figure 4.4 was given originally in the reference [29] for BBC2008 model. Since it is a general flow chart, it can also be used for the other models.

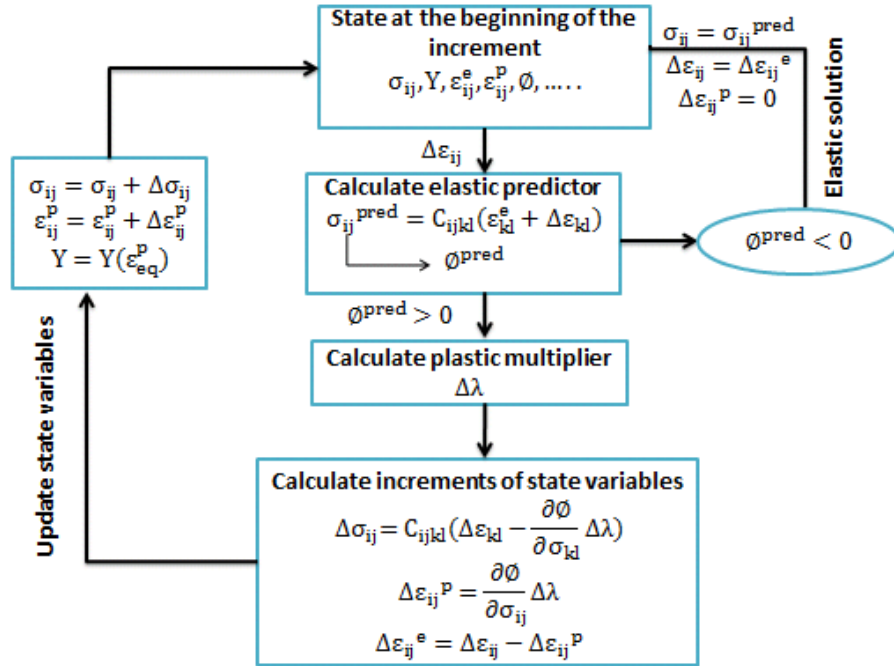


Figure 4.4. Flow chart of the BBC2008 model [29].

CHAPTER 5

EXPERIMENTAL STUDIES

5.1 Tension Test

The normal anisotropy (r) for a test specimen shown in Figure 5.1 is,

$$r = \frac{\text{width strain}}{\text{thickness strain}} = \frac{\epsilon_w}{\epsilon_t} \quad (5.1)$$

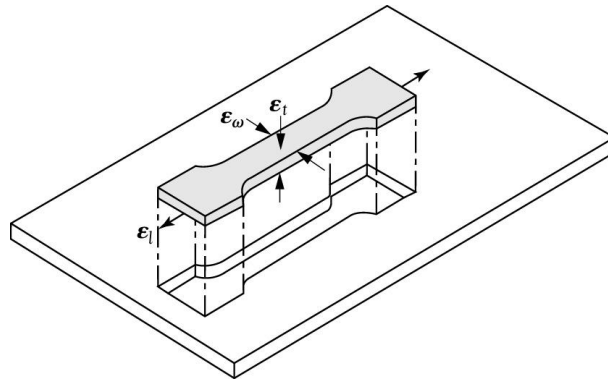


Figure 5.1 Strains on a tensile specimen.

and the average anisotropy (r_m) is,

$$r_m = \frac{r_0 + 2r_{45} + r_{90}}{4} \quad (5.2)$$

The planar anisotropy (Δr) is

$$\Delta r = \frac{r_0 - 2r_{45} + r_{90}}{2} \quad (5.3)$$

Here, r_0 , r_{45} and r_{90} are the r values obtained from tensile specimens extracted at 0° , 45° and 90° with respect to rolling direction of the sheet material. The planar anisotropy determines whether earing will occur. If $\Delta r = 0$ then no ears will form. It is also known that ear height increases with Δr . Although, the low Δr and high r_m are desirable in sheet metal drawing processes, this case is not hold commonly since both values are tend to increase together.

Tension tests were performed by using Zwick/Roel Z020 19.62 kN tensile testing machine (Figure 5.2) in the Solid Mechanics Laboratory of Mechanical Engineering (ME) Department at Middle East Technical University (METU) to obtain the mechanical behavior of sheet metals used in the study. Specimens used in tension tests (Figure 5.3) were prepared according to ASTM E517 standard. The dimensions for both SS304 and DKP6112 tensile

test specimen were given in Figure 5.4. The SS304 stainless steel (1mm thickness) and DKP6112 steel (1mm thickness)) specimens were cut by using laser cutting machine. The tests were repeated three times for the reliability of the results. The SS304 and DKP6112 steel specimens were cut from 0°, 45°, 90° directions with respect to rolling direction of the sheet material to find the yield stress and anisotropy coefficients in the rolling, diagonal and transverse direction ($\sigma_0, \sigma_{45}, \sigma_{90}, r_0, r_{45}, r_{90}$) of the materials.



Figure 5.2 Zwick/Roel Z020 tension test machine.



Figure 5.3 The SS304 specimens.

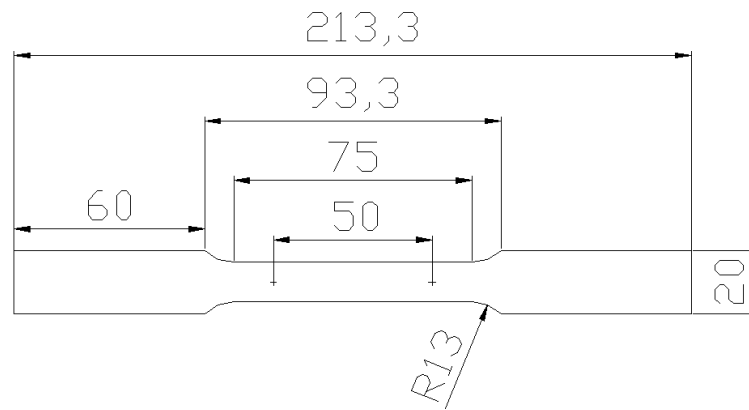


Figure 5.4 Tensile test specimens dimensions.

As shown in Figure 5.5, the elongations of SS304 specimens for 0°, 45°, 90° directions were different due to the existence of anisotropy of the material. The highest and the lowest elongations were observed in the rolling (0°) and in the transverse (90°) directions, respectively. On the other hand, for DKP6112 specimens, the highest and the lowest elongations were observed in the rolling (0°) and in the diagonal (45°) directions, respectively.

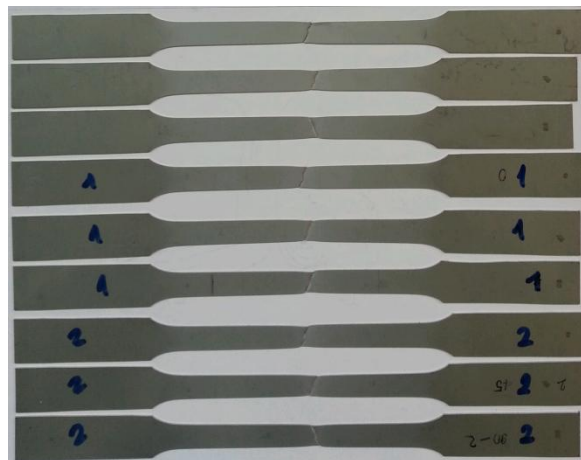


Figure 5.5 The SS304 specimens after tensile testing.

The SS304 stainless steel sheet used in this study is annealed by the manufacturer to reduce the anisotropic characteristic and to improve the homogeneity of the material. The experimentally found Elastic Modulus (E), Poisson's ratio (ν) and mechanical properties and true stress-strain behaviors of the two materials are given in Tables 5.1, 5.2 and Figures 5.6, 5.7, respectively.

Table 5.1 Elastic Modulus, Poisson's ratio of SS304 and DKP 6112 steels.

Material	E [MPa]	ν
SS304	194000	0.22
DKP 6112	141394	0.32

Table 5.2 Mechanical properties of SS304 and DKP 6112 steels. (K: strength coefficient, n: strain hardening exponent, r: Lankford coefficient)

Mechanical Properties						
	SS304	DKP 6112	SS304	DKP 6112	SS304	DKP 6112
	0°		45°		90°	
σ_y [MPa]	339	245	325	258	342	238
σ_{UTS} [MPa]	675	349	657	364	706	342
K [MPa]	1325	571	1261	578	1367	545
n	0.31	0.16	0.32	0.15	0.33	0.16
r	0.72	1.34	1.19	0.99	0.33	0.16

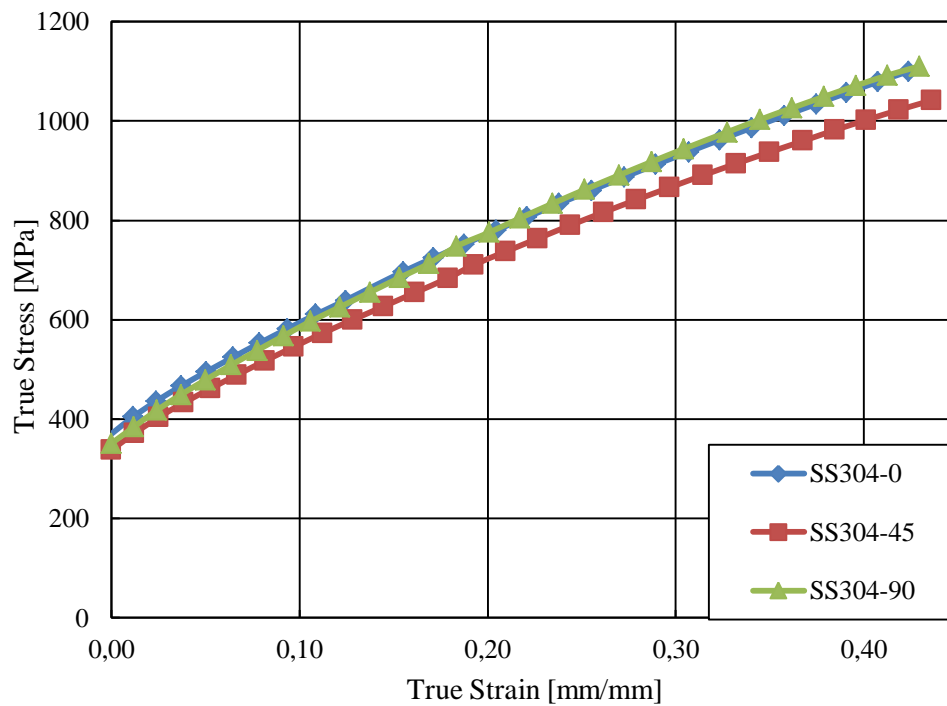


Figure 5.6 True stress-strain behaviors of SS304 material.

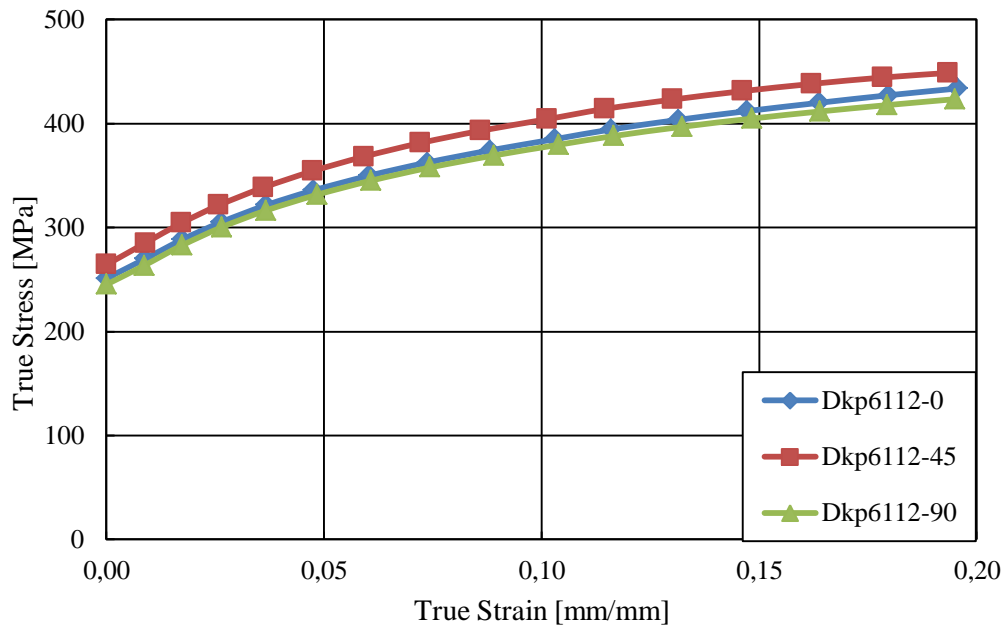


Figure 5.7 True stress-strain behaviors of DKP6112 material.

The SS304 steel showed almost the same true stress-strain characteristics for 0° and 90° specimens. The 45° specimen gave slightly lower true stress values than the 0° and 90° specimens. The DKP6112 steel showed nearly the same true stress-strain characteristics for 0° and 90° specimens. The 45° specimen gave slightly higher true stress values than the two other specimens. True stress-strain behaviors of SS304 steel indicate higher strain hardenability characteristics compared to DKP6112 steel. This fact is also evident from the calculated n values given in Table 5.2.

5.2 Erichsen Test

The Erichsen tests were conducted to obtain equibiaxial yield stress (σ_b) and r-values (r_b) of the SS304 and DKP6112 sheet materials. In the test, the blank was fixed (by means of a blankholder) on the die (Figure 5.8). The test was performed by pressing spherical punch until the first crack appears on the sheet metal. Later, the major and minor strains were measured using the deformed circle patterns with Grid Pattern Analyzer (GPA-100). The major and minor strains were used in calculation of r_b . The tests were also repeated at 10, 14, 18 and 22 mm punch travels for SS304 steel and 6, 8, 10, 12 and 14 mm punch travels for DKP6112 steel.

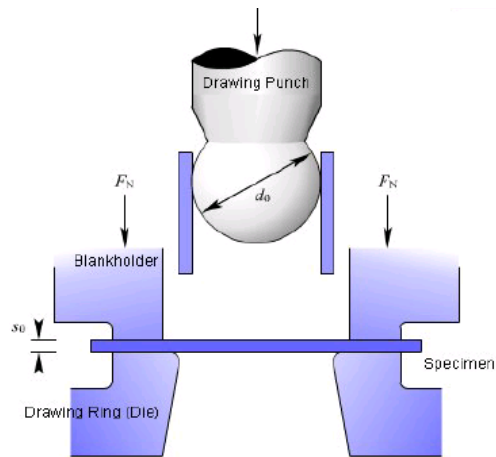


Figure 5.8 Erichsen test setup.

For SS304 and DKP6112 steels the cracks appeared at 24 mm and 16 mm punch travels, respectively. 10, 14, 18, 22 and 24 mm drawn (punch travel) SS304 steel cups are shown in Figure 5.9. The cup on the right side of the figure is cracked at 24 mm punch travel. The equibiaxial yield stresses and r-values are given in Table 5.3.



Figure 5.9 10, 14, 18, 22 and 24 mm drawn SS304 steel cups.

Table 5.3 The Equibiaxial yield stresses (σ_b) and r-values (r_b) of SS304 and DKP6112 steels.

	SS304	DKP6112
σ_b [MPa]	354	281
r_b	0.60	0.76

5.3 Deep Drawing Tests

Deep drawing tests were conducted by using Tinius-Olsen deep drawing testing machine (Figure 5.10) located in Plasticity and Metal Forming Laboratory of ME Department at METU. Cylindrical, square and round bottom cup forms were selected in simulation and experimental phases of this study since the die-punch sets of these geometries were available in the laboratory. The DKP6112 steel and SS304 stainless steel materials both with 1 mm thickness were used in the tests. Grease was applied on blank, die and punch surfaces to reduce the friction between them. Also, a nylon sheet was placed between the sheet and the die surface to reduce the coefficient of friction as well as to prevent the removal of laser markings on the blank during the test. In this study, the blankholder forces used in different types of cup drawing geometries, materials and different punch travels were decided by using the results of preliminary deep drawing experiments and ABAQUS cup drawing simulations which do not result in wrinkles and tearings.



Figure 5.10 Tinius-Olsen deep drawing machine.

5.3.1 Cylindrical Cup Drawing

Dimensions of the blank, die and punch were as follows:

Blank diameter	:	110 mm
Punch diameter	:	50 mm
Die diameter	:	115 mm
Die opening diameter	:	53 mm
Die shoulder diameter	:	13.5 mm

In the tests, 400 and 600 N blankholder forces at 20 mm punch travel, 400, 600, 700 and 900 N blankholder forces at 35 mm punch travel and 400, 600, 700 and 900 N blankholder forces

at 45 mm punch travel were used for SS304 steel blanks. A 500 N blankholder force at 15 and 25 mm punch travels and a 600 N blankholder force at 35 mm punch travel were used for DKP6112 steel blanks. The friction coefficients in between die-blank and punch-blank sets were both taken as 0.06 in accordance with the preliminary ABAQUS simulations.

As clearly seen in Figure 5.11, four earing peaks were placed at 45°, 135°, 225° and 315° angles with respect to the rolling direction due to the anisotropy of the SS304 steel. For DKP6112 steel, four earing valleys were seen at 45°, 135°, 225° and 315° angles. For SS304 material, the earing formations were less evident than the DKP6112 steel. This is attributed to the highly homogenous inner structure of the SS304 steel material which would lead slight anisotropic characteristics than the DKP6112 steel. It is also found that the earing formations were observed especially after 35 mm depth of punch travel for SS304 steel and after 25 mm for DKP6112 steel.



Figure 5.11 20, 35, 45 mm drawn SS304 steel cylindrical cups.

5.3.2 Square Cup Drawing

Dimensions of the blank, die and punch were as follows:

Blank dimensions	:	80 x 80 mm
Punch dimensions	:	40 x 40 mm
Punch radius	:	10 mm
Punch corner radius	:	4.50 mm
Die opening	:	42 x 42 mm
Die shoulder radius	:	4.50 mm

In the tests, a 900 N blankholder force was applied at 15, 20 and 25 mm punch travels for SS304 blanks. A 500 N blankholder force at 15 mm punch travel and a 600 N blankholder force at 20 and 25 mm punch travels were used for DKP6112 steel blanks. The friction coefficients in between die-blank and punch-blank sets were both taken as 0.06 in accordance with the preliminary ABAQUS simulations.

The SS304 steel cups drawn at 15, 20, 25 mm punch travels were shown in Figure 5.12. The variations in rim geometries with increasing punch travels were evident for both SS304 and DKP6112 steels.



Figure 5.12 15, 20, 25 mm drawn SS304 steel square cups.

5.3.3 Round Bottom Cup Drawing

Dimensions of the blank, die and punch were as follows:

Blank diameter	: 110 mm
Punch diameter	: 50 mm
Die diameter	: 115 mm
Die opening diameter	: 53 mm
Die shoulder diameter	: 13.5 mm

In the tests, a 1400 N blankholder force at 25 and 45 mm punch travels were applied for SS304 steel blanks. A 900 N blankholder force at 20, 35 and 45 mm punch travels were used for DKP6112 steel blanks. The friction coefficients in between die-blank and punch-blank sets were both taken as 0.06 in accordance with the preliminary ABAQUS simulations.



Figure 5.13 25 and 45 mm drawn SS304 steel round cups.

As shown in Figure 5.13, four earing peaks were observed especially at 45 mm punch travel at 45°, 135°, 225° and 315° angles with respect to the rolling direction due to the anisotropy of the SS304 material. For DKP6112 steel, four earing valleys were observed at 45°, 135°, 225° and 315° angles. The earing formations were more evident in DKP6112 steel cups than the SS304 steel cups due to the stronger anisotropy of the DKP6112 steel than the SS304 steel.

5.4 Material Constants

The SS304 and DKP6112 steel blanks were marked before tests by using laser marking machine to analyze the strains experienced during the deep drawing and Erichsen tests. Various laser marking patterns used for different types of blanks are shown in Figure 5.14.

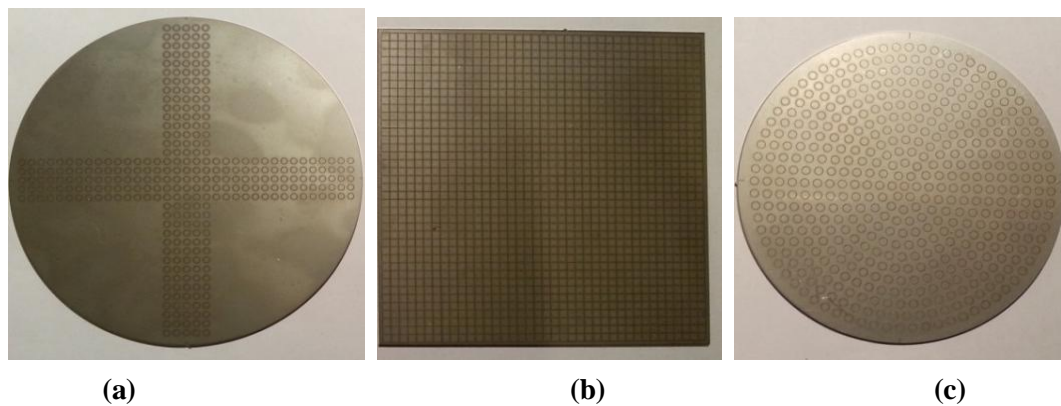


Figure 5.14 Laser marking patterns of blanks: (a) Circular blanks for cylindrical and round bottom cup drawing, (b) square blanks for square cup drawing, (c) circular blanks for Erichsen tests.

The strains on the cup forms were measured by using Grid Pattern Analyzer (GPA-100). The analyzer measures the dimensions of the deformed circle (Figure 5.15) or square patterns optically and calculates the major and minor strains by using their initial (undeformed) dimensions (Figure 5.14.a). The GPA100 analyzer automatically calculates the local strains and forms the FLD of the sheet material by means of embedded software in the analyzer. The size of the circular (for cylindrical and round bottom cup drawing cases and for Erichsen tests) and square (for square cup drawing case) patterns used in the study were 2 mm and 2x2 mm, respectively.



Figure 5.15 The deformed patterns on the drawn cup.

The values of $\sigma_0, \sigma_{45}, \sigma_{90}, r_0, r_{45}, r_{90}, \sigma_b$ and r_b that had been obtained from the Tension and Erichsen tests, were used in the calculation of the material constants of the BBC2008-8p and Yld2003-8p yield criteria for the SS304 and DKP6112 steels. The material constants of a model were found by minimizing the error function defined for the model. The error functions for BBC2008-8p and Yld2003-8p models are given before in Eqns. (4.165) and (4.106), respectively. The minimization of the error function for each model was achieved by using of a developed code (which uses the anisotropy parameters to find the material constants) specifically for the MATLAB software.

Material constants found for BBC2008-8p and Yld2003-8p yield criteria are given in Table 5.4 and Table 5.5, respectively. The material constants were used in ABAQUS (FEA) simulation of the cylindrical, square and round cup forms drawn in this study.

Table 5.4 Material constants of BBC2008-8p yield criterion for SS304 and DKP6112 steels.

	SS304	DKP6112
k	4	3
w	1.5	1.5
s	1	1
l_{11}	0.25	1.32
l_{21}	0.70	-1.21
m_{11}	0.60	-0.56
m_{21}	0.60	-0.53
m_{31}	0.72	-0.11
n_{11}	0.50	-0.44
n_{21}	0.35	0.97
n_{31}	0.55	1.19

Table 5.5 Material constants of Yld2003-8p yield criterion for SS304 and DKP6112 steels.

	SS304	DKP6112
m	8	6
a ₁	0.46	-1.45
a ₂	1.23	-1.35
a ₃	1.42	-0.80
a ₄	1.36	-1
a ₅	0.50	1.15
a ₆	0.96	0.8
a ₇	0.9	-0.7
a ₈	1.10	0.05

CHAPTER 6

RESULTS AND DISCUSSION

Cylindrical, square and round bottom drawing processes were analyzed by FEM for seven different models, namely, isotropic hardening, kinematic hardening, combined hardening, Hill'48, Hu2003, Yld2003-8p and BBC2008-8p. The results are presented together with the experimental data by using the thickness strain variations.

In Figures 6.1-6.34, the variations of the thickness strain with respect to distance from the center of the blank are given for the seven models, two different sheet metals (SS304 and DKP6112 steels), three directions (0° , 45° and 90°), three punch travels and three different types of cup geometries.

6.1 Stainless steel 304 material

In this section, the thickness strain distributions of cylindrical, square and round bottom cup drawing for using stainless steel 304 (SS304) material in the diagonal, rolling and transverse directions at different punch displacements are presented.

6.1.1 Cylindrical Cup Drawing

In Figures 6.1 and 6.2, the thickness strain distributions of cylindrical cup drawing are given in rolling and transverse directions, respectively, at 20 mm punch displacement.

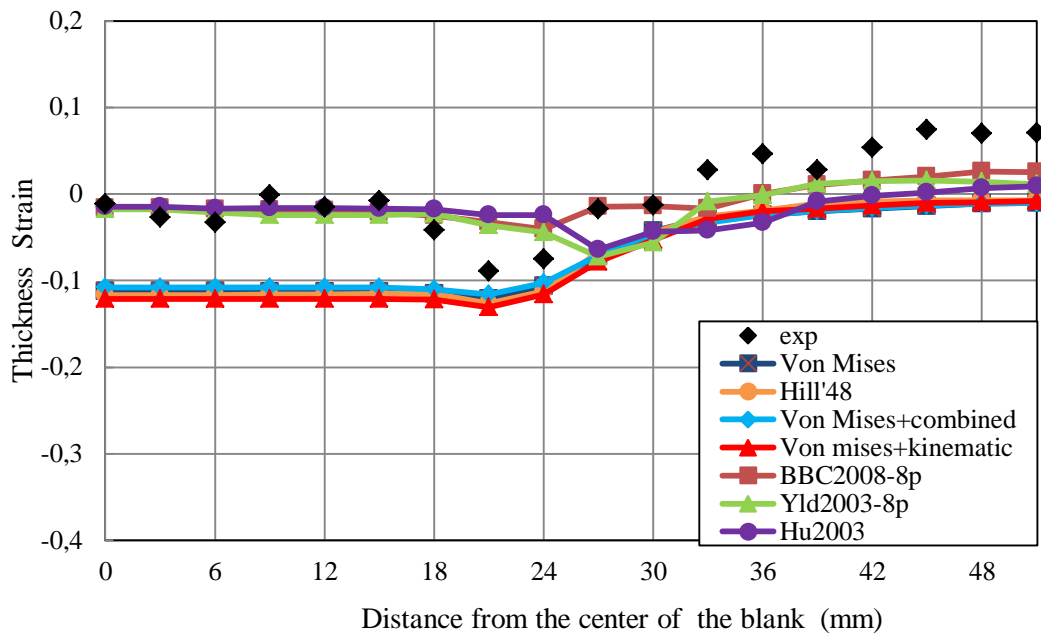


Figure 6.1 Thickness strain distributions obtained from different models and experiment at 20 mm punch travel (SS304, cylindrical, rolling direction).

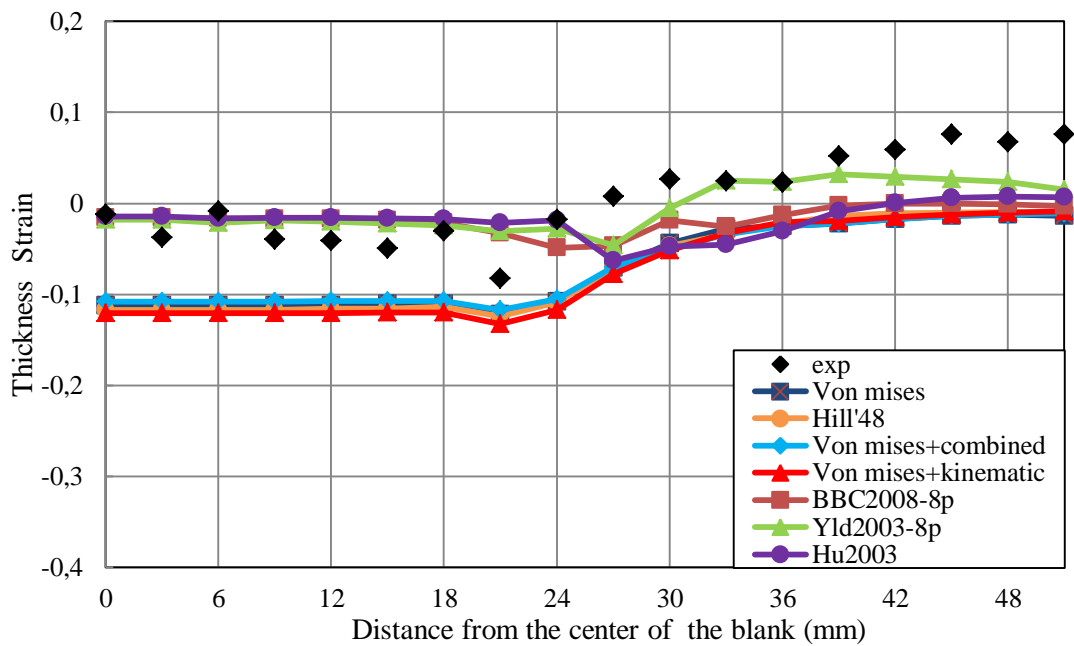


Figure 6.2 Thickness strain distributions obtained from different models and experiment at 20 mm punch travel (SS304, cylindrical, transverse direction).

Figures 6.3 and 6.4 show the thickness strain distributions of cylindrical cup drawing in rolling and transverse directions, respectively, at 35 mm punch displacement.

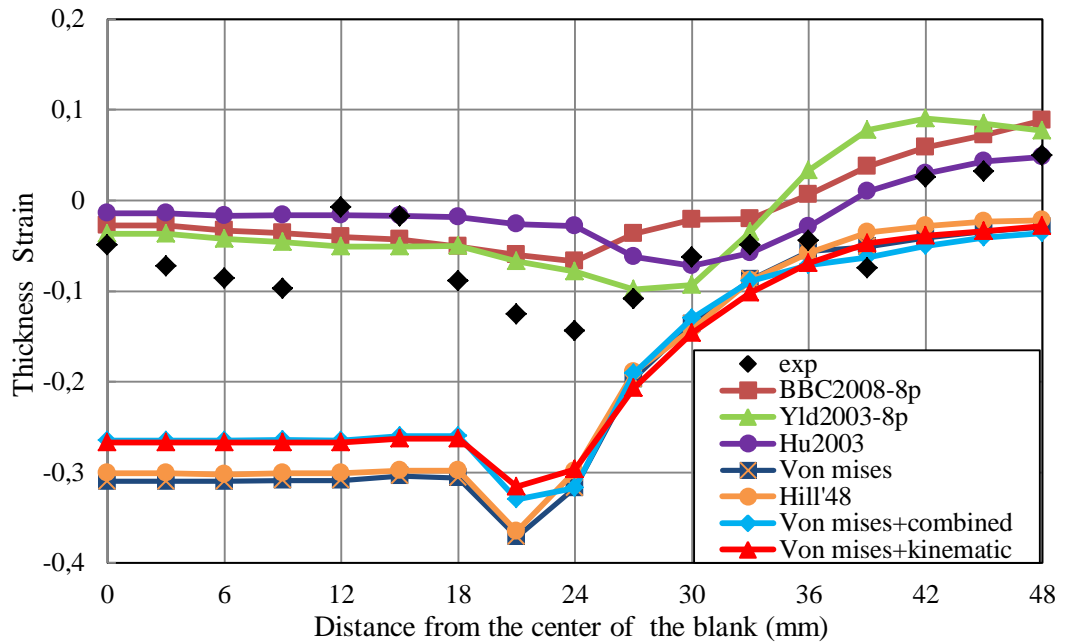


Figure 6.3 Thickness strain distributions obtained from different models and experiment at 35 mm punch travel (SS304, cylindrical, rolling direction).

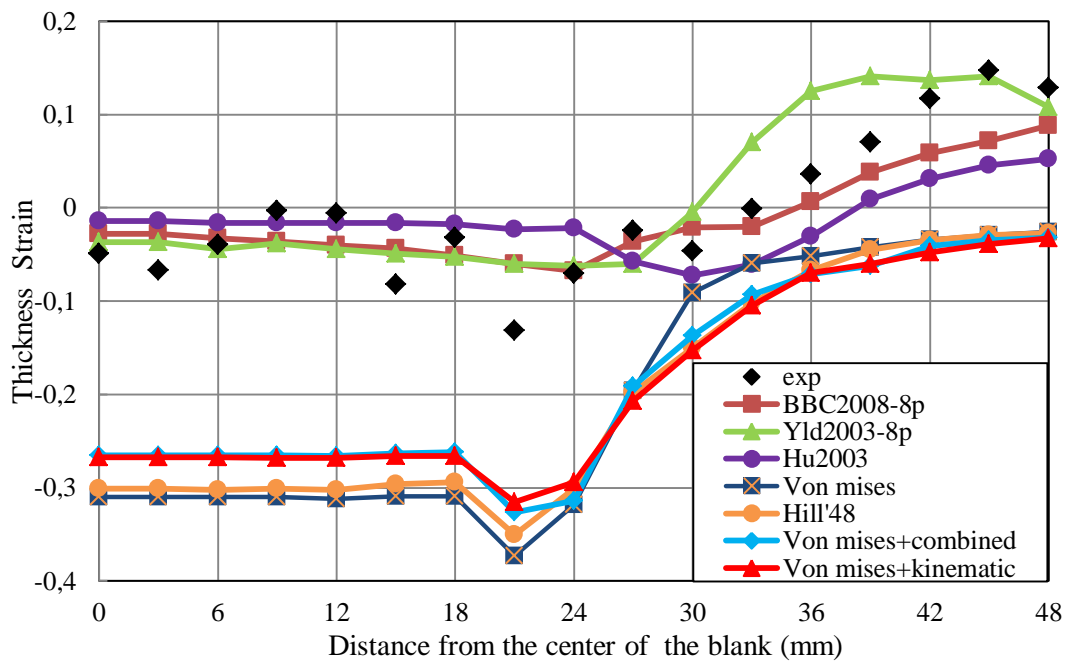


Figure 6.4 Thickness strain distributions obtained from different models and experiment at 35 mm punch travel (SS304, cylindrical, transverse direction).

In Figures 6.5 and 6.6, the thickness strain distributions of cylindrical cup drawing are given in rolling and transverse directions, respectively, at 45 mm punch displacement.

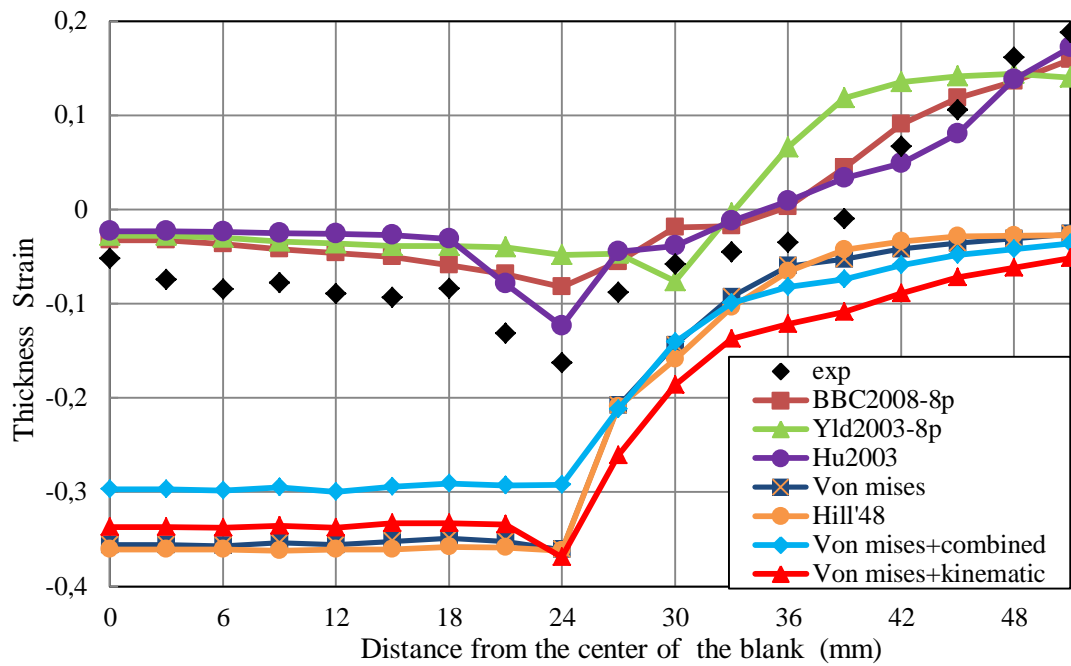


Figure 6.5 Thickness strain distributions obtained from different models and experiment at 45 mm punch travel (SS304, cylindrical, rolling direction).

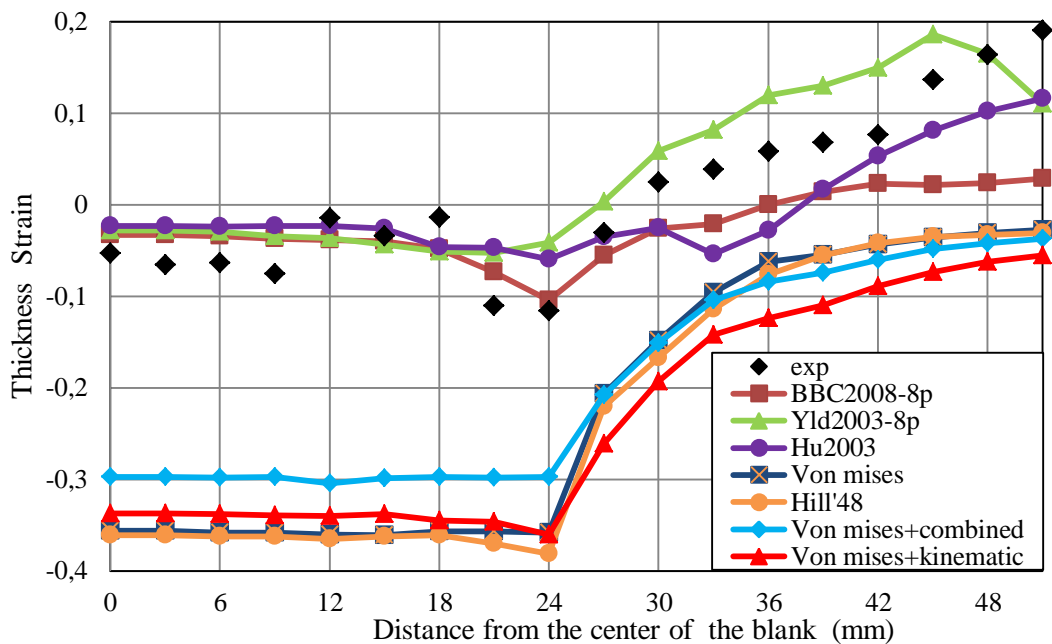


Figure 6.6 Thickness strain distributions obtained from different models and experiment at 45 mm punch travel (SS304, cylindrical, transverse direction).

There are slight deviations in the thickness strains between the seven constitutive models and the experimental data at the bottom region of the cup at 20 mm punch travel. On the other hand, significant thickness strain deviations between Hu2003, Yld2003-8p, BBC2008-8p models and isotropic hardening, kinematic hardening, combined hardening, Hill'48 models

are noticeable at the bottom region of the cup at 35 and 45 mm punch travels. However, the results for Hu2003, Yld2003-8p and BBC2008-8p are in better agreement with experiments. Yet, the observed deviations in thickness strains are reduced significantly at the flange regions. The thickness strain distribution of cylindrical cup drawing for SS304 material at 20, 35 and 45 mm punch travels (Figures 6.1-6.6) showed that the experimental thickness variations are in better agreement with the Hu2003, Yld2003-8p and BBC2008-8p models.

6.1.2 Square Cup Drawing

Figures 6.7 and 6.8 show the thickness strain distributions of square cup drawing in between the midpoint of the sides (rolling) and diagonal directions at 15 mm punch displacement, respectively.

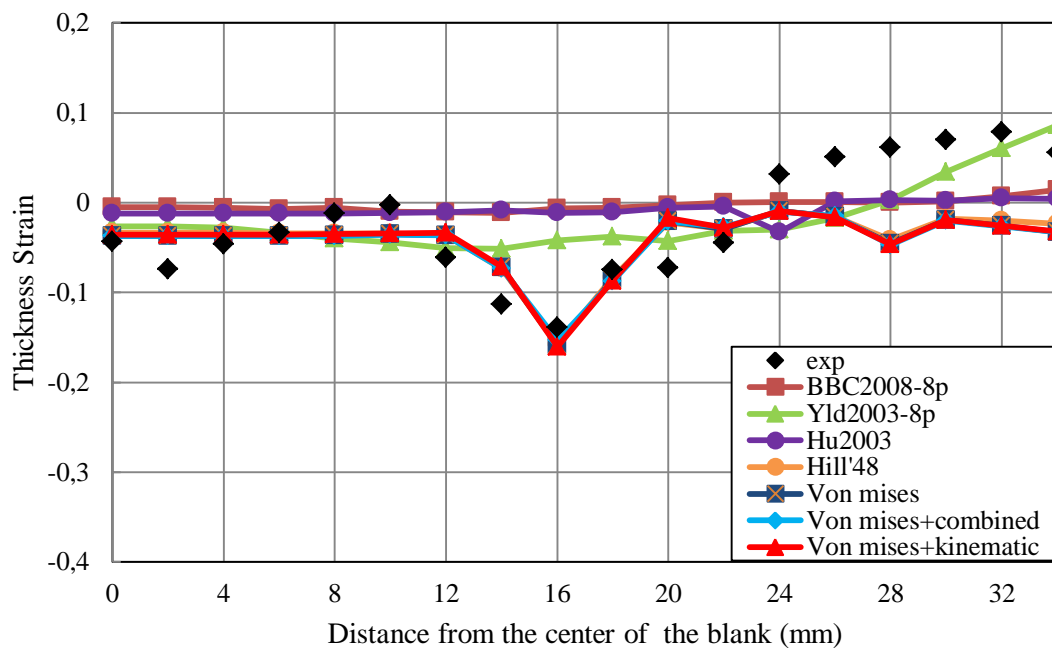


Figure 6.7 Thickness strain distributions obtained from different models and experiment at 15 mm punch travel (SS304, square, rolling direction).

In Figures 6.9 and 6.10, the thickness strain distributions of square cup drawing are given in between the midpoint of the sides (rolling) and diagonal directions, respectively, at 20 mm punch displacement.

The thickness strain distributions (Figures 6.7-6.10) of the seven constitutive models are generally consistent with each other and with the experimental data for square cup drawing with 15 mm and 20 mm punch travels.

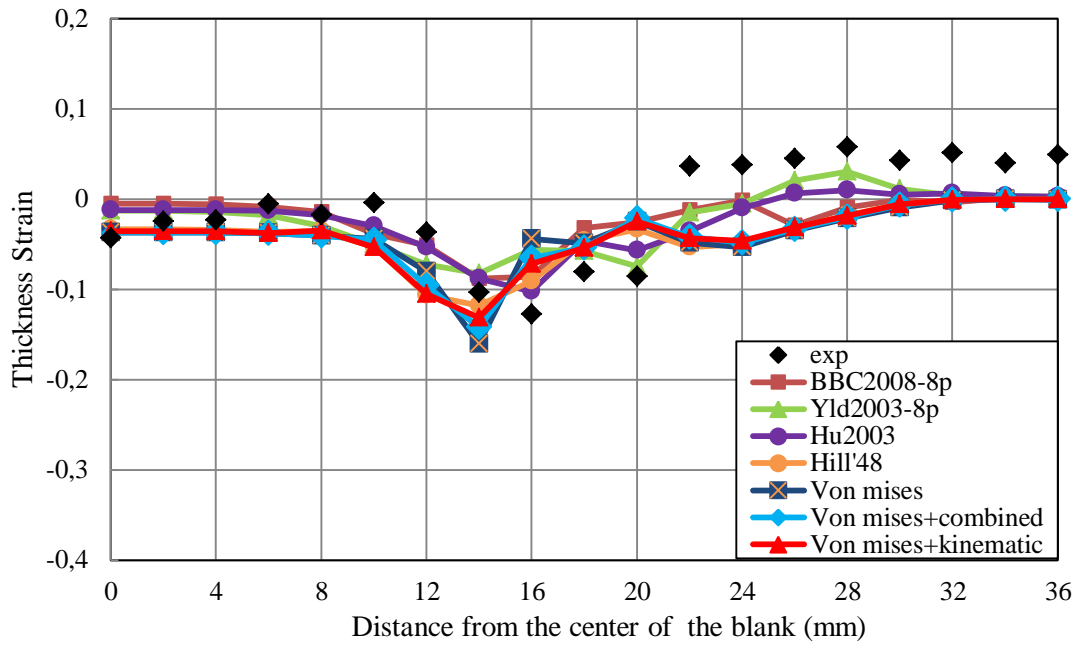


Figure 6.8 Thickness strain distributions obtained from different models and experiment at 15 mm punch travel (SS304, square, diagonal direction).

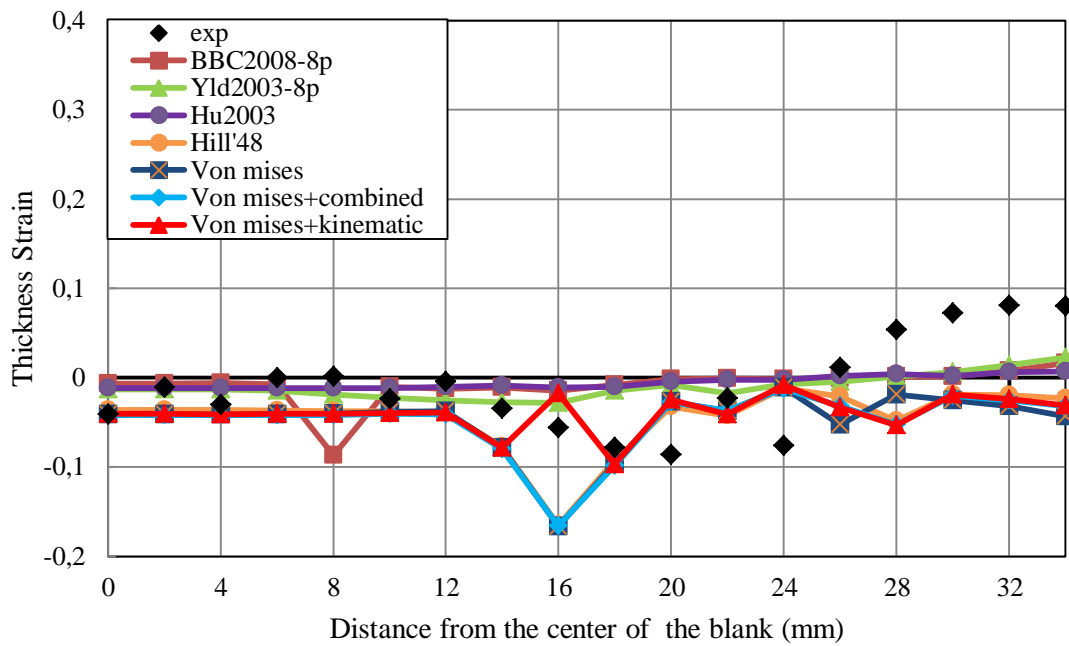


Figure 6.9 Thickness strain distributions obtained from different models and experiment at 20 mm punch travel (SS304, square, rolling direction).

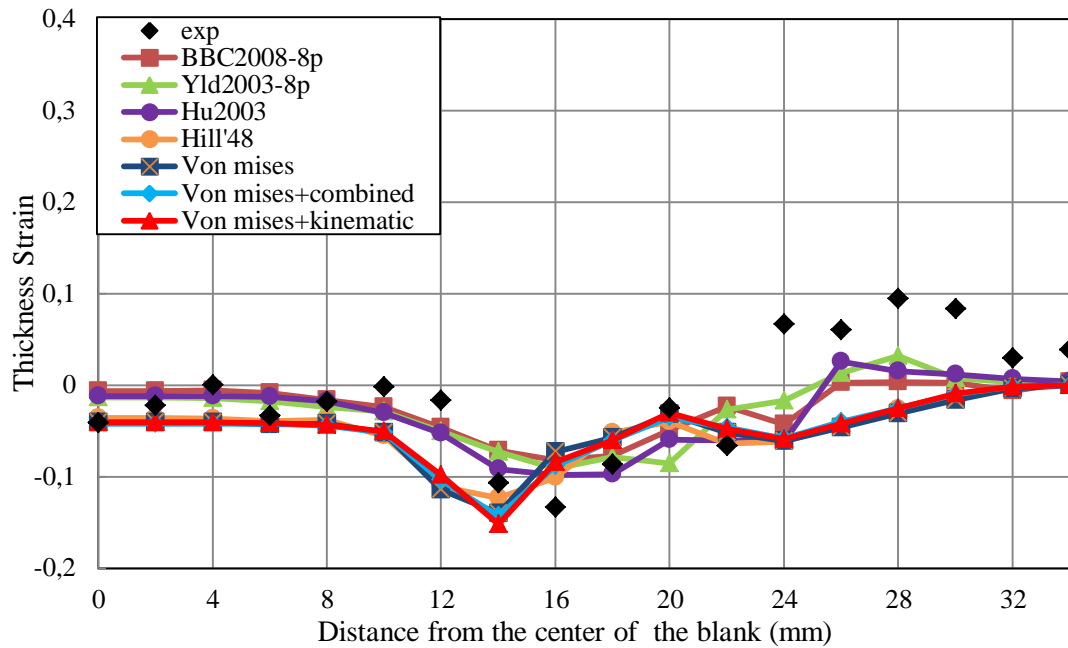


Figure 6.10 Thickness strain distributions obtained from different models and experiment at 20 mm punch travel (SS304, square, diagonal direction).

Figures 6.11 and 6.12 show the thickness strain distributions of square cup drawing in between the midpoint of the sides (rolling) and diagonal directions, respectively, at 25 mm punch displacement. As shown clearly in the figures, the Hu2003, Yld2003-8p, BBC2008-8p models show good agreement with the experimental results at 25 mm punch travel. On the other hand, the other four models group together and show little deviation from the others. The deviation of the thickness strain observed in the Hill'48, isotropic hardening, kinematic hardening and combined hardening constitutive models at the bottom region of the cylindrical cup is not observed in square cup drawing cases.

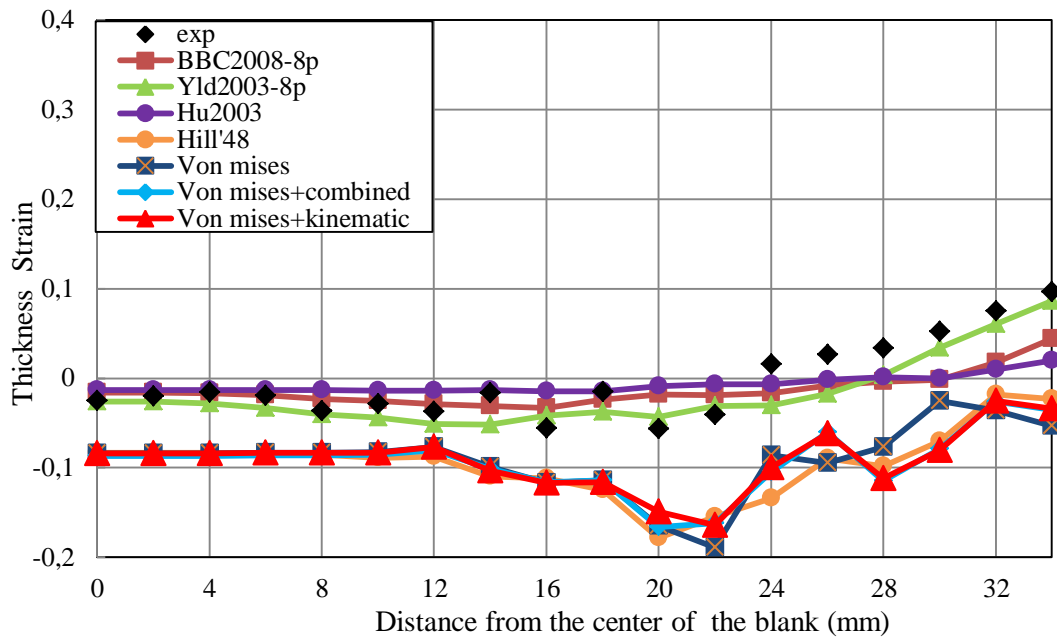


Figure 6.11 Thickness strain distributions obtained from different models and experiment at 25 mm punch travel (SS304, square, rolling direction).

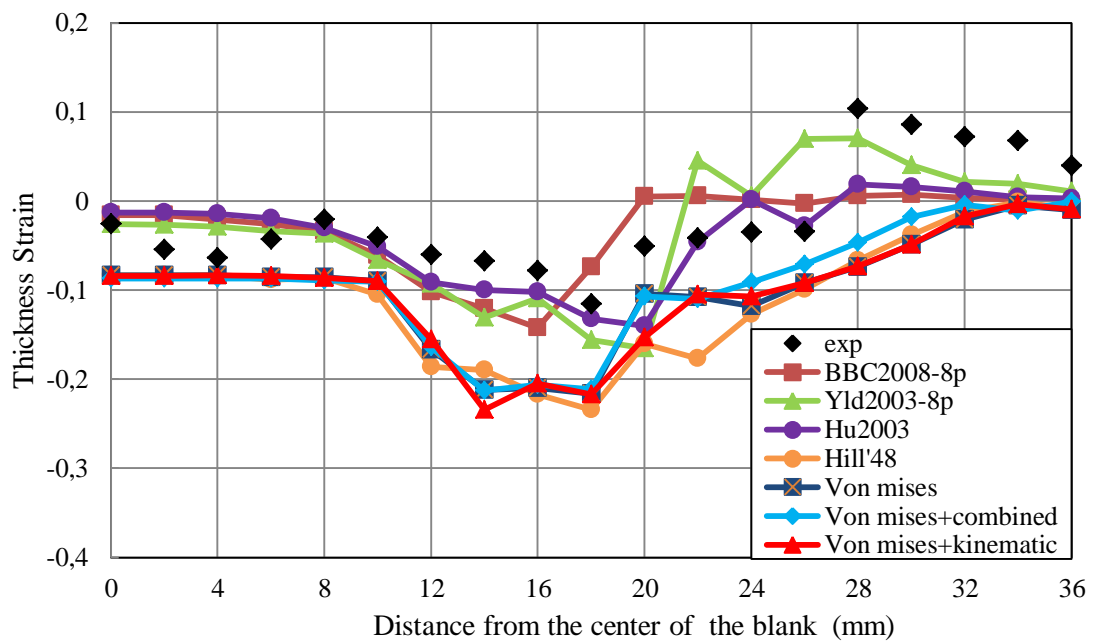


Figure 6.12 Thickness strain distributions obtained from different models and experiment at 25 mm punch travel (SS304, square, diagonal direction).

6.1.3 Round Bottom Cup Drawing

In Figures 6.13 and 6.14, the thickness strain distributions of round cup drawing are given in rolling and transverse directions, respectively, at 25 mm punch displacement. As shown in figures, the experimental results are in better agreement with the Hu2003, isotropic hardening, kinematic hardening, combined hardening, Hill'48 at 25 mm punch travel. Yet, slight thickness strain divergences of the other models are noticeable at the bottom regions of the cup for BBC2008-8p and Yld2003-8p.

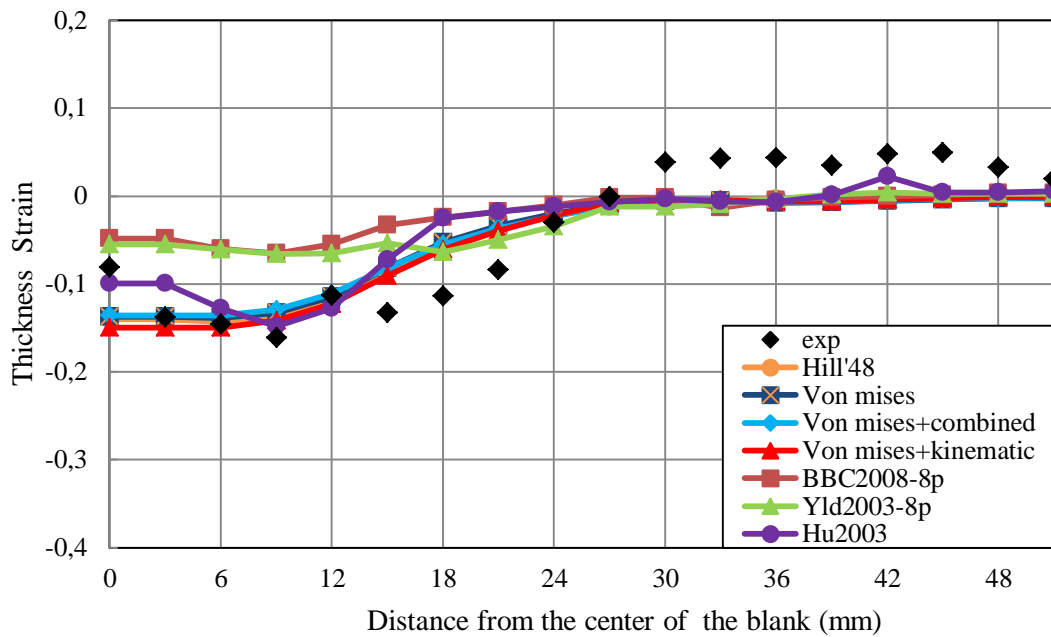


Figure 6.13 Thickness strain distributions obtained from different models and experiment at 25 mm punch travel (SS304, round, rolling direction).

In Figures 6.15 and 6.16 the thickness strain distributions of round cup drawing are given in rolling and transverse directions, respectively, at 45 mm punch displacement. Figures show that the experimental results are consistent with the BBC2008-8p and Yld2003-8p models at 45 mm punch travel. There are considerable deviations between the experimental data and the isotropic hardening, kinematic hardening, combined hardening, Hill'48 models at the bottom region of the cup.

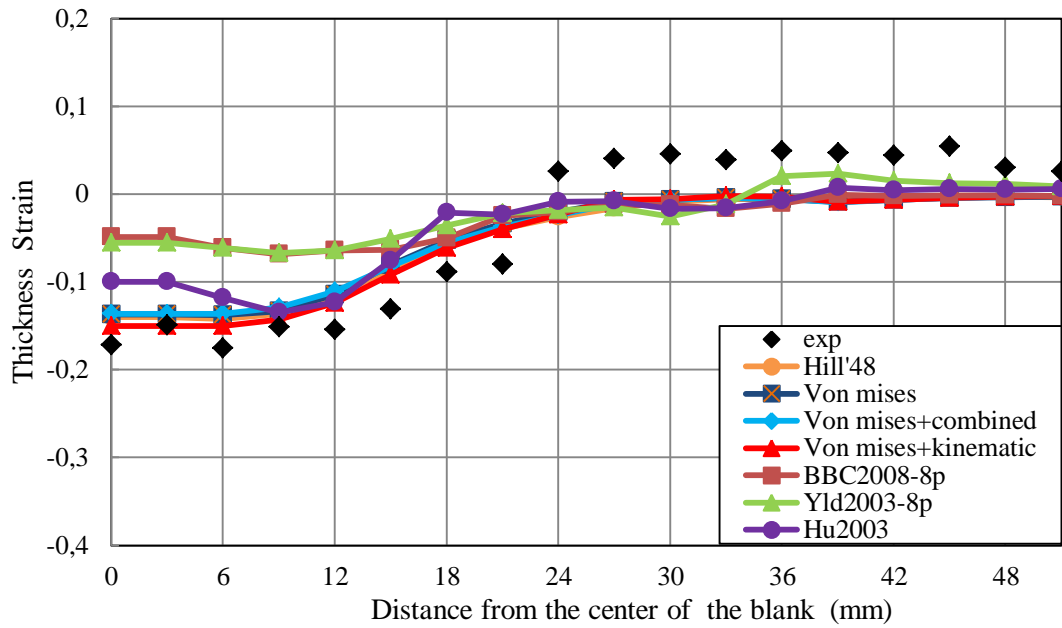


Figure 6.14 Thickness strain distributions obtained from different models and experiment at 25 mm punch travel (SS304, round, transverse direction).

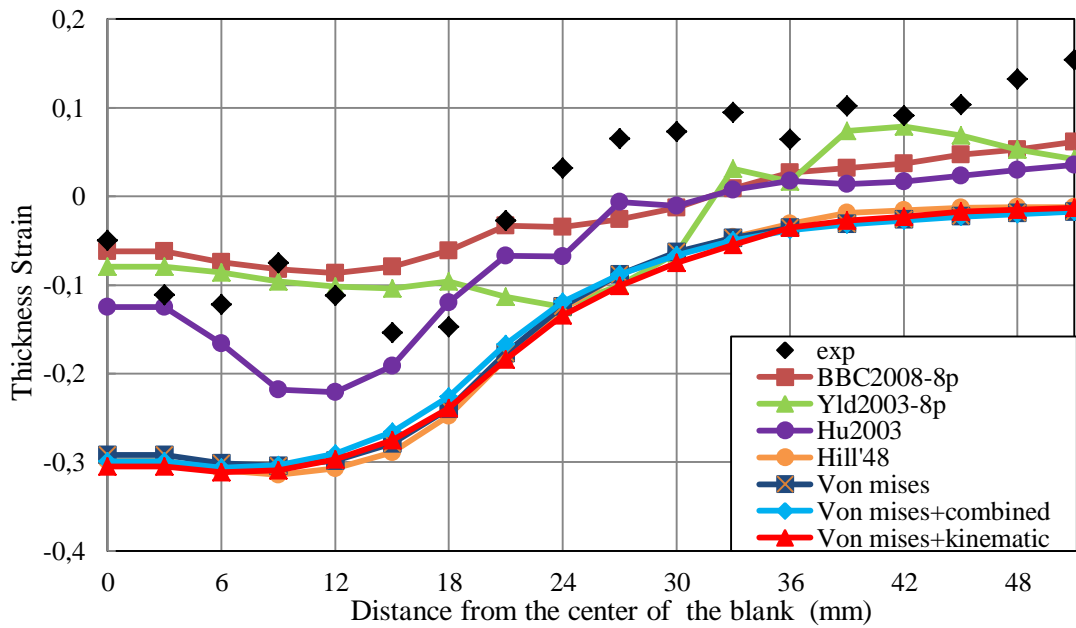


Figure 6.15 Thickness strain distributions obtained from different models and experiment at 45 mm punch travel (SS304, round, rolling direction).

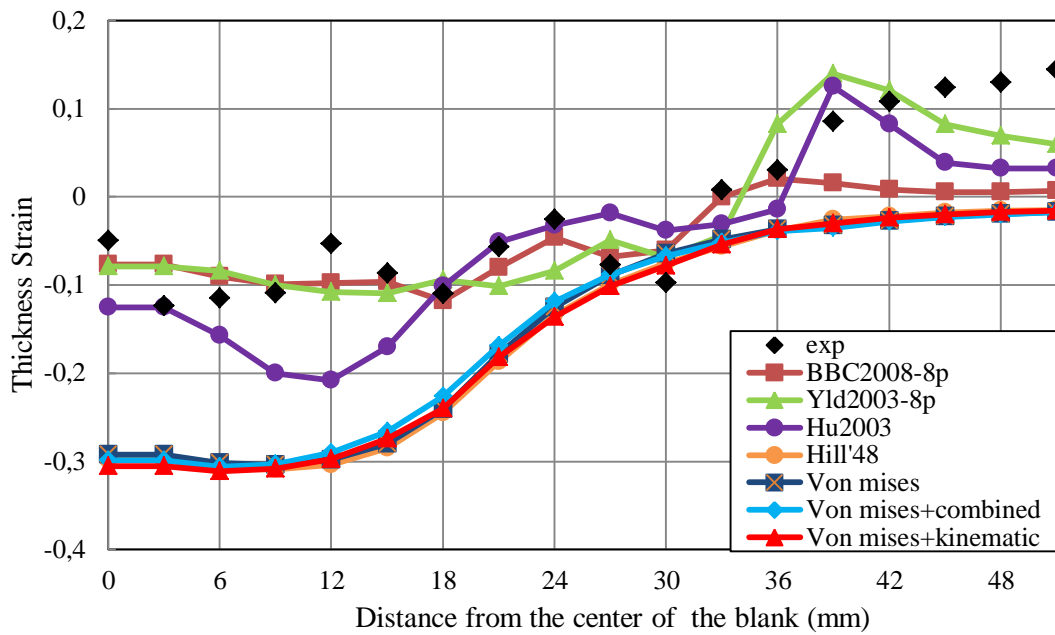


Figure 6.16 Thickness strain distributions obtained from different models and experiment at 45 mm punch travel (SS304, round, transverse direction).

6.2 DKP6112 material

In this section, the thickness strain distributions of cylindrical, square and round bottom cup drawing for using DKP6112 material in the diagonal, rolling and transverse directions at different punch displacements are presented.

6.2.1 Cylindrical Cup Drawing

Figures 6.17 and 6.18 show the thickness strain distributions of cylindrical cup drawing in rolling and transverse direction, respectively, at 15 mm punch displacement.

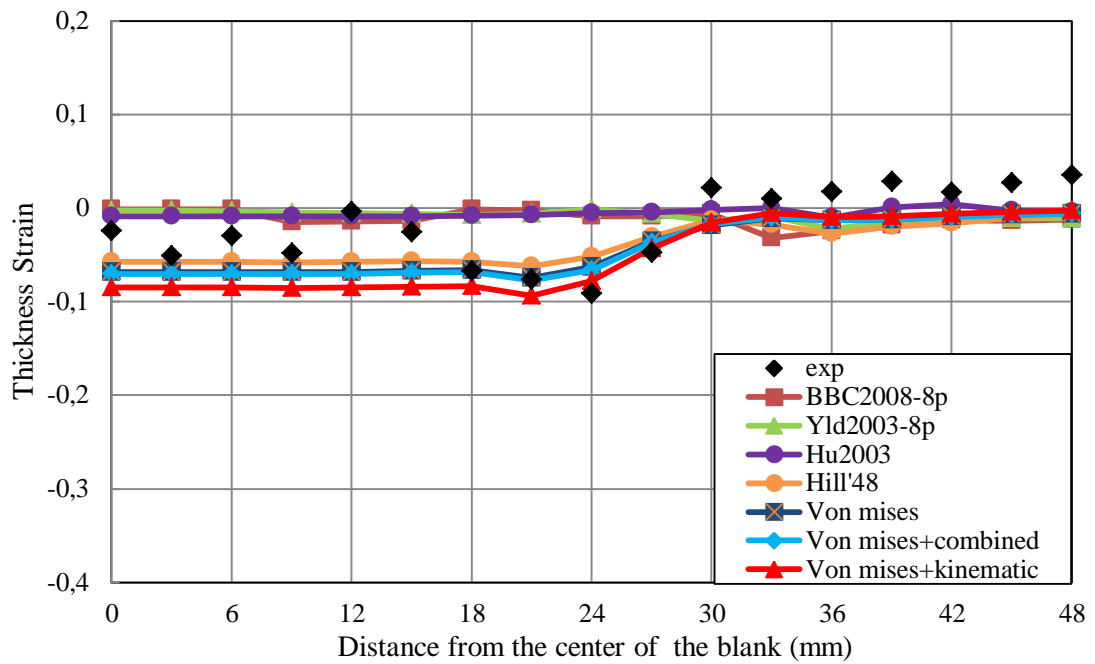


Figure 6.17 Thickness strain distributions obtained from different models and experiment at 15 mm punch travel (DKP6112, cylindrical, rolling direction).

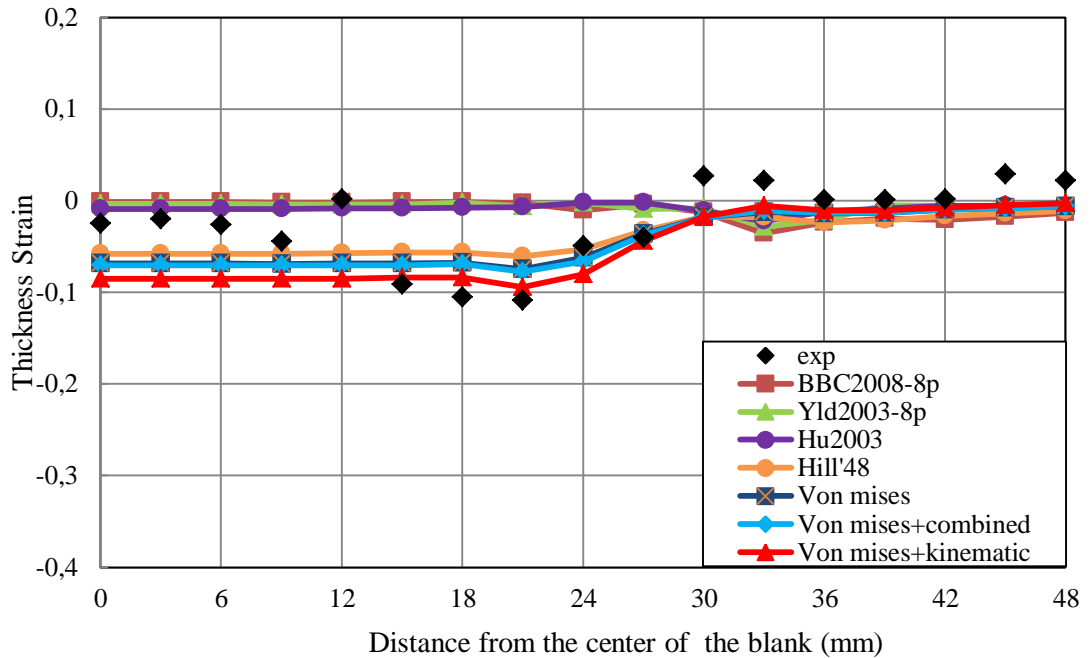


Figure 6.18 Thickness strain distributions obtained from different models and experiment at 15 mm punch travel (DKP6112, cylindrical, transverse direction).

In Figures 6.19 and 6.20, the thickness strain distributions of cylindrical cup drawing are given, in rolling and transverse direction, respectively, at 25 mm punch displacement.

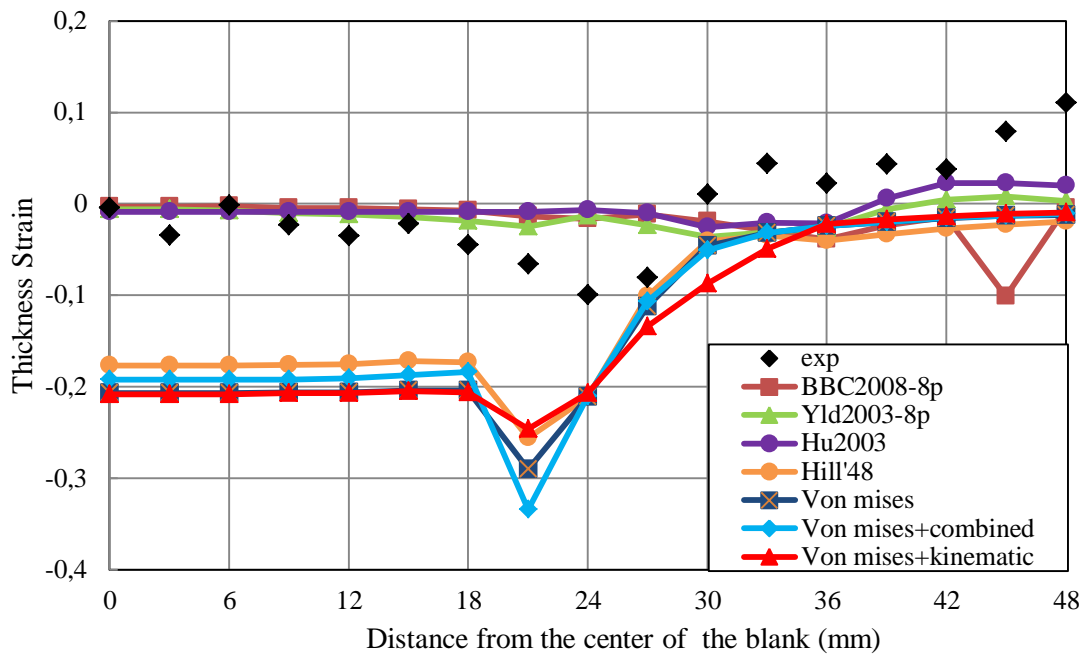


Figure 6.19 Thickness strain distributions obtained from different models and experiment at 25 mm punch travel (DKP6112, cylindrical, rolling direction).

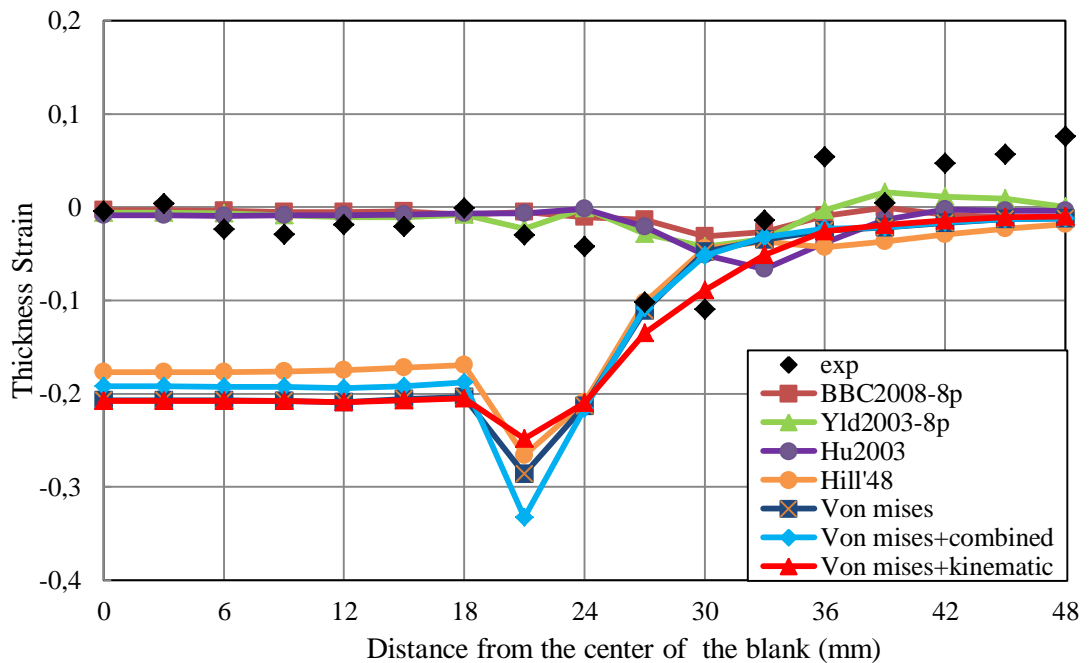


Figure 6.20 Thickness strain distributions obtained from different models and experiment at 25 mm punch travel (DKP6112, cylindrical, transverse direction).

Figures 6.21 and 6.22 show the thickness strain distributions of cylindrical cup drawing in rolling and transverse direction, respectively, at 35 mm punch displacement.

In Figures 6.17-6.22, the experimental thickness variations are in better agreement with the Hu2003, Yld2003-8p and BBC2008-8p models at 15, 25 and 35 mm punch travels. A significant deviation between the experimental data, Hu2003, Yld2003-8p, BBC2008-8p models and isotropic hardening, kinematic hardening, combined hardening, Hill'48 models are also observed at the 25 and 35 mm punch travels.

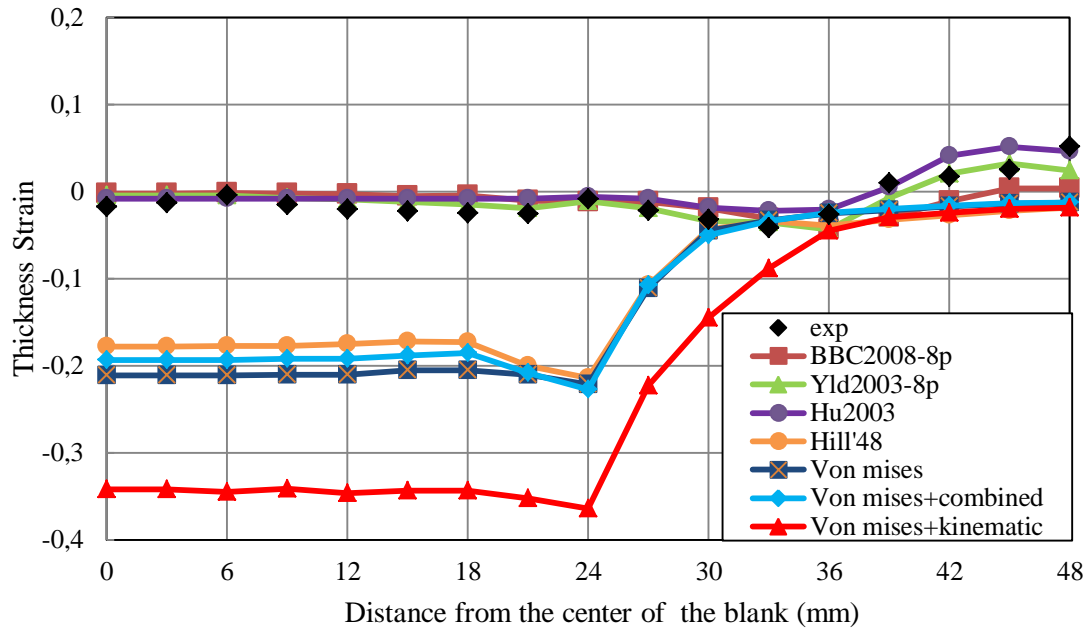


Figure 6.21 Thickness strain distributions obtained from different models and experiment at 35 mm punch travel (DKP6112, cylindrical, rolling direction).

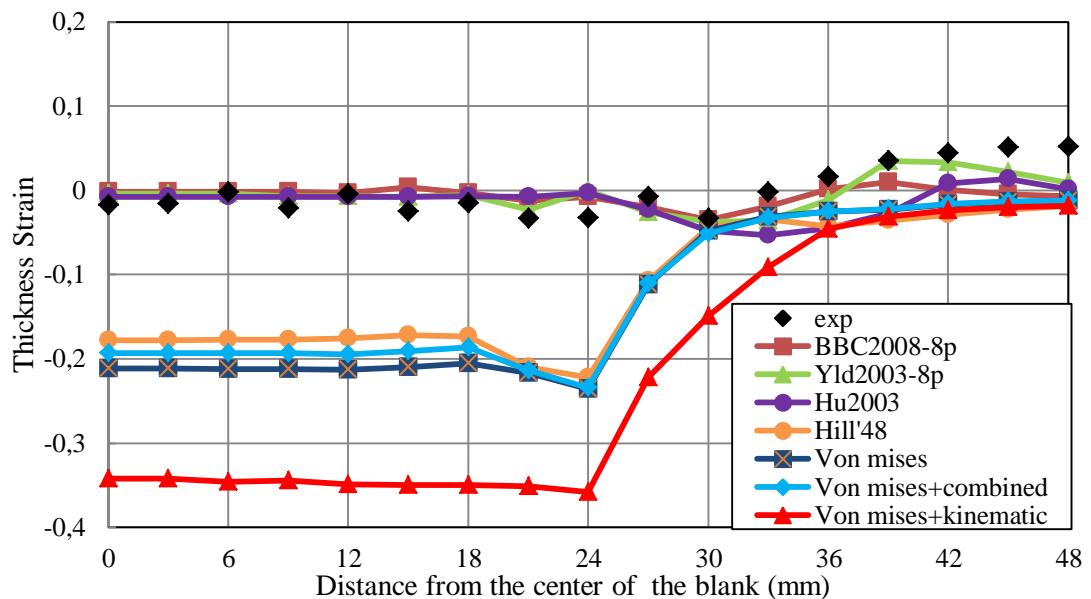


Figure 6.22 Thickness strain distributions obtained from different models and experiment at 35 mm punch travel (DKP6112, cylindrical, transverse direction).

6.2.2 Square Cup Drawing

In Figures 6.23 and 6.24, the thickness strain distributions of square cup drawing are given in between the midpoint of the sides (rolling) and diagonal direction, respectively, at 15 mm punch displacement. As shown in the figures, the thickness strain values of the seven constitutive models are generally consistent with each other and with the experimental data at 15 mm punch travels. Yet, local deviations in thickness strain values from experimental results at the bottom corner region of the cup are observed in Figure 6.23 for kinematic hardening, combined hardening, isotropic hardening and Hill'48 models.

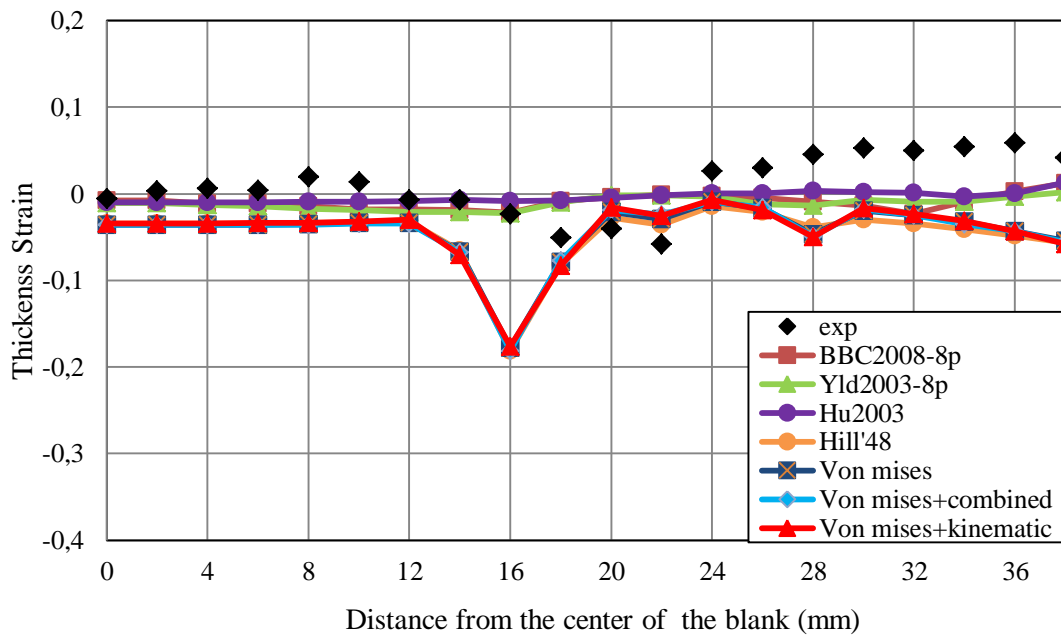


Figure 6.23 Thickness strain distributions obtained from different models and experiment at 15 mm punch travel (DKP6112, square, rolling direction).

Figures 6.25 and 6.26 show the thickness strain distributions of square cup drawing in between the midpoint of the sides (rolling) and diagonal direction, respectively, at 20 mm punch displacement. As shown in Figure 6.25, the experimental results are generally consistent with the seven models at 20 mm punch travel in between the midpoint of the sides (rolling) direction except for bottom corner region of the cup. Significant thickness strain differences from the experimental results are observed at the bottom corner region of the cup especially at BBC2008-8p and Hu2003 models. In Figure 6.26, the thickness strain values of BBC2008-8p and Hu2003 models show better fit with the experimental results at 20 mm punch travel in diagonal direction. The Yld2003-8p model also shows consistency with the experimental results except for the slight differences observed at the bottom region of the cup. Although, the other four models (isotropic hardening, kinematic hardening, combined hardening and Hill'48) show higher strain values than the experimental data at the bottom region, the differences in strain values are hardly noticeable at flange regions.

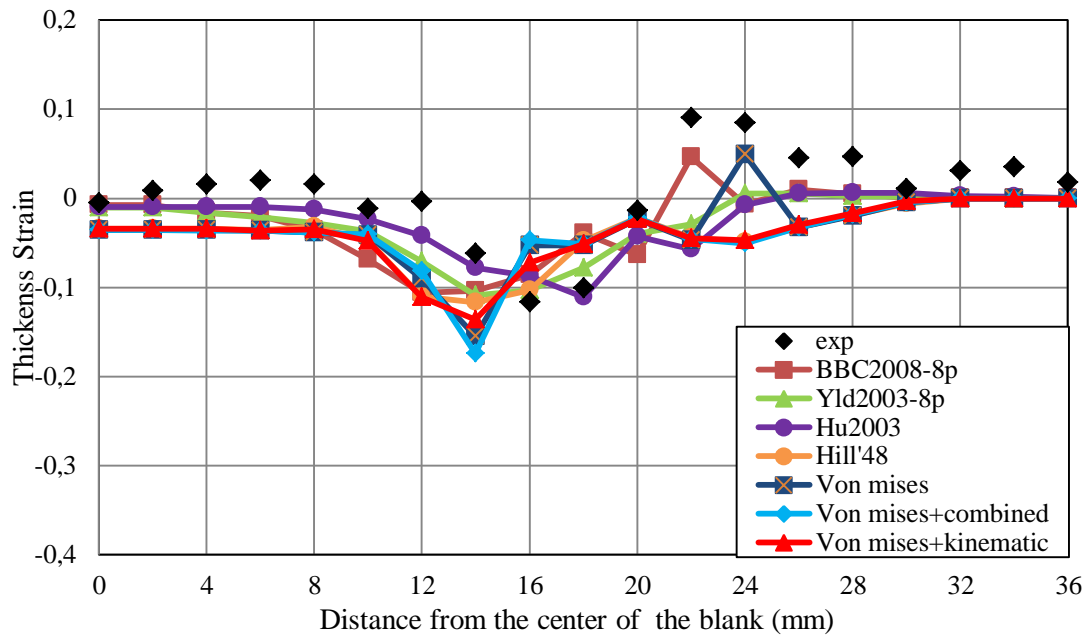


Figure 6.24 Thickness strain distributions obtained from different models and experiment at 15 mm punch travel (DKP6112, square, diagonal direction).

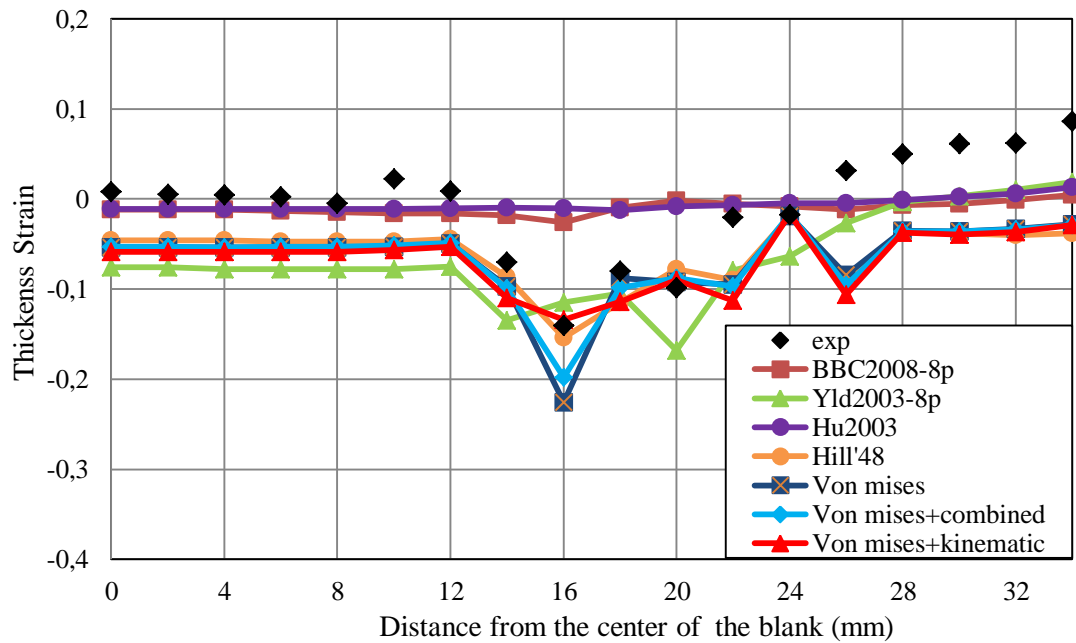


Figure 6.25 Thickness strain distributions obtained from different models and experiment at 20 mm punch travel (DKP6112, square, rolling direction).

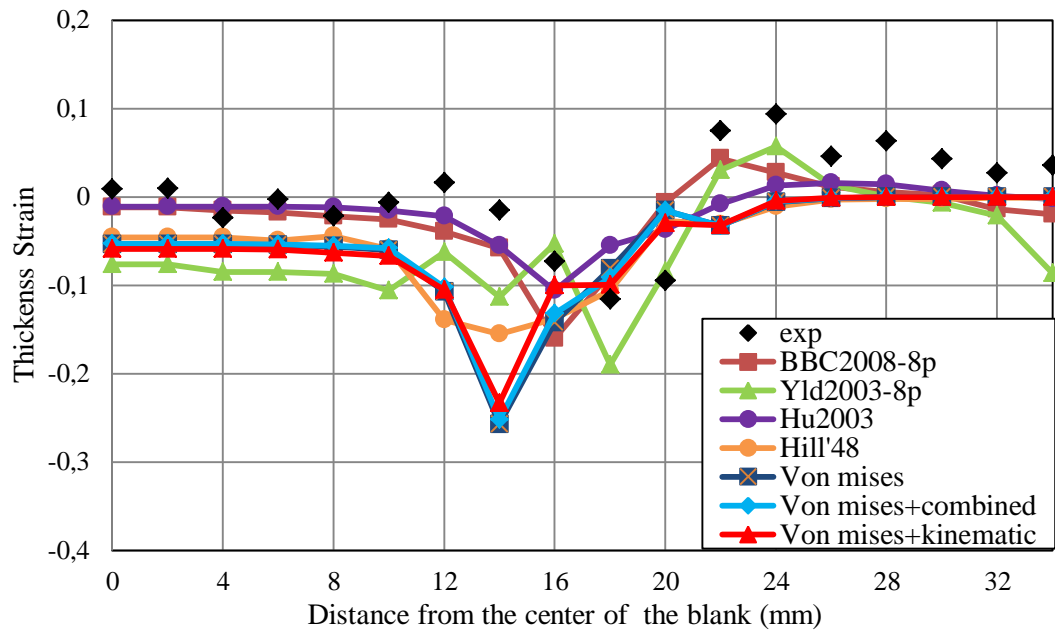


Figure 6.26 Thickness strain distributions obtained from different models and experiment at 20 mm punch travel (DKP6112, square, diagonal direction).

In Figures 6.27 and 6.28, the thickness strain distributions of square cup drawing are given in between the midpoint of the sides (rolling) and diagonal direction, respectively, at 25 mm punch displacement. As shown in Figure 6.27, the experimental thickness distributions are in better agreement with Yld2003-8p and BBC2008-8p in between the midpoint of the sides (rolling) direction. The figure indicates that the Hu2003 model does not reflect the experimental strain behavior at the bottom corner region of the cup. Although, some deviations in strain values are observed at the bottom corner region of the cup in Figure 6.28, the seven models and the experimental data show almost the same trend.

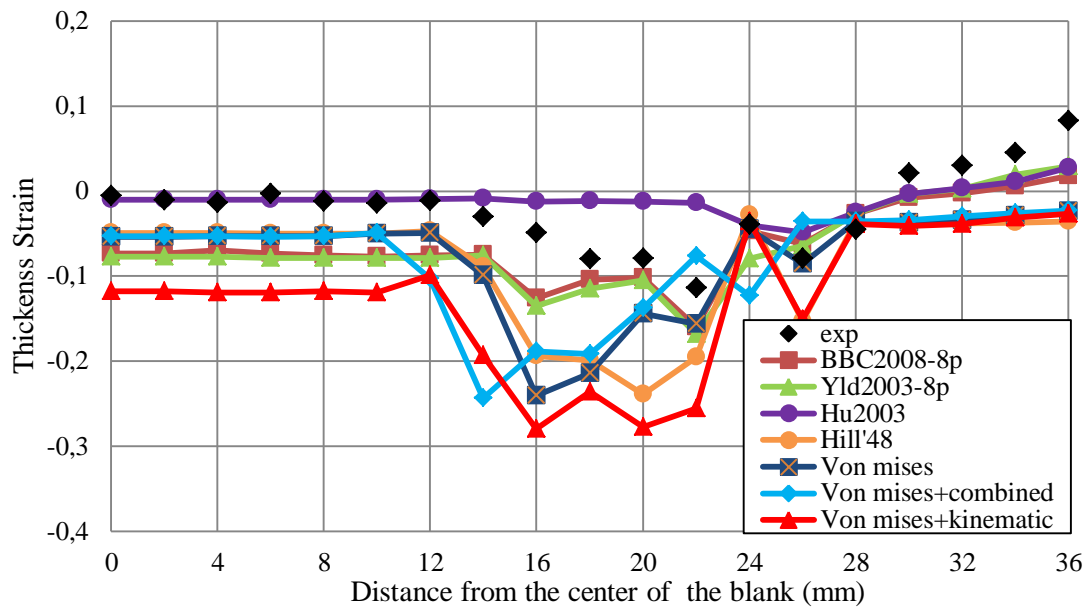


Figure 6.27 Thickness strain distributions obtained from different models and experiment at 25 mm punch travel (DKP6112, square, rolling direction).

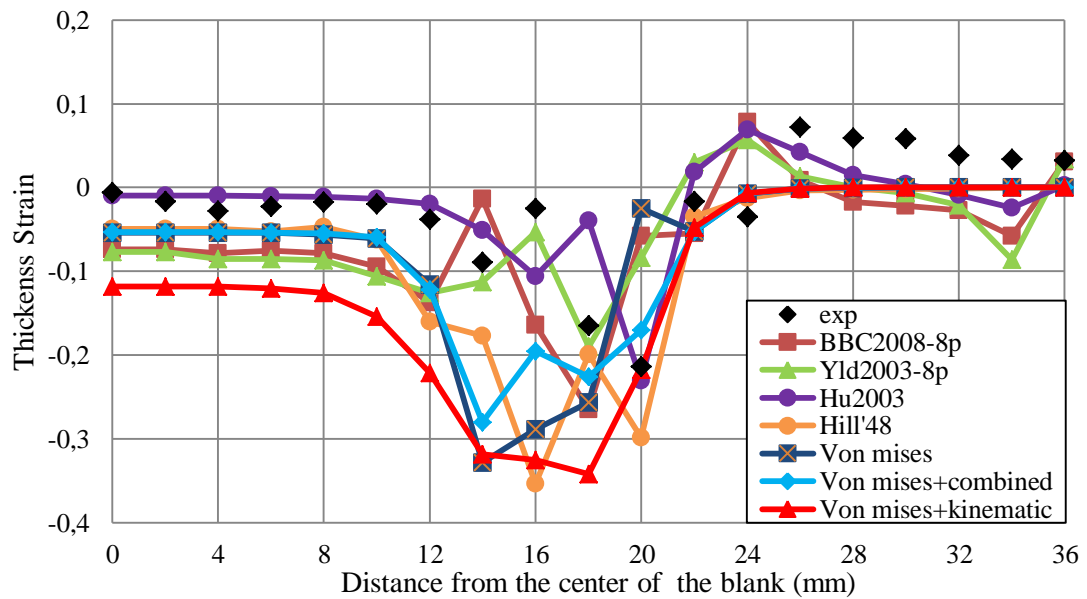


Figure 6.28 Thickness strain distributions obtained from different models and experiment at 25 mm punch travel (DKP6112, square, diagonal direction).

6.2.3 Round Bottom Cup Drawing

Figures 6.29 and 6.30 show the thickness strain distributions of round bottom cup drawing in rolling and transverse direction, respectively, at 20 mm punch displacement. As shown clearly in both figures, the thickness strain values of the seven constitutive models are highly consistent with each other and the experimental data.

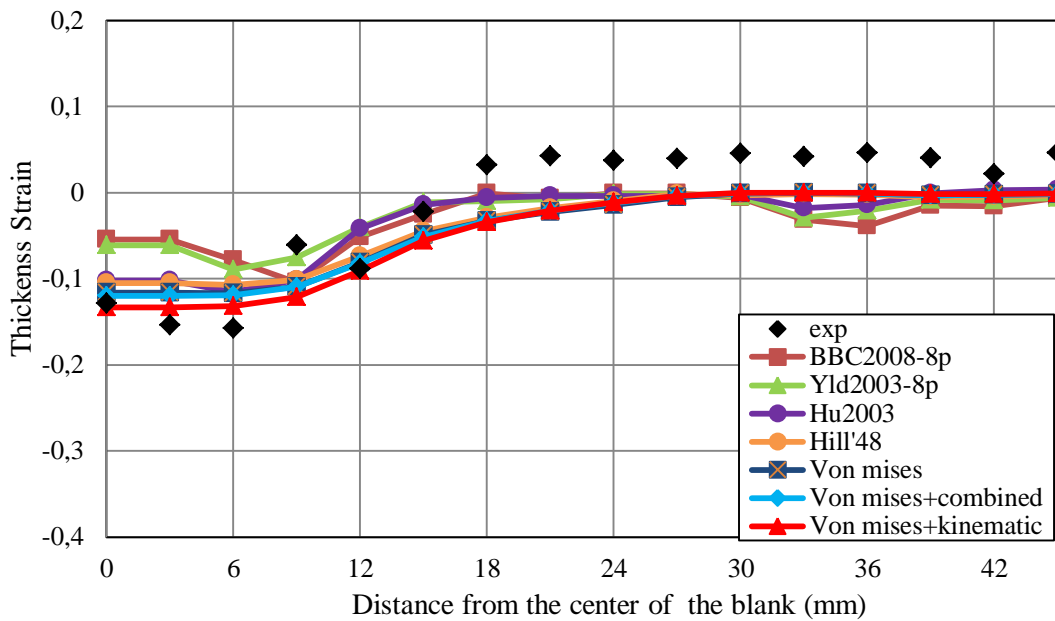


Figure 6.29 Thickness strain distributions obtained from different models and experiment at 20 mm punch travel (DKP6112, round, rolling direction).

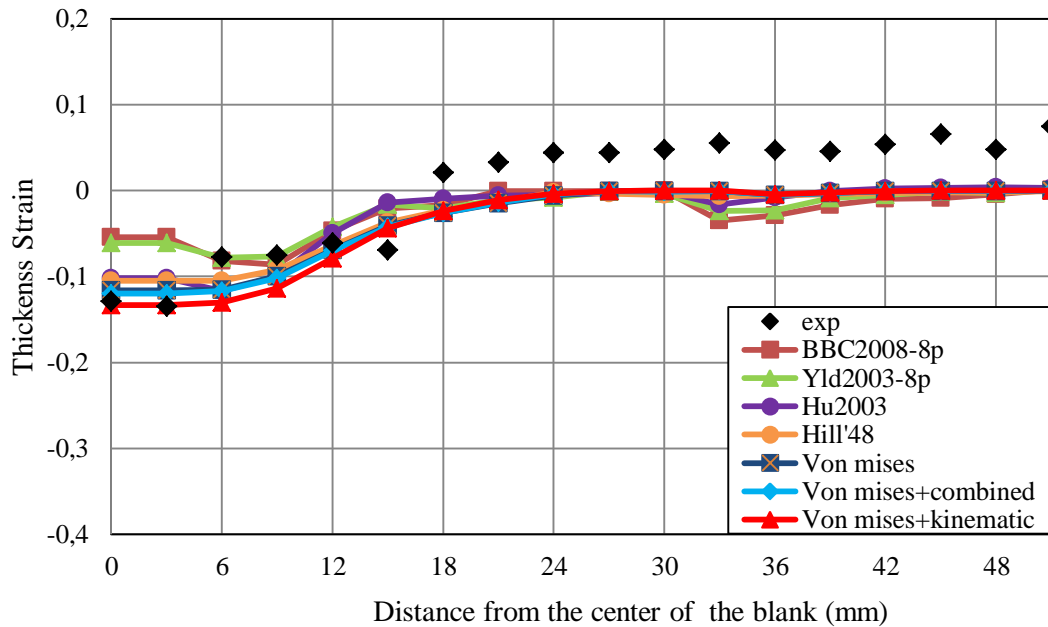


Figure 6.30 Thickness strain distributions obtained from different models and experiment at 20 mm punch travel (DKP6112, round, diagonal direction).

In Figures 6.31- 6.34, the thickness strain distributions of round bottom cup drawing are given in rolling and transverse direction, at 35 and 45 mm punch displacements. It is clear that in all figures, the similar trends are observed. The experimental results are in better agreement with the BBC2008-8p, Hu2003 and Yld2003-8p models. However, there are considerable deviations between the experimental data and the isotropic hardening,

kinematic hardening, combined hardening, Hill'48 models especially at the bottom region of the cup.

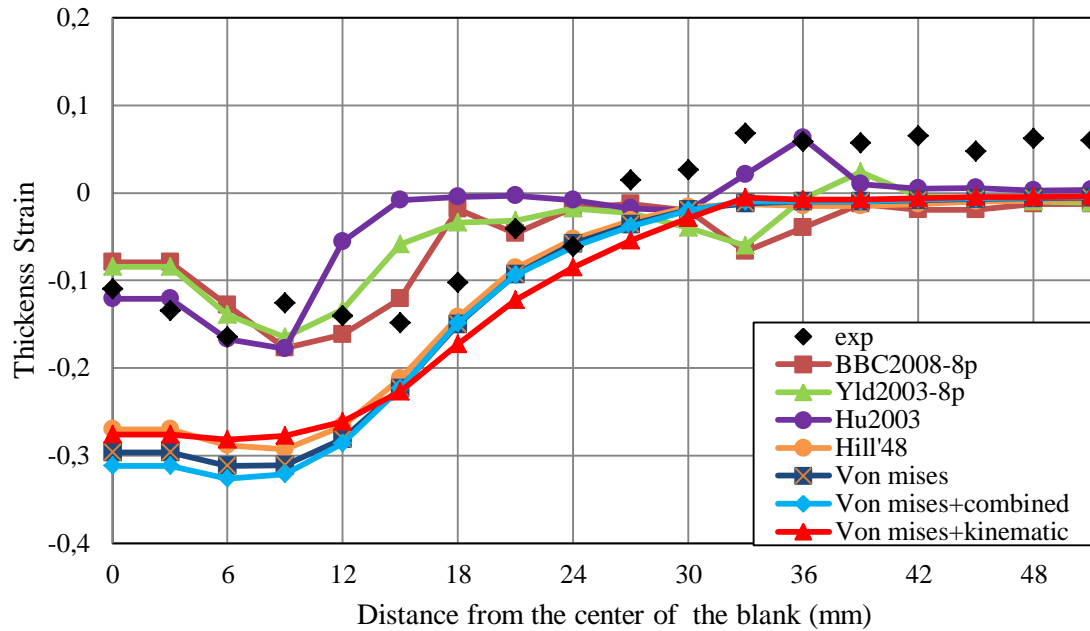


Figure 6.31 Thickness strain distributions obtained from different models and experiment at 35 mm punch travel (DKP6112, round, rolling direction).

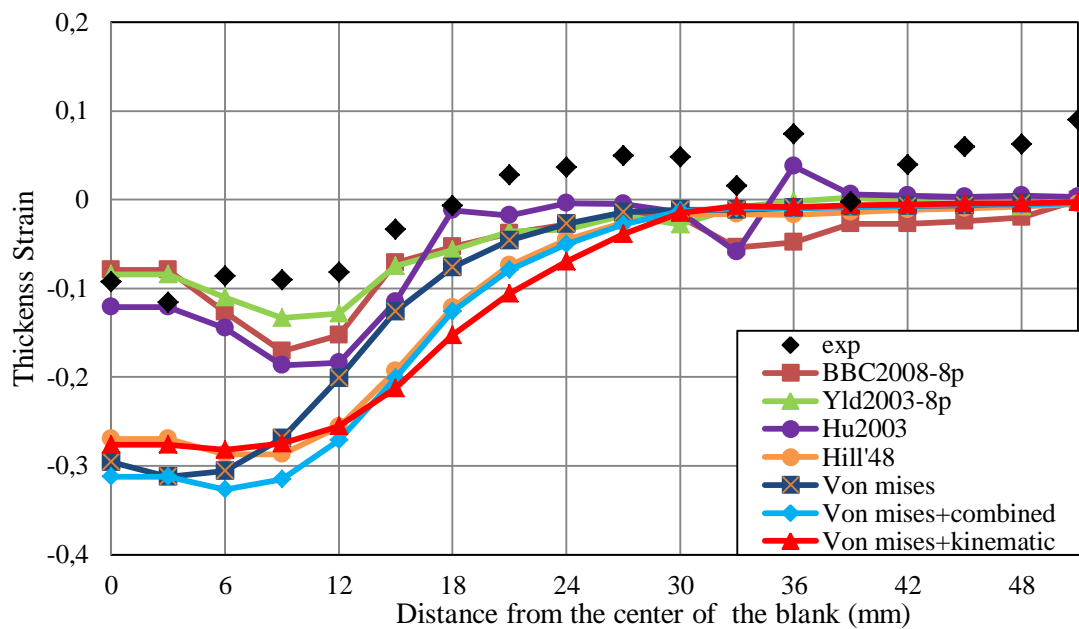


Figure 6.32 Thickness strain distributions obtained from different models and experiment at 35 mm punch travel (DKP6112, round, transverse direction).

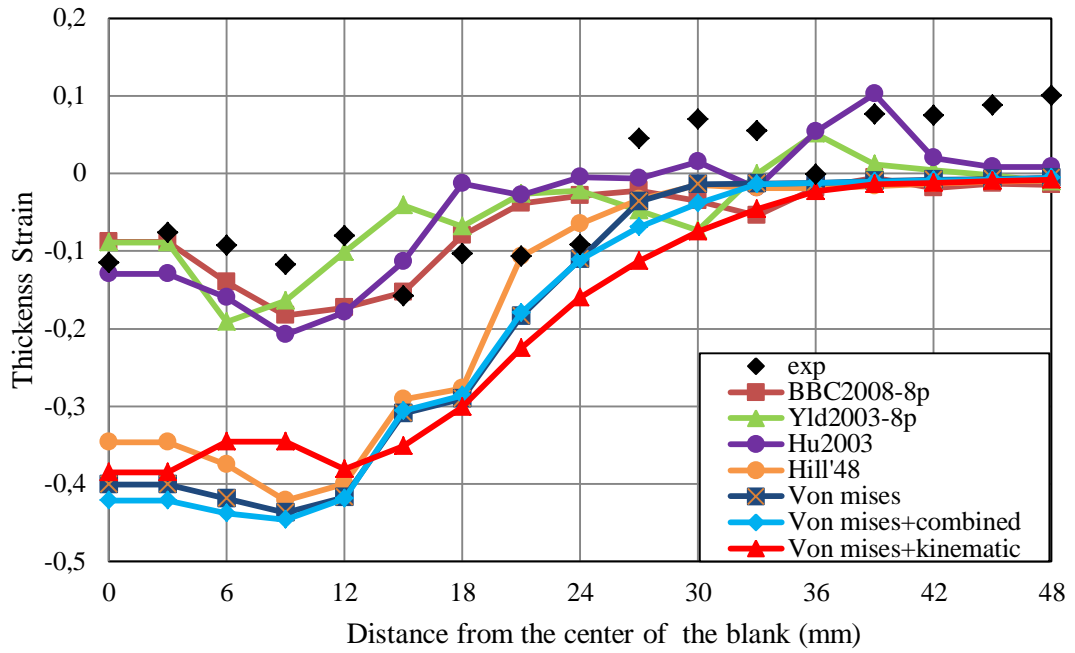


Figure 6.33 Thickness strain distributions obtained from different models and experiment at 45 mm punch travel (DKP6112, round, rolling direction).

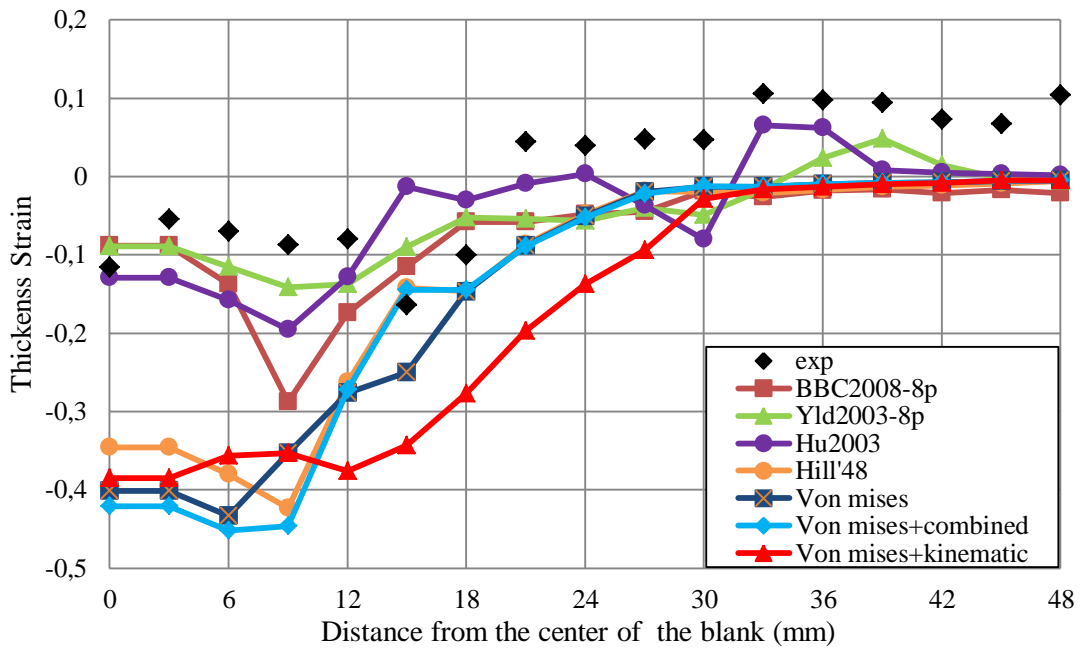


Figure 6.34 Thickness strain distributions obtained from different models and experiment at 45 mm punch travel (DKP6112, round, transverse direction).

CHAPTER 7

CONCLUSIONS AND FUTURE WORK

In this study, seven different models were considered to simulate cylindrical, square and round bottom cup drawing processes for two different sheet metals and three different punch travels. The BBC2008-8p, Yld2003-8p and Hu2003 yield criteria were implemented to ABAQUS software via the user material subroutine, whereas isotropic hardening, kinematic hardening, combined hardening and Hill'48 yield criteria were available in the software. Also, the cylindrical, square and round bottom cup drawing experiments were conducted at various punch travels with the two types of sheet materials. The models tried and the experimental findings allow us to draw the following conclusions:

1. The thickness strain distribution for cylindrical cup drawing of the SS304 and DKP6112 steel materials at various punch travels showed that the Hu2003, Yld2003-8p and BBC2008-8p models are in better agreement with the experimental thickness strain variations. Significant thickness strain deviations between the Hu2003, Yld2003-8p, BBC2008-8p models and the isotropic hardening, kinematic hardening, combined hardening and Hill'48 models are observed at the bottom region of the cup especially at high punch travels. The observed significant deviations in thickness strain reduce into negligible values at flange region of the cups.
2. In square cup drawing;
 - The thickness strain distributions of the seven models are generally close to each other and consistent with the experimental results at all punch travels for SS304 material.
 - The thickness strain distributions of the seven models are generally close to each other and consistent with the experimental results at 15 mm punch travel for DKP6112 material.
 - The experimentally obtained thickness strain values are generally consistent with the seven models at 20 mm punch travel for DKP6112 material in between the midpoint of the sides (rolling) direction especially for bottom corner region of the cup except for BBC2008-8p and Hu2003 models. The thickness strain distributions of BBC2008-8p, Hu2003 and Yld2003-8p models show better fit with the experimental results at 20 mm punch travel in diagonal direction.
 - The experimental thickness strain distributions are in better agreement with Yld2003-8p and BBC2008-8p at 25 mm punch travel for DKP6112 material in between the midpoint of the sides (rolling). Significant thickness strain deviations between the Hu2003 model, isotropic hardening, kinematic hardening, combined hardening, Hill'48 models are observed at the bottom and flange region of the cup. Although, some deviations in strain values are observed at the bottom corner region

of the cup at 25 mm punch travel in diagonal direction, the seven models and the experimental data show the same trend.

3. In round bottom cup drawing;

- The experimental thickness strain distributions are in good agreement with the seven models at 25 mm punch travel for SS304 material.
 - The experimental thickness strain distributions are consistent with the BBC2008-8p, Hu2003 and Yld2003-8p models at 45 mm punch travel for SS304 material.
 - The experimental thickness strain distributions are in good agreement with the seven models at 20 mm punch travel for DKP6112 material. The experimental thickness strain distributions are consistent with the BBC2008-8p, Hu2003 and Yld2003-8p models at 35 and 45 mm punch travels for DKP6112 material. There are considerable deviations between experimental thickness strain distributions and the isotropic hardening, kinematic hardening, combined hardening, Hill'48 models especially at the bottom region of the cup for both materials.
4. The seven models used in this study can be separated into two groups regarding the closeness of the thickness strain distributions with the experiments as; i) the BBC2008-8p, Yld2003-8p and Hu2003 and ii) the isotropic hardening, kinematic hardening, combined hardening and Hill'48 model. The former is better in predicting the material behavior of the deep drawing processes presented in the study.

As future works;

- Other yield and hardening laws can be used in the simulation of the deep drawing process to check their consistency with the tried models and experimental data of this study.
- Different materials can be tried to validate the conclusions drawn in this study. Also, various sheet thicknesses could be used in the simulation studies to find out their effect on thickness strain distribution.

REFERENCES

- [1] Kuwabara, T. and Bael, A.V., “Measurement and analysis of yield locus of sheet aluminum alloy 6XXX”, Proc. Fourth Int. Conf. and Wshop on Numerical Simulation of 3D Sheet Forming Processes, 85–90, Besanc, 1999.
- [2] Hu, W., “An orthotropic yield criterion in a 3-D general stress state”, *Int. J. Plasticity*, 21, 1771–1796, 2005.
- [3] Wang, J., “Principles of The Draw Bend Spring-back Test”, PhD. Thesis, Ohio State University, 2004.
- [4] Taherizadeh, A., Green, D.E., Ghaei, A. and Yoon, J.-W., “A non-associated constitutive model with mixed iso-kinematic hardening for finite element simulation of sheet metal forming”, *Int. J. Plasticity*, 26, 288–309, 2010.
- [5] Hill, R., “The Mathematical Theory of Plasticity”, Clarendon Press (reprint), 1998.
- [6] Kachanov, L.M., “Fundamentals of the Theory of Plasticity”, Dover Publications, 2004.
- [7] Khan, A.S. and Huang, S., “Continuum Theory of Plasticity”, John Wiley and Sons, 1995.
- [8] Mises, R.V., “Mechanik der plastischen Formänderung von Kristallen”, *Zeitschrift für Angewandte Mathematik und Mechanik*, 8, 161–185, 1928.
- [9] Mellor, P.B. and Parmer, A., “Plasticity of sheet metal forming, In: Koistinen, D.P. and Wang, N.M. (Eds.), *Mechanics of Sheet Metal Forming*, Plenum Press, 53–74, New York, 1978.
- [10] Mellor, P.B., “Sheet metal forming”, *Int. Metals. Rev.*, 26, 1–20, 1981.
- [11] Aretz, H. and Barlat, F., “New convex yield functions for orthotropic metal plasticity”, *Int. J. Non-Linear Mechanics*, 51, 97–111, 2013.
- [12] Banabic, D., Aretz, H., Comsa, D.S. and Paraianu, L., “An improved analytical description of orthotropy in metallic sheets”, *Int. J. Plasticity*, 21, 493–512, 2005.
- [13] Barlat, F., Aretz, H., Yoon, J.W., Karabin, M.E., Brem, J.C. and Dick, R.E., “Linear transformation based anisotropic yield functions”, *Int. J. Plasticity*, 21, 1009-1039, 2005.
- [14] Barlat, F., Brem, J.C., Yoon, J.W., Chung, K., Dick, R.E., Choi, S.H., Pourboghrat, F., Chu, E. and Lege, D.J., “Plane stress yield function for aluminum alloy sheets”, *Int. J. Plasticity*, 19, 1297–1319, 2003.
- [15] Karafillis, A.P. and Boyce, M.C., “A general anisotropic yield criterion using bounds and a transformation weighting tensor”, *J. Mech. Phys. Solids*, 41, 1859–1886, 1993.

- [16] Hill, R., "Theoretical plasticity of textured aggregates", *Math. Proc. Camb. Philos. Soc.*, 85, 179–191, 1979.
- [17] Hill, R., "Constitutive modeling of orthotropic plasticity in sheet metals", *J. Mech. Phys. Solids*, 38, 405–417, 1990.
- [18] Hill, R., "A user-friendly theory of orthotropic plasticity in sheet metals", *Int. J. Mech. Sci.*, 35, 19–25, 1993.
- [19] Barlat, F. and Lian, J., "Plastic behavior and stretchability of sheet metals, Part I: a yield function for orthotropic sheets under plane stress conditions", *Int. J. Plasticity*, 5, 51–66, 1989.
- [20] Barlat, F., Lege, D.J. and Brem, J.C., "A six-component yield function for anisotropic materials", *Int. J. Plasticity*, 7, 693–712, 1991.
- [21] Barlat, F., Becker, R.C., Hayashida, Y., Maeda, Y., Yanagawa, M., Chung, K., Brem, J.C., Lege, D.J., Matsui, K., Murtha, S.J. and Hattori, S., "Yielding description for solution strengthened aluminum alloys", *Int. J. Plasticity*, 13, 385–401, 1997a.
- [22] Custom Part Net, Sheet Metal Forming, <http://www.custompartnet.com/wu/sheet-metal-forming>, viewed 2 July 2013.
- [23] Obermeyer, E.J. and Majlessi, S.A., "A review of recent advances in the application of blank-holder force towards improving the forming limits of sheet metal parts", *J. Material Processing Technology*, 75, 222–234, 1998.
- [24] Traversin, M. and Kergen, R., "Closed-loop control of the blank-holder force in deep-drawing: finite-element modeling of its effects and advantages", *J. Material Processing Technology*, 50, 306–31, 1995.
- [25] Gunnarsson, L. and Schedin, E., "Improving the properties of exterior body panels in automobiles using variable blank holder force", *J. Material Processing Technology*, 114, 168–173, 2001.
- [26] Krishnan, N. and Cao, J., "Estimation of optimal blank holder force trajectories in segmented binders using an ARMA mode", *J. Mech. Sci and Engineering*, 125, 763–770, 2003.
- [27] Sheng, Z.Q., Jirathearanat, S. and Altan, T., "Adaptive FEM simulation for prediction of variable blank holder force in conical cup drawing", *Int. J. Machine Tools and Manufacture*, 44, 487–494, 2004.
- [28] Yoshihara, S., Manabe, K.I. and Nishimura, H., "Effect of blank holder force control in deep-drawing process of magnesium alloy sheet", *J. Material Processing Technology*, 170, 579–585, 2005.
- [29] Vrh, M., Halilovi, M., Starman, B., Štok, B., Comsa, D.-S. and Banabic, D., "Earing Prediction in Cup Drawing using the BBC2008 Yield Criterion ", *The 8th Int. Conf. and Workshop on Numerical Simulation of 3D Sheet Metal Forming Processes, AIP Conf. Proc.*, 1383, 142-149, 2011.

- [30] Comsa, D.S. and Banabic, D., “Plane-stress yield criterion for highly-anisotropic sheet metals”, In: Hora R.P (ed), Proceedings of the 7th International Conference and Workshop on Numerical Simulation of 3D Sheet Metal Forming Processes, 43–48, Switzerland, 2008.
- [31] Yoon, J.-H., Cazacu, O., Yoon, J.W. and Dick, R.E., “Earing predictions for strongly textured aluminium sheets”, *Int. J. of Mech. Sci.*, 52, 1563-1578, 2010.
- [32] Moreira, L.P., Ferron, G. and Ferran, G., “Experimental and numerical analysis of the cup drawing test for orthotropic metal sheets”, *J. Materials Processing Technology*, 108, 78-86, 2000.
- [33] Ferron, G., Makkouk, R. and Morreale, J., “A parametric description of orthotropic plasticity in metal sheets”, *Int. J. Plasticity*, 10, 431-449, 1994.
- [34] Banabic, D., Kuwabara, T., Balan, T., Comsa, D.S. and Julean, D., “Non-quadratic yield criterion for orthotropic sheet metals under plane-stress conditions”, *Int. J. Mech. Sci.*, 45, 797–811, 2003.
- [35] Guner, A., Soyarslan, C., Brosius, A. and Tekkaya, A.E., “Characterization of anisotropy of sheet metals employing inhomogeneous strain fields for Yld2000-2D yield function”, *Int. J. Solids and Structures*, 49, 3517–3527, 2012.
- [36] Hill, R., “A theory of the yielding and plastic flow of anisotropic metals”, *Proc. Roy. Soc. London*, 193, 281–297, 1948.
- [37] Eggertsen, P.A. and Mattiasson, K., “On constitutive modeling for springback analysis”, *Int. J. Mech. Sci.*, 52, 804–818, 2010.
- [38] Yoshida, F. and Uemori, T., “A model of large-strain cyclic plasticity and its application to springback simulation”, *Int. J. Mech. Sci.*, 45, 1687–1702, 2003.
- [39] Eggertsen, P.A. and Mattiasson, K., “On the modeling of the bending–unbending behavior for accurate springback predictions”, *Int. J. Mech. Sci.*, 51, 547–563, 2009.
- [40] Soare, S., Yoon, J.W. and Cazacu, O., “On the use of homogeneous polynomials to develop anisotropic yield functions with applications to sheet forming”, *Int. J. Plasticity*, 24, 915–944, 2008.
- [41] Laurent, H., Greze, R., Manach, P.Y. and Thuillier, S., “Influence of constitutive model in springback prediction using the split-ring test”, *Int. J. Mech. Sci.*, 51, 233–245, 2009.
- [42] Barlat, F., Lege, D.J., Brem, J.C., “A six-component yield function for anisotropic materials”, *Int. J. Plasticity*, 7, 693–712, 1991.
- [43] Aretz, H., “A non-quadratic plane stress yield function for orthotropic sheet metals”, *J. Material Processing Technology*, 168, 1–9, 2005.
- [44] Yoon, J.W. and Hong, S.H., “Modeling of Aluminum Alloy Sheets Based on New Anisotropic Yield Functions”, *J. Materials Processing Technology*, 177, 134–137, 2006.

- [45] Aretz, H., and Barlat, F., “General orthotropic yield functions based on linear stress deviator transformations”, In: Ghosh, S., Lee, J.K, Castro, J.C., (Eds.), Proceedings of the 8th International Conference on Numerical Methods in Industrial Forming Processes, AIP Conference Proceedings, 712, 147–156, 2004.
- [46] Hu, W.L., “Characterized behaviors and corresponding yield criterion of anisotropic sheet metals”, *Material Science Engineering, A* 345, 139–144, 2003.
- [47] Hosford, W.F., “On yield loci of anisotropic cubic metals”, Proceedings of the 7th North American Metalworking Conference, SME, 191-/197, Dearborn, 1979.
- [48] Xu, L., Barlat, F. and Ahn, D.C., “Constitutive modelling of ferritic stainless steel sheets”, *Int. J. Material Forming*, 2, Springer/ESAFORM, 2009.
- [49] Soare, S.C. and Barlat, F., “A study of the Yld2004 yield function and one extension in polynomial form: A new implementation algorithm, modeling range, and earing predictions for aluminum alloy sheets”, *European J. Mechanics A/Solids*, 30, 807-819, 2011.
- [50] Banabic, D., Kuwabara, T., Balan, T. and Comsa, D.S., “An anisotropic yield criterion for sheet metals”, *J. Materials Processing Technology*, 157–158, 462–465, 2004.
- [51] Kuwabara, T., Ikeda, S. and Kuroda, K., “Measurement and analysis of differential work hardening in cold-rolled steel sheet under biaxial tension”, *J. Material Processing Technology*, 80/8, 517–523, 1998.
- [52] Banabic, D., Balan, T. and Comsa, D., “A new yield criterion for orthotropic sheet metals under plane–stress conditions”, *The Seventh Conf. “TPR2000”*, 217–224, Cluj Napoca, 2000.
- [53] Banabic, D., Balan, T. and Comsa, D., “Yield criterion for orthotropic sheet metals”, *The 8th Int. Conf. on Metal Forming* , 755–761, Krakow, 2000.
- [54] Mattiasson, K. and Sigvant, M., “An evaluation of some recent yield criteria for industrial simulations of sheet forming processes”, *Int. J. Mech. Sci.*, 50, 774–787, 2008.
- [55] Barlat, F., Yoon, J.W., Cazacu, O., “On linear transformations of stress tensors for the description of plastic anisotropy”, *Int. J. Plasticity*, 23, 876–896, 2007.
- [56] Butuc, M.C., Teodosiu, C., Barlat, F. and Gracio, J. J, “Analysis of sheet metal formability through isotropic and kinematic hardening models”, *European J. Mechanics A/Solids*, 30, 532-546, 2011.
- [57] Teodosiu, C., Hu, Z., “Evolution of the intragranular microstructure at moderate and large strains: modelling and computational significance”, In: Shen, S.-F., Dawson, P.R. (Eds.), *Proc. NUMIFORM’ 95*, 173-182, 1995.
- [58] Swift, H.W., “ Plastic instability under plane stress”, *J. Mech. Phys. Solids*, 1, 1-16, 1952.

- [59] Voce, E., “A Practical Strain-Hardening Function”, *Metallurgica*, 51, 219-220, 1955.
- [60] Marciniak, Z., Kuczynski, K., “Limit strains in the processes of stretch-forming sheet metal”, *Int. J. Mech. Sci.*, 9, 609-620, 1967.
- [61] Wu, H.C.,” Anisotropic plasticity for sheet metals using the concept of combined isotropic-kinematic”, *Int. J. Plasticity*, 18, 1661–1682, 2002.
- [62] Wu, H.C. and Loureiro, M., “An anisotropic plasticity for sheet metals, In: Zabarar, N., Becker, R., Lalli, L., Ghosh, S. (Eds.), *The Integration of Material, Process and Product Design*, 93–102, Balkema, Rotterdam, 1999.
- [63] Wu, H.C., Hong, H.K. and Shiao, Y.P., “Anisotropic plasticity with application to sheet metals”, *Int. J. Mech. Sci.*, 41, 703–724, 1999.
- [64] Wu, H.C. and Hong, H.K., “Endochronic description of plastic anisotropy in sheet metal”, *Int. J. Solids Structures*, 36, 2735–2756, 1999.
- [65] Dasappa, P., Inal, K. and Mishra, R., “The effects of anisotropic yield functions and their material parameters on prediction of forming limit diagrams”, *Int. J. Solids and Structures*, 49, 3528–3550, 2012.
- [66] Hill, R., “A theory of the yielding and plastic flow of anisotropic metals”, *Proc. Roy. Soc. London*, 193, 281–297, 1948.
- [67] Plunkett, B., Cazacu, O., Barlat, F., “Orthotropic yield criteria for description of the anisotropy in tension and compression of sheet metals”, *Int. J. Plasticity*, 24, 847–866, 2008.
- [68] Yoon, J.W., Barlat, F., Chung, K., Pourboghrat, F. and Yang, D.Y., “Earing predictions based on asymmetric nonquadratic yield function”, *Int. J. Plasticity*, 16, 1075–1104, 2000.
- [69] Barlat, F., Maeda, Y., Chung, K., Yanagawa, M., Brem, J.C., Hayashida, Y., Lege, D.J., Matsui, K., Murtha, S.J., Hattori, S., Becker, R.C. and Makosey, S., “Yield function development for aluminum alloy sheets”, *J. Mech. Phys. Solids*, 45, 1727–1763, 1997b.
- [70] Choi, Y., “Modeling Evolution of Anisotropy and Hardening for Sheet Metals”, Master Thesis, Ohio State University, 2003.
- [71] Dixit, U.S., “Finite Element Method: Introduction”, Lecture Notes, Department of Mechanical Engineering, Indian Institute of Technology, India.
- [72] Hutton, D.V., “Fundamentals of finite element analysis”, McGraw-Hill, 2004.
- [73] Ivanco, I.V, “Nonlinear Finite Element Analysis”, Script of Lectures, Faculty of Mechanical Engineering, Technical University of Košice, Slovakia, June 2011.
- [74] Bhavikatti, S. S, “Finite Element Analysis”, New Age International (P) Publishers, 2005.
- [75] “Abaqus 6.10 Theory Manual”, Dassault Systemes Simulia Corporation, 2010.

- [76] Boger, R.K., “Non-Monotonic Strain Hardening and Its Constitutive Representations”, PhD. Thesis, Ohio State University, 2006.
- [77] Neto, S., Peric, D., Owen, D., “Computational Methods for Plasticity, Theory and Applications”, Wiley, 2008.
- [78] Barlat, F., and Richmond, O., “Prediction of tricomponent plane stress yield surfaces and associated flow and failure behavior of strongly textured fcc polycrystalline sheets”, *Materials Science and Engineering*, 95, 15-29, 1987.

APPENDIX A

SAMPLE FEA RESULTS

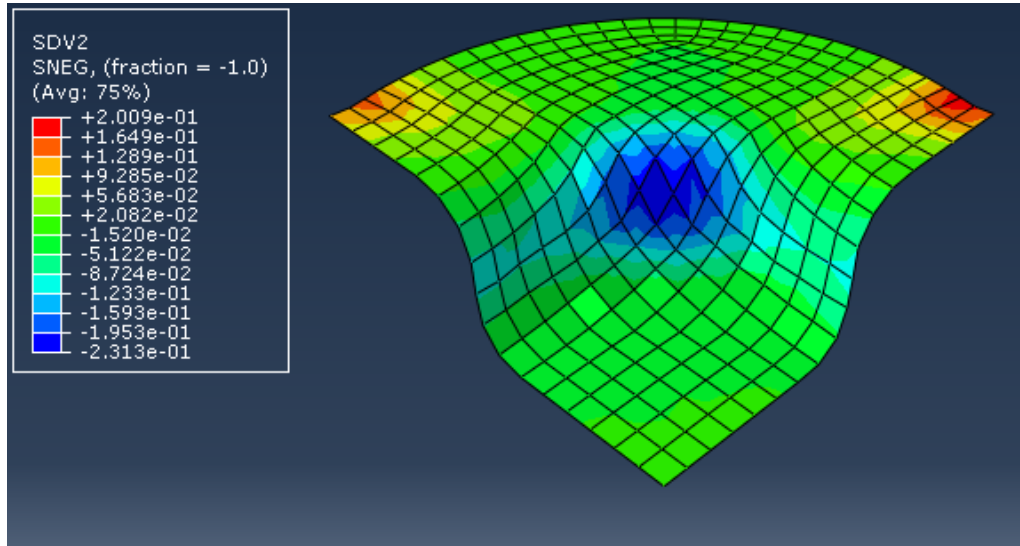


Figure A.1 The cylindrical cup drawn (SS304 steel) according to Hu2003 model (45 mm punch travel).

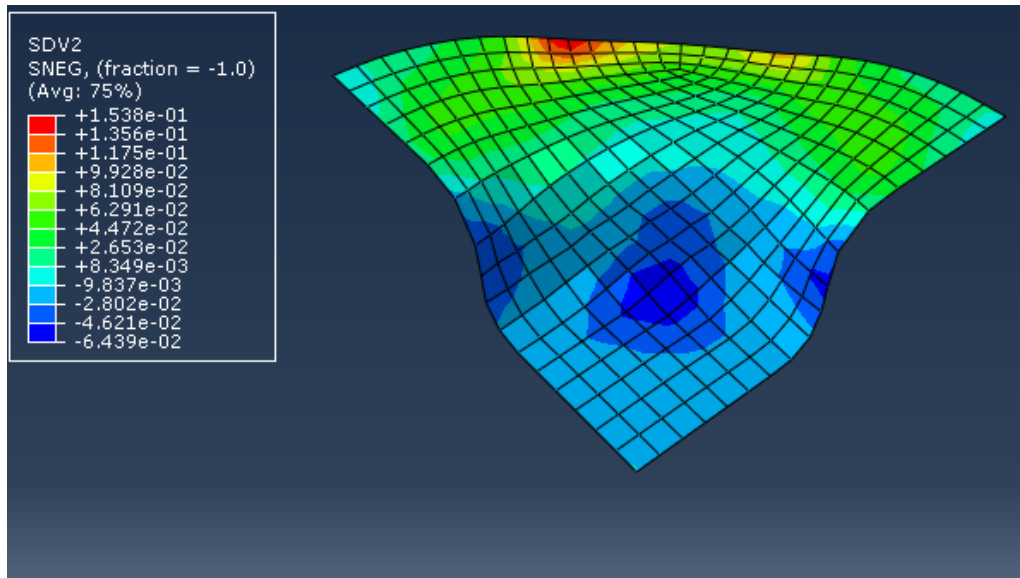


Figure A.2 The cylindrical cup drawn (DKP6112 steel) according to Yld2003 model (35 mm punch travel).

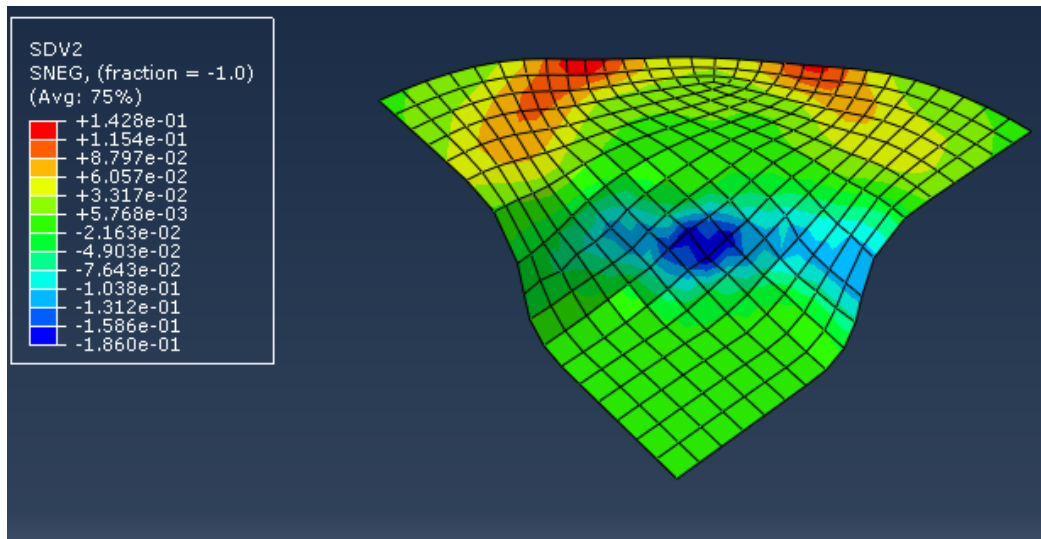


Figure A.3 The cylindrical cup drawn (DKP6112 steel) according to Hu2003 model (35 mm punch travel).

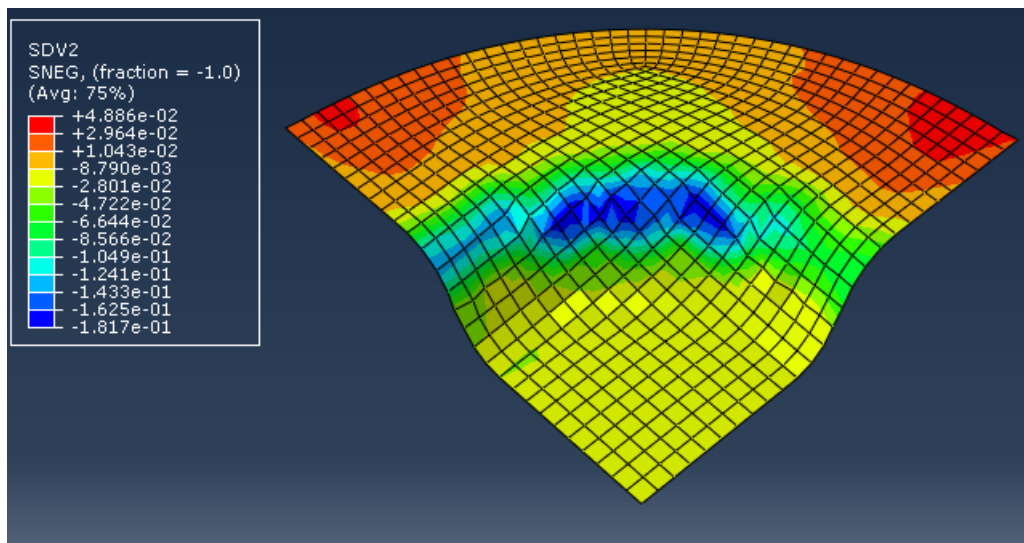


Figure A.4 The cylindrical cup drawn (SS304 steel) according to Hu2003 model (20 mm punch travel).

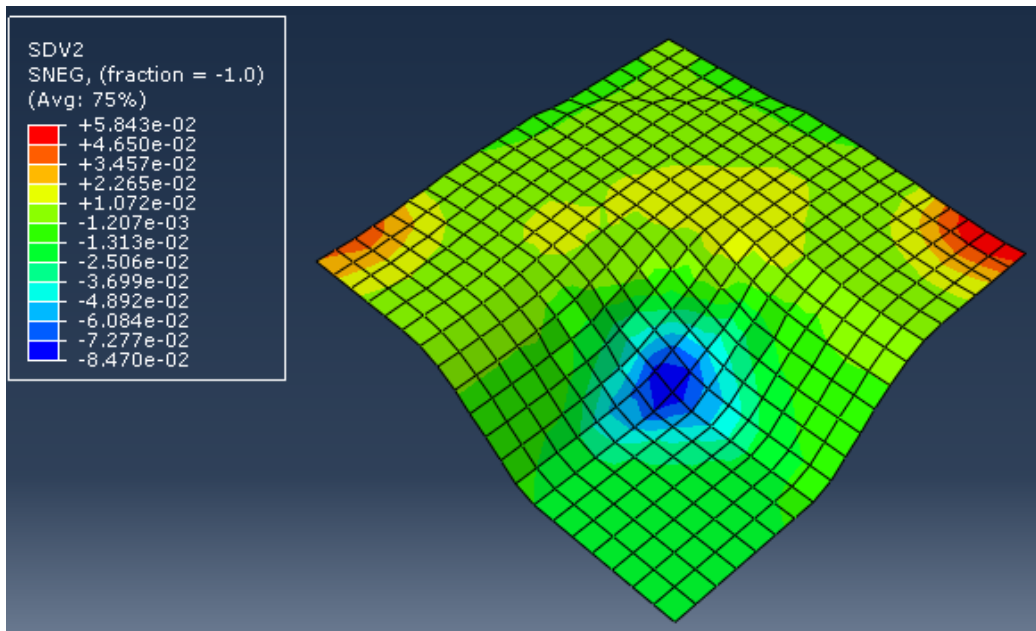


Figure A.5 The square cup drawn (SS304 steel) according to Hu2003 model (15 mm punch travel).

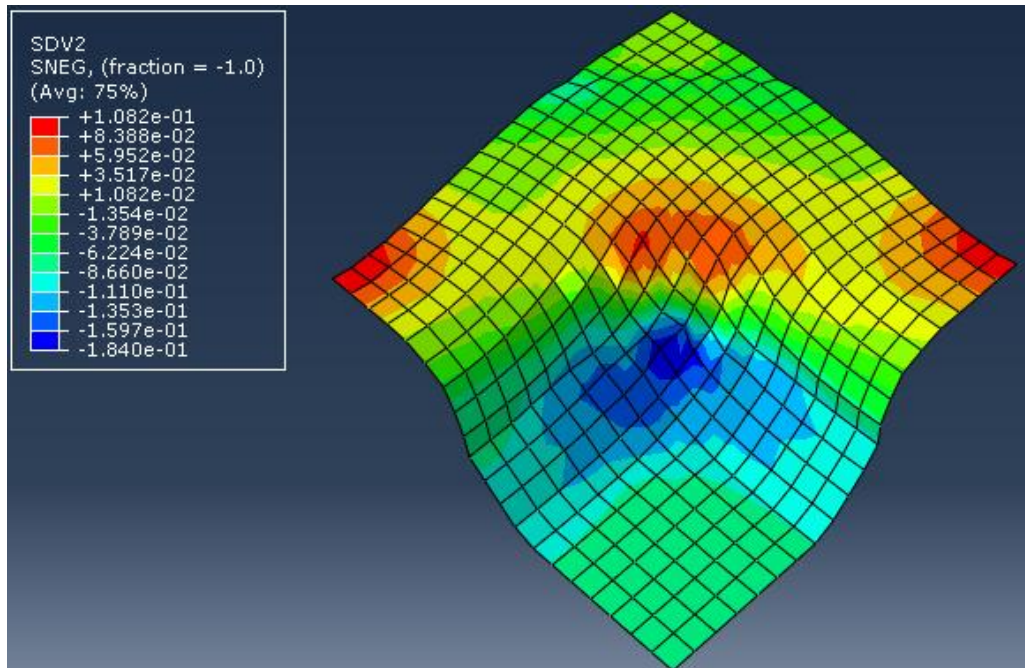


Figure A.6 The square cup drawn (SS304 steel) according to Yld2003 model (25 mm punch travel).

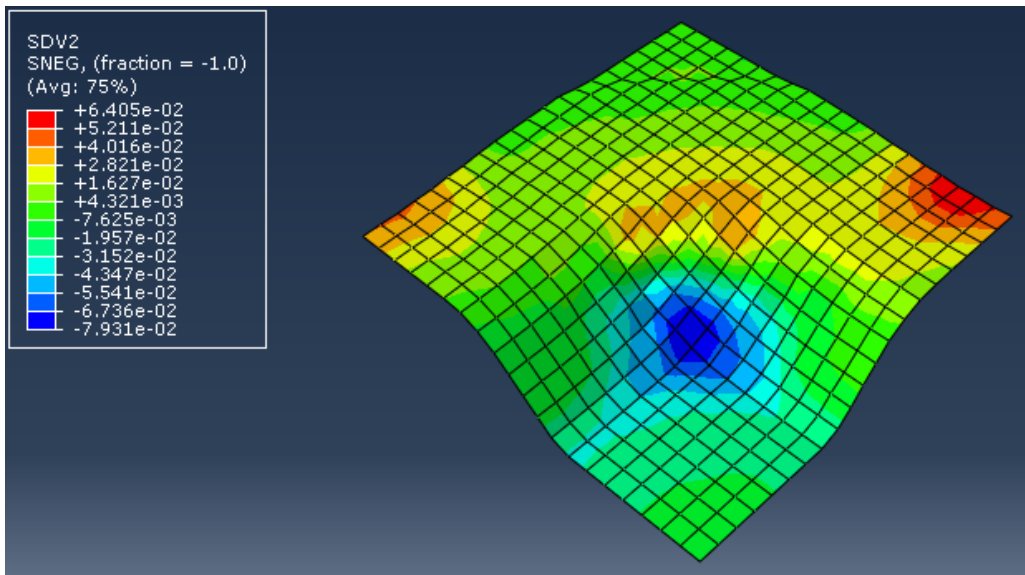


Figure A.7 The square cup drawn (SS304 steel) according to Yld2003 model (15 mm punch travel).

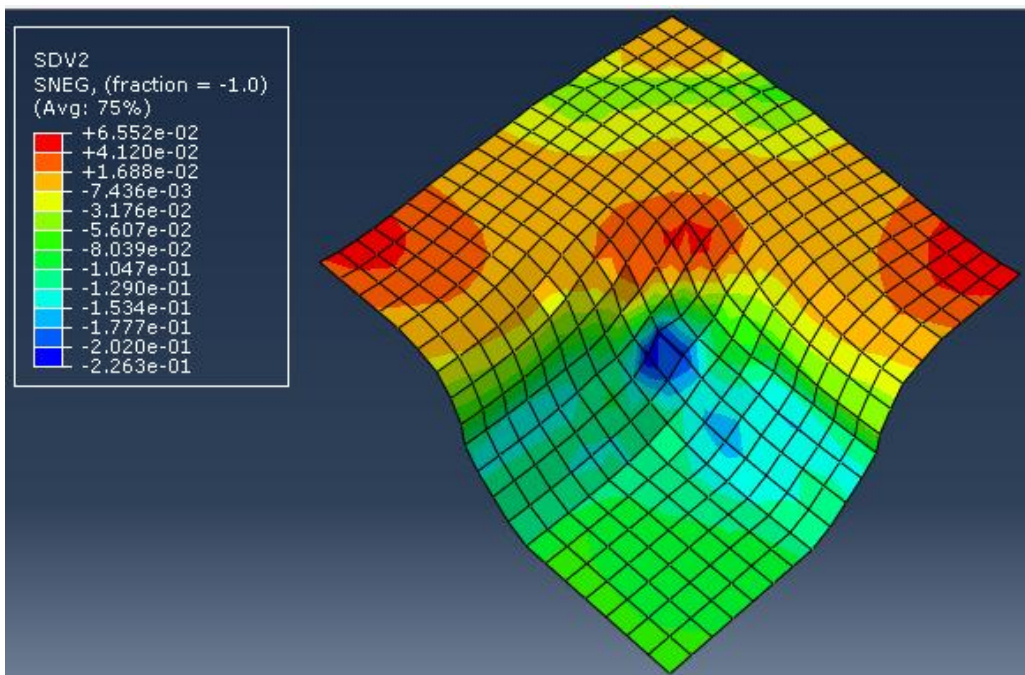


Figure A.8 The square cup drawn (DKP6112) according to Yld2003 model (25 mm punch travel).

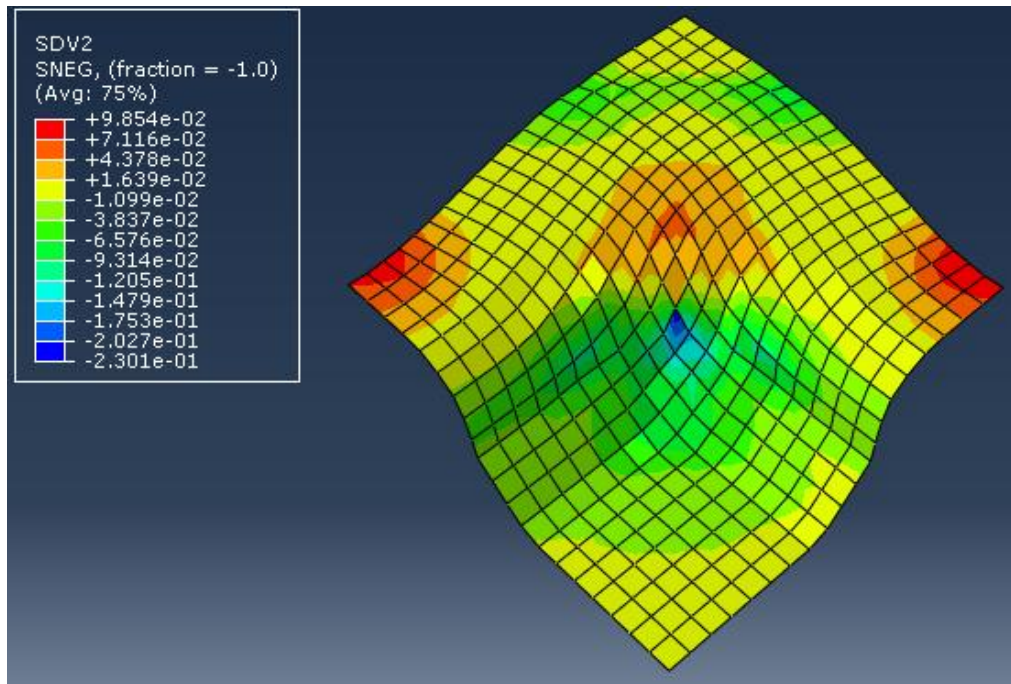


Figure A.9 The square cup drawn (DKP6112) according to Hu2003 model (25 mm punch travel).

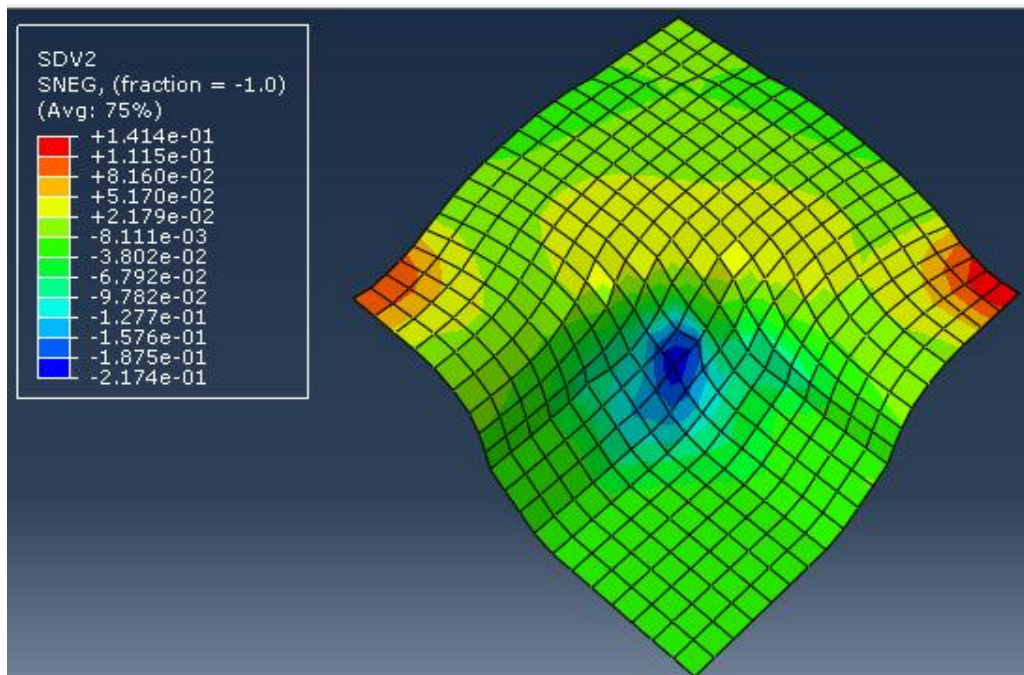


Figure A.10 The square cup drawn (SS304 steel) according to Hu2003 model (25 mm punch travel).

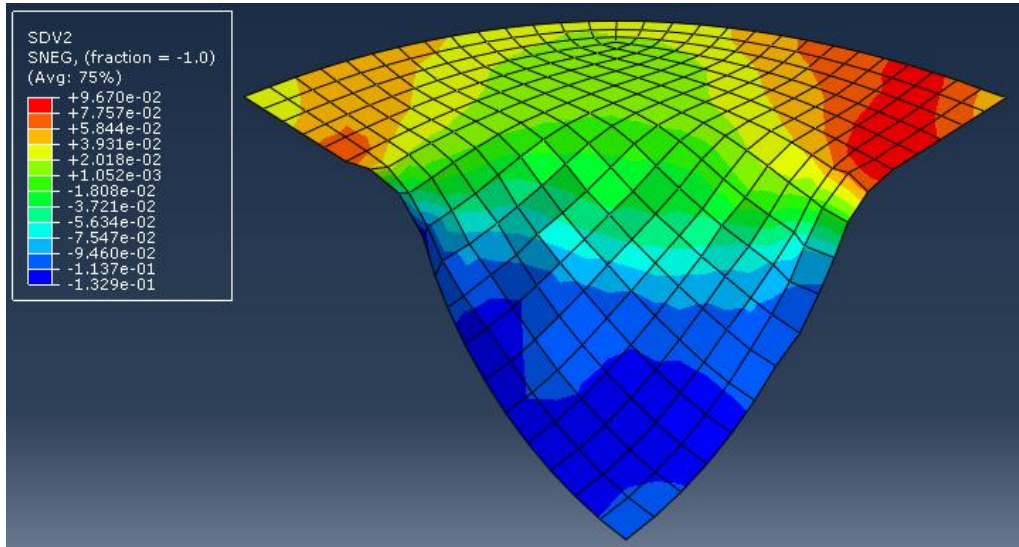


Figure A.11 The round bottom cup drawn (SS304 steel) according to Yld2003 model (45 mm punch travel).

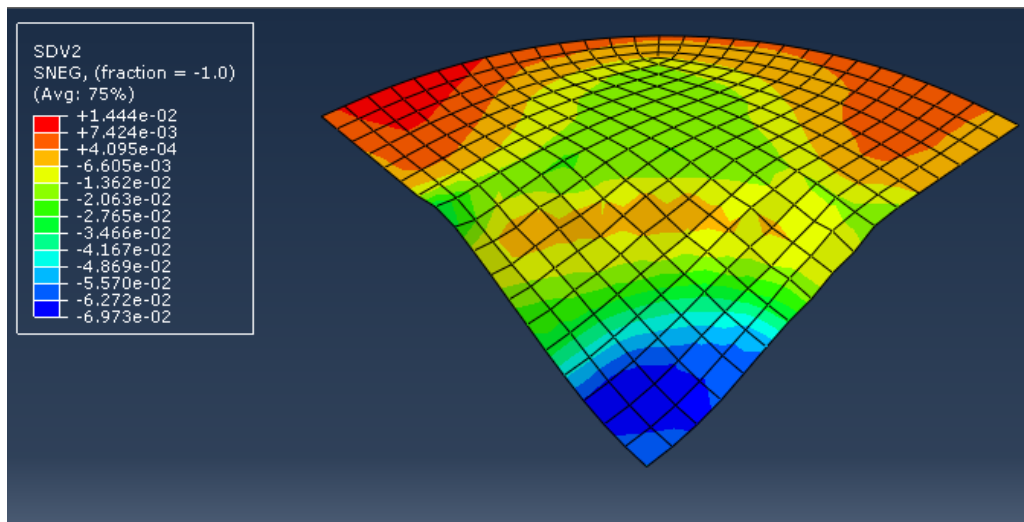


Figure A.12 The round bottom cup drawn (SS304 steel) according to BBC2008 model (25 mm punch travel).

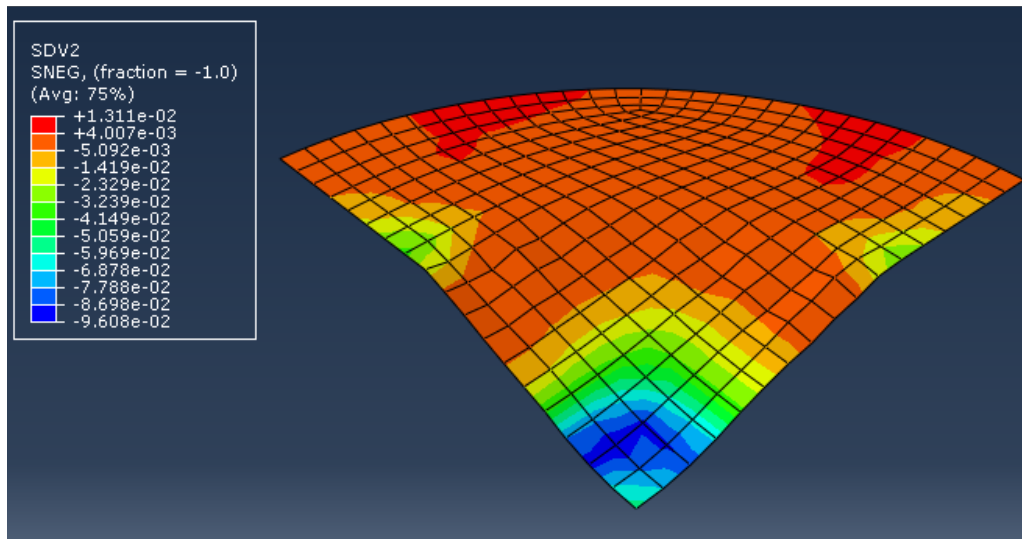


Figure A.13 The round bottom cup drawn (DKP6112) according to BBC2008 model (20 mm punch travel).

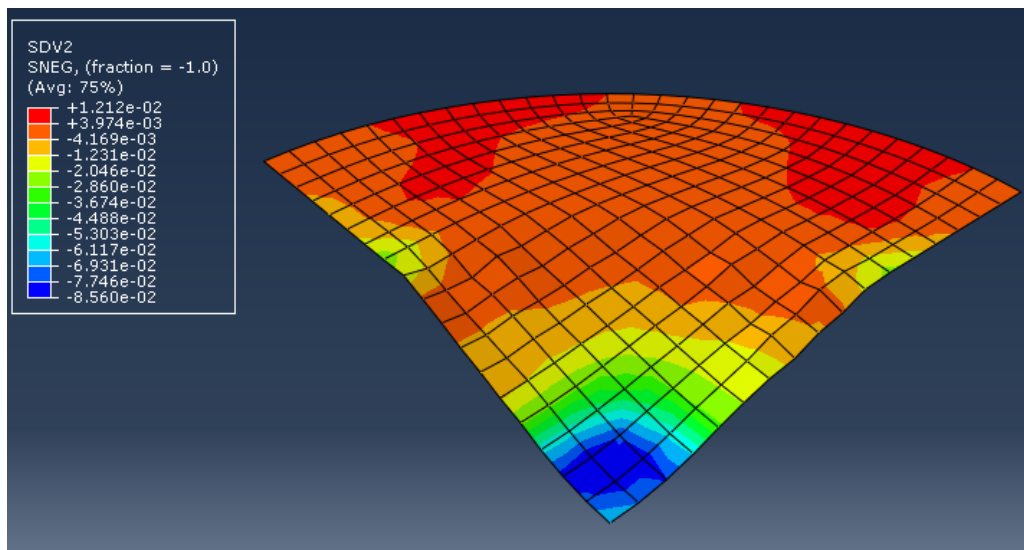


Figure A.14 The round bottom cup drawn (DKP6112) according to Yld2003 model (20 mm punch travel).

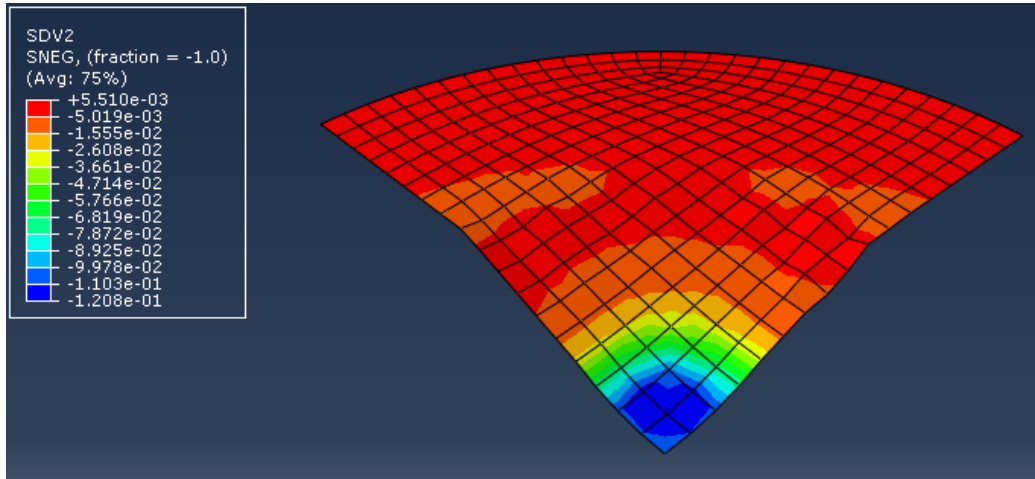


Figure A.15 The round bottom cup drawn (DKP6112) according to Hu2003 model (20 mm punch travel).

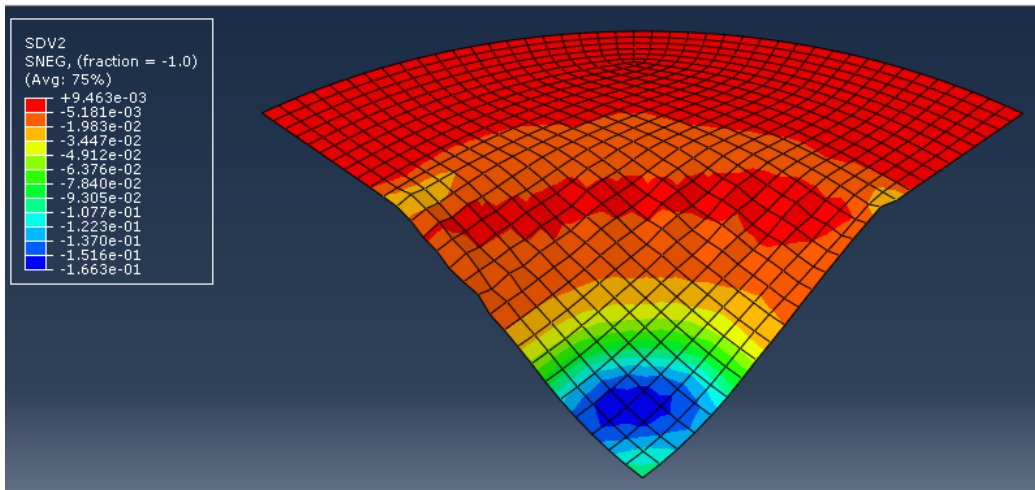


Figure A.16 The round cup drawn (SS304 steel) according to Hu2003 model (25 mm punch travel).